AUS DEM INSTITUT FÜR SCHLAGANFALL- UND DEMENZFORSCHUNG
DER LUDWIG-MAXIMILIANS-UNIVERSITÄT MÜNCHEN
DIREKTOR: PROF. DR. MED. MARTIN DICHGANS

Role of inhaled nitric oxide on vascular inflammation after experimental ischemic stroke

Dissertation
zum Erwerb des Doktorgrades der Naturwissenschaften
an der Medizinischen Fakultät der
Ludwig-Maximilians-Universität zu München

vorgelegt von

Rebecca Isabella Sienel

aus

München

2022

Mit Genehmigung der Medizinischen Fakultät

der Universität München

Betreuer(in):	Priv. Doz. Dr. Christof Haffner
Zweitgutachter(in):	Prof. Dr. Sabine Steffens
Dekan:	Prof. Dr. med. Thomas Gudermann
Tag der mündlichen Prüfung:	10. November 2022

"Tell me and I forget, teach me, and I may remember, involve me and I learn."

(Benjamin Franklin)

Für meine
Familie

Affidavit

I hereby confirm that my thesis entitled

"**Role of inhaled nitric oxide on vascular inflammation after experimental ischemic stroke**"

was the result of my own work.

I did not receive any help or support from commercial consultants. All sources and/or materials applied were listed and specified in the thesis.

Furthermore, I confirm that this thesis has not yet been submitted as part of another examination process neither in identical nor in similar form.

München, 20.11.2022	Rebecca Sienel
Place, Date	Rebecca Sienel

Publication list

Adhesion of leukocytes to cerebral venules precedes neuronal cell death and triggers tissue damage after cerebral ischemia.
Sienel RI*, Kataoka H.**, Seong-Woong Kim, Burcu Fatma Seker and Nikolaus Plesnila*; *Front. Neurol. – Stroke. DOI: 10.3389/fneur.2021.807658*

Neurovascular reactivity in the aging mouse brain assessed by laser speckle contrast imaging and 2-photon microscopy: Quantification by an investigator-independent analysis tool.
Seker B, Fan Z, Gesierich B, Gaubert M, ***Sienel RI****, Plesnila N; Front. Neurol. - Applied Neuroimaging. DOI: 10.3389/fneur.2021.745770*

Interaction of FGF9 with FGFR3-IIIb/IIIc, a putative driver of growth and aggressive behavior of hepatocellular carcinoma.
Paur J, Valler M, ***Sienel R****, et al. [published online ahead of print, 2020 May 7]. Liver Int. 2020;10.1111/liv.14505. doi:10.1111/liv.14505*

(authors contributed equally to the manuscript)*

Abstract

Inhaled nitric oxide (iNO) reduces ischemic brain damage by increasing collateral blood flow to the ischemic penumbra. Next to its vasoactive activity, NO is also known to reduce vascular inflammation. The adhesion of leukocytes to cerebral vessels is recognized to contribute to ischemic brain injury. However, the underlying mechanisms are unclear. Therefore, the current thesis aimed to investigate whether iNO may protect the brain by inhibiting post-ischemic leukocyte adhesion through anti-inflammatory properties.

To answer this question, mice underwent middle cerebral artery occlusion (MCAo; 1 hour) and received 50 ppm NO by inhalation upon reperfusion. Leukocyte-endothelial interaction was visualized *in vivo* by 2-photon microscopy. Plasma and tissue samples were collected five hours after reperfusion. Pro-inflammatory cytokines, adhesion molecules, leukocyte numbers, nitric oxide synthases, and NO metabolites were analyzed by qPCR, western blot, ELISA, or chemiluminescence.

Cerebral ischemia reduced the number of circulating monocytes and neutrophils by 18% and increased the expression of endothelial NOS (eNOS) by 50%. Cortical IL-1β, IL-6, and TNF-α were upregulated by 15-20-fold, while adhesion molecules such as E/P-selectin, ICAM-1, and VCAM-1 were upregulated five-fold in the ischemic cortex. Consequently, rolling and adhesion to venous and capillary endothelium increased by 80%. iNO elevated NO-related metabolites such as nitrite and nitrate in plasma four-fold and reduced leukocyte rolling and adhesion by 75% and 98%, respectively. Moreover, iNO exhibited beneficial effects through lowering cytokine and ICAM-1 expression by 60% and 75%, respectively. Additionally, iNO normalized the number of circulating leukocytes and the expression of eNOS.

The current study results indicate that iNO treatment blunted leukocyte adhesion and reduced inflammatory signaling in cerebral vessels and cortex after focal cerebral ischemia. Hence, reducing neuroinflammation may represent a novel mechanism by which iNO protects the brain after stroke. These findings further support the clinical evaluation of iNO as a potential therapeutic approach for ischemic stroke.

Zusammenfassung

Inhaliertes Stickstoffmonoxid (iNO) reduziert den ischämischen Hirnschaden indem es die kollaterale Durchblutung zur ischämischen Penumbra erhöht. Neben seiner vasoaktiven Wirkung ist NO auch dafür bekannt, dass es die Gefäßentzündung reduziert. Es ist bekannt, dass die Adhäsion von Leukozyten an den Hirngefäßen zu einer ischämischen Hirnschädigung beiträgt, die zugrundeliegenden Mechanismen sind jedoch unklar. Das Ziel der vorliegenden Arbeit war daher zu untersuchen, ob iNO das Gehirn schützen kann, indem es die postischämische Leukozytenadhäsion durch entzündungshemmende Eigenschaften hemmt.

Um diese Frage zu beantworten, wurden Mäuse einem Verschluss der mittleren Hirnarterie (MCAo; 1 Stunde) unterzogen und erhielten nach der Reperfusion 50 ppm NO durch Inhalation. Die Leukozyten- Endothelium Interaktion wurde *in vivo* mit Hilfe der 2-Photonen-Mikroskopie visualisiert. Plasma- und Gewebeproben wurden fünf Stunden nach der Reperfusion entnommen, und pro-inflammatorische Zytokine, Adhäsionsmoleküle, Leukozytenzahlen, Stickstoffmonoxid-Synthasen und NO-Metaboliten wurden mittels qPCR, Western Blot, ELISA oder Chemilumineszenz analysiert.

Die zerebrale Ischämie verringerte die Zahl der zirkulierenden Monozyten und Neutrophilen um 18 % und erhöhte die Expression der endothelialen NOS (eNOS) um 50 %. Kortikales IL-1β, IL-6 und TNF-α waren um das 15-20-fache erhöht, während Adhäsionsmoleküle wie E/P-Selektin, ICAM-1 und VCAM-1 im ischämischen Kortex um das Fünffache erhöht waren. Folglich nahmen das Rollen und die Adhäsion am Venen- und Kapillarendothel um 80 % zu. iNO erhöhte die NO-verwandten Metaboliten wie Nitrit und Nitrat im Plasma um das Vierfache und verringerte das Rollen und die Adhäsion der Leukozyten um 75 % bzw. 98 %. Darüber hinaus zeigte iNO positive Auswirkungen, indem es die Expression von Zytokinen und ICAM-1 um 60 % bzw. 75 % verringerte. Darüber hinaus normalisierte iNO die Anzahl der zirkulierenden Leukozyten und die Expression von eNOS.

Die Ergebnisse der aktuellen Studie zeigen, dass eine iNO-Behandlung die Adhäsion von Leukozyten und die Entzündungssignale in den Hirngefäßen und der Hirnrinde nach einer fokalen zerebralen Ischämie reduziert. Die Verringerung der Neuroinflammation könnte daher ein neuer Mechanismus sein, durch den iNO das Gehirn nach einem Schlaganfall schützt. Diese Ergebnisse unterstützen die klinische Bewertung von iNO als potenziellen therapeutischen Ansatz für ischämische Schlaganfälle.

Table of contents

I. Introduction

Stroke affects 15 million people worldwide every year. With a mortality rate of 30%, stroke is the second leading cause of death and the leading cause of severe and long-term disability.[1] Stroke causes an immediate deprivation of oxygen and nutrients in the brain due to a sudden loss of blood flow caused by blockage (ischemic stroke) or rupture (hemorrhagic stroke) of a cerebral artery provoking tissue infarction.[2,3] Common known risk factors for stroke are advanced age and lifestyle-related factors such as hypertension, smoking, diet, and physical inactivity.[4] The ischemic brain tissue can be divided into two regions: an ischemic core, with rapid, severe unrecoverable damage, and a salvageable ischemic penumbra, where damage develops rather slowly due to the blood supply via collaterals.[5]

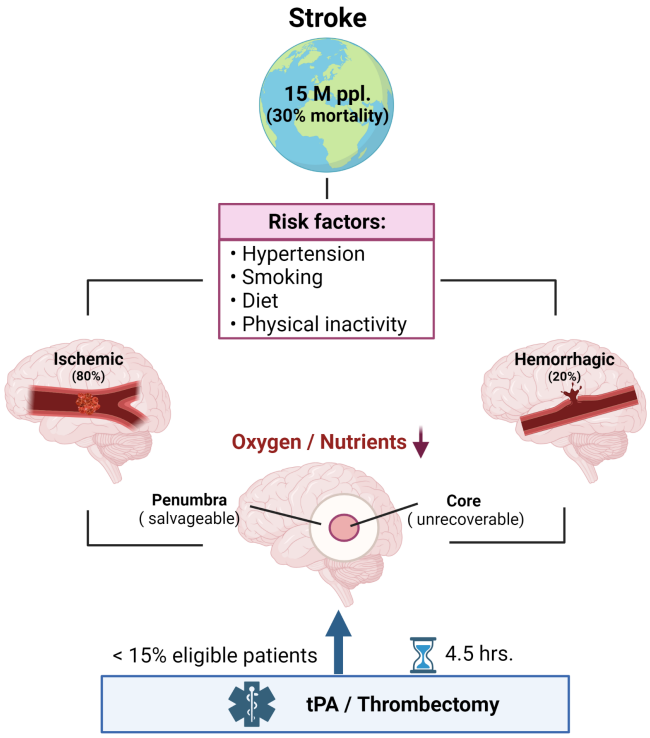

Figure 1: Overview of stroke epidemiology, causes, impacts, and therapeutic approaches. Insufficient supply of the brain with blood either by a blocked (ischemic) or disrupted (hemorrhagic) vessel causes a medical condition named stroke. Stroke is one of the most prevalent and devastating diseases globally. Advanced age and lifestyle-related factors are among the common know risk factors for stroke. Medical thrombectomy and thrombolysis (tPA) are the first treatment choices, however, with a small therapeutic window (4.5 hrs.) and less than 15% of eligible patients. (created with BioRender.com)

Ischemic stroke represents 80% of all stroke cases.[1] Therapeutic approach encompasses the intravenous application of tissue-type plasminogen activator (tPA) and endovascular thrombectomy to recanalize the occluded vessel. Intravenous tPA is the only approved pharmacological treatment with clinical benefit.[6] Yet, the therapeutic window of only 4.5 hours and other contraindications [6,7] limit the number of eligible patients to less than 15% of all affected individuals.[8-14] After acute treatment, multiple approaches such as anti-platelet drugs, statins, and anticoagulants are available to reduce recurrent ischemic events. Nevertheless, the overall prognosis of stroke patients remains poor and stresses the urgent need for novel therapeutic options.[15]

1. Inflammation cascade in ischemic stroke

Cerebral ischemia initiates metabolic, neurologic, and immunologic reactions that subsequently cause irreversible tissue injury within minutes after its onset.[16] Successful restoration of cerebral blood flow to limit brain injury causes reperfusion damage. Besides activation of transcriptional processes and programmed cell death, this also causes the no-reflow phenomenon. In essence, this refers to the observation that recanalization of a large cerebral blood vessel does not necessarily restore perfusion to the microvasculature, thereby hindering recovery after stroke.[17] At the same time, stroke elicits a strong inflammatory response from acute vascular events to parenchymal processes. Thereby, the immunologically privileged brain tissue becomes prone to local and peripheral production of various mediators such as cytokines, chemokines, reactive oxygen species, and secondary messengers by resident inflammatory brain cells (microglia), endothelial cells, and lymphoid organs. These elements contribute to blood-brain barrier (BBB) damage and enable peripheral immune cells to invade the brain parenchyma.[18,19] The breakdown of the BBB further allows locally generated inflammatory mediators to enter the systemic circulation, thereby inducing a systemic immune response that manifests itself in peripheral immunodepression resulting in pulmonary, urinary, cardiovascular, gastrointestinal, musculoskeletal, and endocrine system dysfunction.[20-22] In essence, intravascular and parenchymal immune components communicate with each other to promote the inflammatory response contributing to the local and systemic stroke pathology promoting mortality and long-term disability. Therefore, neuroinflammation has been identified as a major pathomechanism contributing to brain injury besides its beneficial effect of restoring tissue homeostasis following an ischemic stroke. Thus, it appears that there is a driving need to fill the knowledge gaps regarding the inflammatory response and consider bidirectional interactions between the brain and the rest of the body after stroke to develop effective immunomodulatory therapeutic strategies beyond the restoration of blood flow to the brain.[23,24]

1.1 Intravascular events initiating inflammation after stroke

Immediately after arterial occlusion, inflammatory signaling begins in the vascular compartment. Inflammation induces the recruitment of leukocytes from the circulation to the wall of post-capillary cerebral venules.[23] This process consists of three significant, fine-regulated steps, namely, rolling, adhesion, and transmigration. All these steps are mediated by the expression of adhesion molecules located on the cerebral endothelium.[25]

Rolling, the initial step of the leukocyte adhesion cascade, is mediated by transmembrane glycoproteins known as selectins. The selectin family consists of three members, namely L- (leukocyte), P- (platelet), and E- (endothelial) selectin. In response to an ischemic insult, P-selectin appears to be the leading player in the rolling step since it is stored in Weibel-Palade bodies in the cytoplasm of endothelial cells (and platelets) and can be immediately translocated to the endothelial membrane. Once E-selectin is expressed and translocates to the luminal surface of endothelial cells, both selectins interact with carbohydrate (sialyl Le^X) moieties or P-selectin glycoprotein ligand-1 (PSGL-1) on circulating immune cells. This low-affinity interaction is easily disrupted by shear stress resulting in repetitive detachment, binding, and rolling leukocytes along the endothelial surface.[26-28] Several studies demonstrated the involvement of P-selectin release and E-selectin upregulation along with an increased inflammatory response to be involved in ischemic brain injury.[29,30]

Adhesion is initiated by the interaction between ß2-integrins on leukocytes and immunoglobulin superfamily proteins on endothelial cells. Integrins are heterodimeric transmembrane glycoproteins consisting of an α- and a β-subunit. The most prominent members of the integrin family are lymphocyte function-associated antigen 1 (LFA-1: CD18/CD11a), macrophage-1 antigen (Mac-1: CD18/CD11b) and very late antigen-4 (VLA-4: CD49d/CD29).[28,31,32] Evaluation of post-ischemic animal brains and blood samples from stroke patients showed an accumulation of LFA-1- and Mac-1-expressing leukocytes on the endothelium of cerebral venules.[33-35] Endothelial cell-derived chemokines bind to chemokine receptors on rolling leukocytes, thereby initiating clustering and activation of integrins through a conformational change, allowing them to bind their ligands on the endothelial surface.[36] The most important integrin ligands on the vascular endothelium are intercellular adhesion molecule 1 (ICAM-1), the counterpart for LFA-1 and Mac-1, and vascular cell adhesion molecule 1 (VCAM-1), the binding partner of VLA-4. ICAM-1 and VCAM-1 have been documented to be increased in the human and animal vasculature, blood, and cortico-spinal fluid after stroke, and expression was shown to correlate with the severity of neurological deficits.[37,38]

Transmigration is the last step in the leukocyte recruitment cascade and may occur either between adjacent endothelial cells (paracellular) or through endothelial cells (transcellular). Tight junctions (cadherins, junctional adhesion molecule (JAM) family, occludin, and claudins) which connect adjacent endothelial cells and form the BBB are believed to regulate transendothelial migration of leukocytes.[38,39]

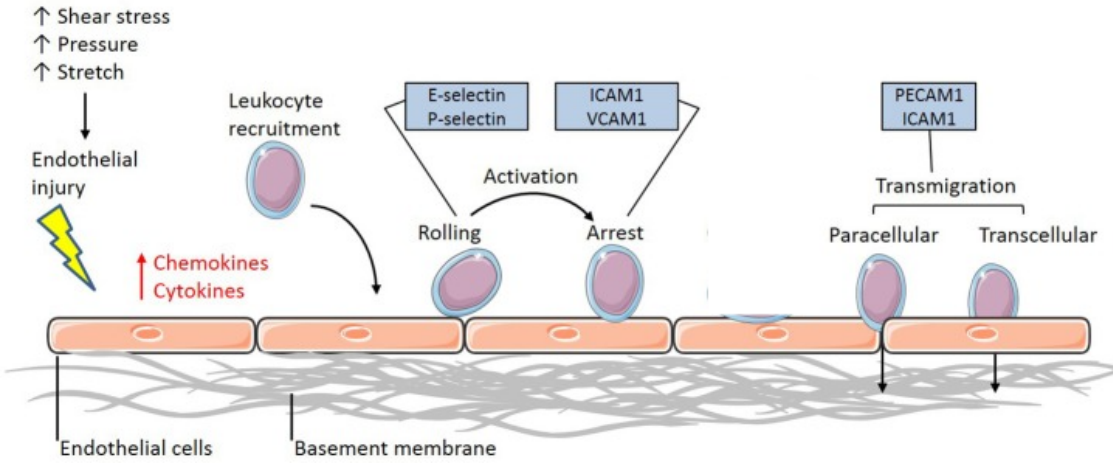

Figure 2: Leukocyte recruitment cascade. At sites of inflammation, cytokines activate endothelial cells to produce selectins, integrin ligands, and chemokines. This process results in rolling, adhesion, and transmigration of leukocytes. (adapted from Shiata et al. 2016)

In addition to the vascular route, some leukocyte populations, e.g., lymphocytes, may enter the central nervous system (CNS) by alternative ways, such as the choroid plexus (blood-CSF-barrier) or the meninges (blood-meningeal barrier).[41-43]

1.2 Cerebral leukocyte migration time course after stroke

Peripheral immune cells invade the tissue through the aforementioned sequential steps via different routes upon inflammatory stimuli. Moreover, brain invasion occurs in an orchestrated manner following various stages of stroke progression, namely, acute, sub-acute, and chronic phases. [44-47] These stages are discussed in detail in the following sections.

Immune response in the acute phase

The acute phase of cerebral ischemia starts within minutes after the occlusion. In this period, resident phagocytic cells clear dead cells. The innate immune system, rapidly activated due to its low-affinity interactions, allows neutrophils and monocytes/macrophages to invade the tissue.[25]

Neutrophils

Early adhesion following reperfusion is attributed to blood-borne neutrophils that arrive at the injury site within the first hour after cerebral ischemia.[48] However, up to now, there is no direct

evidence that neutrophils invade the ischemic tissue before the onset of neuronal death.[45] In fact, neutrophils have been shown to exert their effects already by interacting with the vessel wall. Further, neutrophils are involved in the no-reflow phenomenon by plugging capillaries.[49]

Neutrophils have also been localized in perivascular areas and leptomeningeal spaces in the ischemic rodent brain.[50] A massive accumulation of neutrophils in the perivascular spaces following experimental stroke has been observed.[51] On the other hand, neutrophils remain in the tissue over a month after stroke. However, their presence is masked after three days due to the over-activation of microglia/macrophages in the inflammatory area.[48] This has been confirmed by analyzing postmortem brain samples of ischemic stroke patients in which neutrophils could be found in the leptomeninges and perivascular spaces but scarcely in the infarcted parenchyma. [52] Very recently, an elegant study using microcatheter aspiration to collect blood during the acute occlusion phase investigated a high elevation of neutrophils distal to the clot.[53] Furthermore, an increase in circulating blood neutrophils was seen at six hours and continues to be present up to 72 hours in stroke patients.[54,55] Patient studies indicated a negative correlation between high neutrophil count in the blood and infarct volume.[56] Furthermore, clinical studies suggested that the neutrophil/lymphocyte ratio appears to be a prognostic marker in stroke patients.[57] This is important because neutrophils pave the way for further immune cell migration to the brain by releasing cytokines/chemokines, proteolytic enzymes that obstruct endothelial cells, and extracellular matrix. Besides, they secrete neutrophil extracellular traps (NETs) containing DNA, histones, and proteolytic enzymes that activate platelets and contribute to the thrombotic process, which also increased in patients with stroke.[52]

Monocyte/ Macrophage

Peripheral monocytes, which can maturate to macrophages, are also attracted to the injured brain tissue within the first 24 hours post-ischemia, where they persist for weeks.[55,58-60] Based on similar morphology and gene expression, it is challenging to differentiate invading monocytes from brain resident microglia. However, with evolving techniques, peripheral monocytes could be shown to infiltrate the ischemic brain to potentiate stroke damage by acquiring morphological and functional properties of tissue macrophages.[60] Around two hours following ischemia, blood-borne and activated brain resident macrophages can be detected in the brain and remain detectable for up to one week.[61] Depending on the tissue environment, macrophages either have a pro- or anti-inflammatory phenotype. Investigation of human ischemic infarcts led to the result that macrophages initially showed pro-inflammatory properties that switched to an anti-inflammatory feature with the maturation of the lesion.[62]

Immune response in the sub-acute/chronic phase

The inflammatory response following cerebral ischemia continues for days to a month after the insult.[47] During this sub-acute/chronic phase, the adaptive immune system, which is based on specific antigen recognition by lymphocytes and antigen-presenting cells, is dominant in this late stage.[23]

Dendritic cells (DCs)

DCs build the bridge between innate and adaptive immunity due to their crucial antigen-presentation capability and importance in facilitating a T-cell response. In rodent models of acute cerebral injury, an increasing number of infiltrating DCs into the brain was determined.[63,64] In a murine stroke model, DCs accumulated as early as 24 hours post-stroke in the border region of the infarct and were identified as brain resident DCs. In contrast, peripheral DCs populated the infarct core starting 72 hours after the insult.[64] Patients showed a decrease in circulating DCs post-stroke that normalized within a few days. Computer tomography scans show a correlation of low DC levels in the circulation with larger infarct size. This was further supported by analysis of post-mortem brain tissue where patients with more significant infarct sizes had more DC-T-cell clusters located near intracerebral vessels, suggesting that upon cerebral injury, DCs rapidly infiltrate the CNS to interact with other immune cells.[65]

Lymphocytes

The adaptive immune response is based on lymphocytes, classified into T-cells, B-cells, and natural killer cells (NK).[25]

T-cells play a crucial role in amplifying inflammation in the later stages after ischemia. Their numbers increase three days after stroke onset, with a peak around one week after that and a decline in the later stages.[66] First, cytotoxic T-cells ($CD8^+$) are recruited, followed by $CD4^+$ T-cells and NK cells.[67] T-cells have been found to infiltrate the ischemic lesion from pial and cortical vessels and through the choroid plexus.[67-69] Cytotoxic T-cells were observed in human ischemic infarcts, and increased T-cell counts in the blood were reported to be associated with stroke severity. Overall, evidence supports that T-cells exert adaptive functions that could affect stroke outcomes in the long term.[62,70]

B cells are thought to have a protective role following stroke. Animal studies investigated larger infarct volumes, worse functional outcomes, and higher mortality if B-cells were deleted.[71,72] On the contrary, other studies failed to show improvements or neuroprotection and even suggest that B cells have harmful effects in post-stroke recovery.[73,74] Furthermore, aggregation of B cell and

immunoglobulin synthesis in the infarct region four to seven weeks post-stroke correlated with cognitive deficits.[75] The synthesis of immunoglobulin was also detected in the cerebrospinal fluid of stroke patients for months.[76] As opposed to the beneficial role of B-cells for neuroprotection, these cells may play a detrimental role in post-stroke long-term cognitive impairment. However, further studies are needed to clarify their role in ischemic stroke.[75]

In the ischemic brain, NK lymphocytes show a rapid and transient increase.[55] There are conflicting reports regarding their post-stroke effects. One study showed no benefit of depleting NK cells in a murine stroke model, whereas another suggested a pathogenic action promoting inflammation and neuronal cytotoxicity.[77,78] This was seen in ischemic human and mouse brain tissue where NK cell numbers peaked three hours following stroke and then declined.[78] Nicotinic acetylcholine receptors were involved in the NK cell decline. Interference with the receptor had no impact on the lesion size but increased systemic interferon γ, protecting from bacterial infection and enhancing post-stroke survival. However, more studies are required to better understand and validate the pathogenic role of NK cells in ischemic stroke.[79]

Taken together, there is general agreement that leukocytes accumulate in the brain following an ischemic insult in a time-dependent manner. However, the role of leukocytes in tissue damage is still unclear. In most of the studies mentioned above, the leukocyte accumulation after stroke was studied using static, histopathological techniques that restrict the knowledge about this dynamic process. [45,51,80] Furthermore, the time point in most concepts was chosen unfavorable either too early, when the neuronal injury was not yet present, or later after the ischemic injury had occurred.[49,81] A recent study of our group showed that leukocytes start to invade the ischemic tissue around three hours after the onset of neuronal cell death already occurred. Hence, the late and low numbers of leukocytes can only be responsible for the ischemic injury to a certain extend. In the same study hindering leukocyte adhesion to pial venules increased the number of surviving neurons. Suggesting that already the interaction of leukocytes with the endothelium triggers post-ischemic neuronal cell death. These investigations further underpin the important role of immune cells in tissue damage after stroke and provide new insights into the underlying mechanisms, especially in the spatial-temporal relationship of leukocyte invasion and neuronal loss. Hence, it is crucial to limit immune-mediated injury to minimize long-lasting damages.

1.3 Parenchymal events contributing to inflammation after stroke

Acute intravascular events, as described previously, are not the only inflammatory events occurring after stroke. Hypoperfused brain areas face an energy failure due to continuous consumption of adenosine triphosphate (ATP).[82,83] The subsequent dysfunction of ATP-dependent

ionic pumps, mainly Na^+/K^+ ATPase, lead to the breakdown of the membrane potential and excessive release of the neurotransmitter glutamate.[84,85] This leads to the activation of ionotropic glutamate receptors (NMDA and AMPA) that triggers further Ca^{2+} influx to the cell and causes activation of cell death signaling, a process called excitotoxicity.[86-88] Eventually, neuronal necrosis and apoptosis are initiated by activating catabolic proteases, lipases, nucleases, and oxidative and nitrosative cascades.[86,89] Excitotoxicity is further potentiated by the impaired glutamate uptake by astrocytes. [86-88] Injured cells start releasing danger-associated molecular patterns (DAMPs).[90,91] These comprise a pretty diverse group of dis-compartmentalized molecules of different origin such as mitochondrial DNA (mtDNA) and ATP, heat shock proteins, intracellular DNA binding protein (HMGB1= high-mobility group protein1), β-amyloid (Aβ), histones, and uric acid.[92-95] In this way, "danger signals" immediately activate astrocytes and microglia/macrophages via their interaction with toll-like receptors (TLRs) to prompt the production and release of pro-inflammatory mediators.[96-98] These include pro-inflammatory mediators such as interleukin-1ß (IL-1ß), interleukin-6 (IL-6), tumor necrosis factor-α (TNF-α). [99-102] Microglia change their phenotype from a resting to a phagocytic state and secrete IL-1β, TNF-α, and IL-6 that further promote astrocyte and endothelial cell (EC) activation, which contributes to endothelial adhesion molecule expression and BBB damage and further facilitate the trans-endothelial migration of leukocytes into the ischemic area. [99-103]

1.4 Immunomodulatory treatments after stroke

Promising results in experimental studies lead to the development of immunomodulatory therapies, e.g., by inhibiting microglia activation, blocking cytokine receptors, or preventing leukocyte migration, which was evaluated in clinical trials.[104]

Therapeutic strategies targeting cytokine receptor

Several clinical trials tested the effectiveness of a recombinant IL-1 receptor antagonist (Anakinra) after ischemic stroke. The idea was to prevent IL-1 from binding to its receptor, thereby inhibiting the activation of intracellular inflammatory signaling pathways. The intravenous administration of this drug upon hospital arrival had a good safety profile and showed beneficial effects three months after stroke.[105] Changes in the administration to a subcutaneous injection lowered circulating pro-inflammatory molecules associated with a worse outcome in stroke. However, no significant reduction in disability level could be detected compared to placebo three and six months after stroke. The potential positive effects are proposed to be masked by a negative interaction of IL-1 receptor antagonist and tPA, which needs further investigation. [106]

Therapeutic strategies targeting activated microglia

Another neuroprotective compound tested in preclinical stroke models is the tetracycline antibiotic Minocycline. Minocycline has anti-inflammatory properties and additionally hinders microglia activation. A small human study confirmed the safety of intravenous drug application within 24 hours of stroke onset. However, it did not elicit any favorable effects on infarct size or functional outcome.[107,108]

Therapeutic strategies targeting leukocyte-endothelial interaction (LEI)

Several approaches have been followed to avoid the invasion of peripheral immune cells into the brain tissue by either targeting molecules on leukocytes or endothelial cells.

Natalizumab is a humanized antibody targeting a binding protein on leukocytes (VLA-4) thereby, hindering their interaction with endothelial cells. Natalizumab has already been successfully used in multiple sclerosis (MS) with efficacious reduction of inflammation and was repurposed for treating stroke (ACTION trial). No effects on infarct volume were observed, although improvements in functional outcome were shown, leading to further investigations. However, the follow-up phase did not meet the primary endpoint, and results are still awaited.[109,110]

A further approach was to target integrins. Two clinical trials (HALT and ASTIN) had been carried out targeting the CD11b/CD18 (LFA-1) antigen or CD18 alone; however, they were stopped due to missed primary endpoints.[111,112]

Another focus has been on targeting molecules on vascular endothelial cells to prevent leukocytes-endothelia interaction. Enlimomab, a murine antibody, targets ICAM-1. Preclinical studies indicated its beneficial role in post-ischemic brain damage. Patients were treated intravenously within six hours after stroke onset for five days in the clinical setting. However, Enlimomab showed more adverse effects than the placebo group. Therefore, the study was terminated prematurely.[113]

To tackle the infiltration of lymphocytes in the chronic phase, a strategy to avoid the egress of lymphocytes from lymph nodes was tested via the application of Fingolimod (sphingosine-1-phosphate receptor agonist). Experimental stroke models that presented a decrease in infarct size accompanied by improvements in neurological deficits led to clinical studies.[114] There, the oral application within 72 hours after stroke onset decreased microvascular permeability, reduced neurological deficits, and increased recovery. So overall, Fingolimod reduced secondary tissue

injury. In combination with alteplase, it even reduced circulating lymphocytes. Still, further large-scale clinical trials are required for this compelling inflammation-modulating strategy.[115]

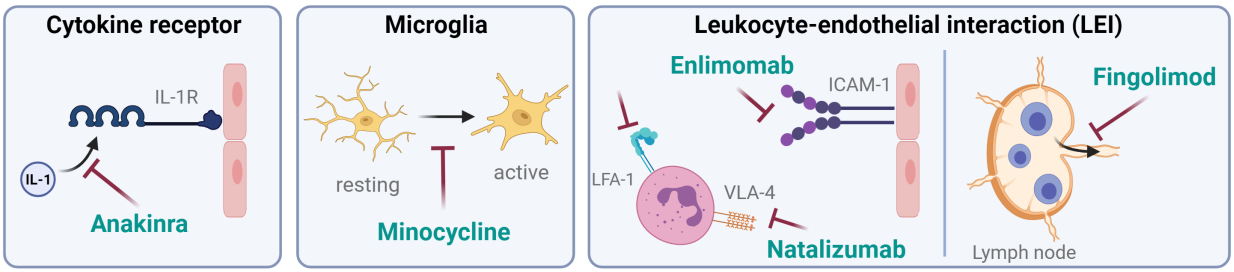

Figure 3: Overview of immunomodulatory strategies after stroke evaluated in clinical trials. Experimental studies identified a variety of different targets to reduce inflammation after stroke. Promising approaches are the inhibition of cytokine receptors (Anakinra), blocking microglia activation (Minocycline), or preventing leukocyte migration (Enlimomab, Natalizumab, Fingolimod). (created with BioRender.com)

Translational setbacks of anti-inflammatory procedures

There are multifactorial reasons for the failure of translating immunomodulatory therapies into clinical application. The discrepancies between human pathophysiology and experimental stroke models represent one of the main issues. Other reasons might include poorly designed preclinical trials with, for instance, irrelevant therapeutic windows or underpowered clinical trials.[116] To this end, the complexity and variability of the immunological response in human stroke should also not be disregarded. Neuroinflammation does not only have detrimental effects but is also important for healing and repair and thereby restoring tissue integrity via clearance of tissue debris and production of anti-inflammatory molecules. Through immunomodulatory therapies, the beneficial characteristics of the inflammatory response are also inhibited, which might also affect the clinical translation.[117] Despite the translational drawbacks of anti-inflammatory treatments after stroke, the promising experimental results indicate that implementing new strategies is most needed and promising. Therefore, a better understanding of the inflammatory process following an ischemic insult might help develop a local anti-inflammatory drug that only acts on the detrimental effects of the inflammatory cascade without inhibiting the regenerative process and further improves the microcirculatory flow by preventing endothelial dysfunction.[104] An alternative approach might be the local restoring of endogenous molecules with well-validated physiological roles and moderate the inflammation processes. One of these molecules is nitric oxide which has multiple functions in the body clarified in the following chapter. On one side, it regulates the endothelial function, and on the other side, it has anti-adhesive roles in the vasculature. Therefore, NO is a potential molecule maintaining an anti-inflammatory state after stroke by carrying these dual actions.[118]

2. Nitric oxide as a potential anti-inflammatory approach for stroke

Two and a half centuries ago, Joseph Priestly first identified nitric oxide (NO) as a gas consisting of one oxygen and one nitrogen atom.[119] Another two hundred years passed until researchers described endothelium-derived relaxing factor (EDFR) as an indispensable molecule for the vasodilation of blood vessels. Further research demonstrated that NO was, in fact, EDRF, and these findings were awarded with the Nobel Prize for Medicine or Physiology in 1998.[120,121] Up to now, many studies have revealed a wide range of key roles of NO in so many regulatory pathways in the body ranging from controlling cell homeostasis to regulating neural, endothelial or immune processes. Especially its known vascular cytoprotective actions such as vasodilation, anti-thrombotic, and anti-inflammatory effects make NO a unique molecule with a potential for therapeutic interventions in ischemic diseases such as stroke. [122-124]

2.1 Biological synthesis of NO

NO is synthesized in nearly all cell types in the human body by the enzyme nitric oxide synthase (NOS). The NOS family includes three isoforms, namely endothelial (eNOS), neuronal (nNOS), and inducible nitric oxide synthase (iNOS).[125-127] This homodimeric protein has an oxygenase domain (place of NO production) and a reductase domain (provides necessary electrons) linked via a calmodulin (CaM) binding region. CaM is a messenger protein that is activated by the binding of calcium. Once activated and bound, it causes a conformational change, thereby enabling a close contact of the two domains of NOS, an essential electron transfer process. The amino acid L-arginine and oxygen serve as a substrate and are further converted into citrulline and NO. At the reductase domain, the cofactor nicotinamide adenine dinucleotide phosphate (NADPH) donates electrons shuttled via two other cofactors (FAD and FMN) to the heme group of the oxygenase domain. The iron ion within the heme group is reduced, driving the reaction in the oxygenase domain.[128,129] Despite their homology in structure and function, nNOS and eNOS show Ca^{2+} CaM-dependent activity, unlike iNOS, which has CaM permanently bound and, therefore, is under transcriptional control.[130]

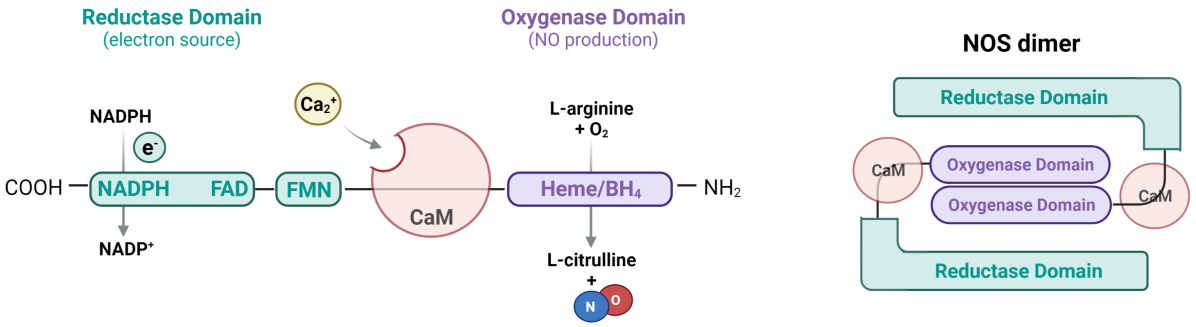

Figure 4: Nitric oxide synthase simplified structure (left) and the active homodimeric NOS protein (right). Each NOS protein monomer consists of two domains, a reductase domain (green) that provides the electrons, linked via calmodulin (CaM) binding region to the oxygenase domain (purple), which generates nitric oxide. Upon activation of CaM via binding of calcium, NOS dimer undergoes a conformational change to transfer the electrons necessary to drive the reaction to produce nitric oxide. (created with BioRender.com)

As the name suggests, endothelial NOS is constitutively expressed by the vascular endothelium.[131] Over time, eNOS was found in other cell types, such as neuronal cells, astrocytes, lymphocytes, bone marrow cells, and dermal fibroblasts.[132-136] The activity of eNOS is not only regulated via reversible Ca^{2+} CaM-binding but can also be activated through heat shock protein 90 (hsp90) that serves as an allosteric modulator.[137-139] The fraction of eNOS localized in caveolae (lipid-rich flask-shaped structures) is coupled to caveolin-1 (caveolae coat protein) that inhibits eNOS activity which can be dissolved via the recruitment of CaM or hsp90.[140,141] Moreover, shear stress, estrogen, vascular endothelial growth factor (VEGF), insulin or bradykinin can activate eNOS. Different residues (serine, threonine, and tyrosine) at variable positions within the synthase are phosphorylated via various kinases (protein kinase A (PKA), Akt, AMP-activated protein kinase (AMPK), CaM-dependent protein kinase II (CaMKII)) depending on the stimuli.[142-144]

Neuronal NOS is constitutively expressed in developing as well as mature neurons.[145] Like eNOS, nNOS is activated via reversible Ca^{2+}-CaM interaction. Upon glutamate receptor stimulation, calcium influx increases in neurons, thus activating nNOS and resulting in the production of nitric oxide or, in the absence of the substrate L-arginine, of superoxide (O_2^-).[146] Regulation can also be performed at the post-translational level through kinases (protein kinase A or C (PKA/PKC), CaM-dependent kinases) that phosphorylate neuronal NOS.[126,145,147]

Inducible NOS is not present under physiological conditions. Inflammatory stimuli (lipopolysaccharide (LPS), interferon-γ (INFγ), IL-1β, TNF- α) activate transcription factors (nuclear factor kappa B (NF-κB) and JAK/STAT pathway) that induce iNOS expression in any cell and tissue.[142,148] However, primarily upregulation of iNOS occurs in macrophages.[149-151] Macrophage-derived NO is essential for the immune response of T- and B-cells and myeloid-derived suppressor

cells. The permanently tight connection to CaM allows iNOS to be activated independently from calcium levels or phosphorylation.

Although NOS is the primary source of NO production, NO can also be synthesized by other mechanisms. One example is the generation of NO via nitrite (NO_2^-) reduction. In mammals, nitrite can derive from endogenous NO, dietary sources or are generated from commensal bacteria in the digestive system by nitrate reduction.[152,153] Several pathways for the NO generation from nitrite have been described. Acidic reduction of nitrite is most significant in the stomach due to the low pH and high nitrite concentrations. The evolving high NO levels eliminate bacteria, enhance mucus generation, and increase blood flow in the gastric mucosa.[154,155] The acid-catalyzed nitrite reduction to NO was shown to also take place in blood vessels.[156] Another NO production pathway is reducing nitrite or nitrate by the enzyme xanthine oxidase (XO).[157] XO-catalyzed NO production has mainly been observed under hypoxic and acidic conditions.[158] Several studies suggest that nitrite is recycled to bioactive NO through deoxyhemoglobin that enables NO generation in regions of poor oxygenation, whereas nitrate is the predominant reaction product under normoxia.[159]

2.2 Signaling pathway and physiology of NO

Nitric oxide signaling is mainly mediated through its primary receptor soluble guanylate cyclase (sGC) that produces the second messenger guanosine 3',5'-cyclic monophosphate (cGMP). cGMP regulates smooth muscle relaxation, blood pressure regulation, leukocyte recruitment, platelet aggregation, and neurotransmission.[160,161] The heterodimeric sGC consists of an α- and a β-subunit. The heme domain is located on both subunits, whereas only the β-subunit can bind NO and activate sGC. This leads to a conformational change enabling the generation of cGMP from guanosine 5'-triphosphate (GTP). The diverse physiological actions of cGMP are conveyed via the activation of several effector molecules: cGMP-dependent protein kinases, cGMP-gated ion channels, and cGMP-regulated phosphodiesterases. [162,163] Protein kinase G (PKG) regulates platelet activation/inhibition, cell growth, and differentiation, apoptosis, vascular smooth muscle relaxation/contraction, calcium signaling, and transcription events in a tissue-specific manner.[164] The binding of cGMP to cyclic nucleotide-gated channels leads to the exchange of non-selective cations. These are important in the signal transduction pathway of vision and olfaction. The various functions of cGMP signaling require continuous control of its intracellular concentration supervised by the enzyme superfamily of phosphodiesterase (PDE), cleaving the phosphodiester bond in cyclic nucleotides such as cGMP, thereby generating guanosine monophosphate (GMP).[165]

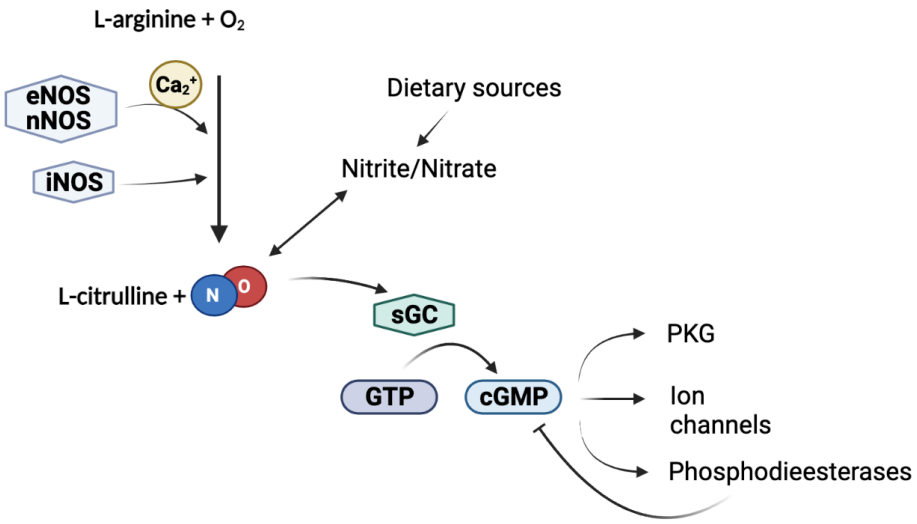

Figure 5: General overview of NO signaling pathway. Besides NOS as the primary source of NO, it can also be produced by dietary sources. Once generated, NO binds to its primary receptor soluble guanylate cyclase (sGC), generating the second messenger guanosine 3',5'-cyclic monophosphate (cGMP). Physiological actions are further conveyed by several effector molecules such as cGMP-dependent protein kinases (PKG), cGMP-gated ion channels, and cGMP-regulated phosphodiesterases (PDE) with different functions. (created with BioRender.com)

2.3 NO pathology in ischemic stroke

NO elicits neuroprotective and neurotoxic effects after an ischemic insult. NO's dual-action depends on the cellular compartment where NO is produced, its concentration, and when NO is active after stroke. The physiological concentration in the CNS derives from nNOS/eNOS activity, while iNOS is not expressed.[166] During ischemia, NO concentrations in the ischemic tissue decline due to oxygen deficiency. Shortly after the ischemic damage (acute phase), elevated levels of eNOS and nNOS activity related to the calcium overload could be detected to improve blood supply and limit the degree of damage, lasting from 30 minutes up to hours.[167,168] One hour after reperfusion, NO concentrations return to physiological levels.[168,169] Conversely, iNOS expression started 12 hours after ischemia and remained upregulated up to seven days after stroke, thus potentially contributing to the ischemic brain damage.[170] At this stage, microglia, astrocytes, endothelial cells, and infiltrated leukocytes upregulated iNOS and produced excess NO amounts.[166,171] As mentioned before, iNOS expression is transcriptionally regulated by inflammatory stimuli such as NF-κB, TNF-α, IL-1β, and oxidative radicals that are found to be increased in ischemic injury.[172] The pathological role of NO in cerebral ischemia was investigated in NOS knockout animals or by NOS overexpression via drug application. These experiments showed reduced neuronal death if mice lacked iNOS or nNOS, whereas deleting eNOS entailed an increase in dead neurons.[173-175] Ischemic lesions further showed reduced excitotoxicity, nitrosative stress, and superoxide production if nNOS was abolished.[167,176,177] Despite the neurotoxic effect of iNOS and nNOS in the acute phase after

experimental stroke, they have an essential role in promoting and attenuating neurogenesis in the chronic phase.[178-180] Additionally, mice deficient in the α-subunit of sGC showed a larger infarct size suggesting that cGMP generation is protective.[181]

2.4 Potential therapeutic applications restoring NO in stroke

Based on the evidence for NO-mediated neuroprotection post-stroke, several therapeutic strategies have been proposed to restore post-ischemic NO levels: direct administration of NO, application of NO donors or precursors, enhancing eNOS activity, and inhibition of iNOS.[182,183]

Stimulation of NO production via donors

In rats' injection of the NOS substrate, L-arginine following middle cerebral artery occlusion (MCAo) improved cerebral blood flow within the penumbra. It minimized the infarct size,[184]; however, clinical trials applying L-arginine to stroke patients failed to improve the outcome. The most likely cause of this translational failure was the fact that L-arginine reduced the systemic mean arterial blood pressure and thus cerebral blood flow to the ischemic penumbra.[182]

Nitric oxide donors (NOD) are a heterogeneous group of drugs able to release NO. Organic nitrates, S-nitrosothiols, sydnonimines, NONOates, and sodium nitroprusside are the most frequently studied substances in clinical and basic research. NODs reduced tissue injury and increased cerebral blood flow if administered soon after stroke induction in rodent models of cerebral ischemia.[185] In this category, the only successful application of an NOD without affecting the cerebral blood flow was the transdermal glyceryl trinitrate (nitroglycerin) administration. Clinically, transdermal nitroglycerin improved systemic blood flow. However, there was no effect on the size of the cerebral infarct (Efficacy of nitric oxide in stroke trial (ENOS), Rapid Intervention with GTN in Hypertensive stroke Trial (RIGHT), and RIGHT-2). [186]

Nitric oxide synthase modulators

An alternative strategy to manage the excessive production of NO in an ischemic insult represents the inhibition of NOS. Common inhibitors include Nω-nitro-l-arginine methyl ester hydrochloride (L-NAME). This non-selective inhibitor reduced the stroke volume in rodents in low dosages and a time window of nine hours after ischemia.[187] More selective approaches such as pharmacological inhibition of nNOS with 7-nitroimidazole given acutely after vessel occlusion decreased the infarct volume in a rodent stroke model.[188] Post-ischemic brain damage reduction was also achieved through selective iNOS inhibitors in animal models of stroke.[189] Long-term application of statins (HMG-CoA reductase inhibitors) induced eNOS upregulation, thus increasing NO bioavailability, saving brain tissue, and improving cerebral perfusion in ischemic stroke.[190]

However, patients treated with statins also were prone to post-stroke infections.[191] Downregulation of eNOS during and after ischemia has been related to the activation of Rho kinase (ROCK) in endothelial cells, rendering the kinase a potentially promising target.[192] ROCK inhibitors had neuroprotective effects in experimental stroke models but caused hypotension, a limiting factor in acute stroke treatment. Therefore, ROCK inhibitors selective for cerebral circulation are currently developed.[193]

Inhibition of cGMP degradation

Another target of the NO/cGMP signaling pathway is elevating cGMP levels in the ischemic brain. This can be achieved by phosphodiesterases inhibitors that prevent the cleavage of cGMP. Despite the neuroprotective effects of PDE inhibitors, its clinical use is so far restricted to secondary prevention due to its well-known antiplatelet properties that possibly increase bleeding risk. The complications also arise due to the widespread distribution of PDE in the body and the reversibility of clinically used PDE inhibitor effects.[194]

As noted above, there are many promising strategies enabling NO's availability, however, with different problems in the acute phase of ischemia.

2.5 NO supplementation via inhalation

Initially, it was hypothesized that inhaled nitric oxide (iNO) was rapidly inactivated, thus restricting its vasodilatory effects to the lung without systemic effects. This led to the approval of iNO for the treatment of persistent pulmonary hypertension in adults and pulmonary vasoconstriction in preterm babies.[195] iNO was initially studied in the context of intensive care. Clinical studies showed the beneficial effects of iNO after traumatic brain injury by reducing intracranial pressure, increasing cerebral perfusion pressure, and reducing systemic inflammatory responses.[196-198] In parallel to the human data, experimental studies showed beneficial cerebrovascular effects of iNO. Kuebler et al. showed that increasing concentrations of iNO application in healthy pigs increased the cerebral blood volume without influencing CBF.[199] This insight of iNO led to various studies investigating its cerebrovascular effects in more detail in brain-related injuries. Inhaled NO physiologically dilated cerebral venules in mice, whereas iNO under ischemic stroke conditions caused arterial dilatation, thus reducing lesion size, improving CBF, and reducing neurological deficits. These effects of iNO were attributed to the improved collateral blood flow to the penumbra.[200] In a model of traumatic brain injury (TBI), iNO improved CBF and reduced intracranial pressure, lesion volume, and edema formation.[201] Further investigations showed that iNO prevents impairment of cerebral autoregulation and limits histopathological damage after TBI

through preservation of ion channel function via blocking signaling pathways.[202] In experimental subarachnoid hemorrhage (SAH), iNO reversed microvascular dysfunction and prevented the formation of microvasospasms.[203]

The anti-inflammatory effects of iNO are less well investigated. Studies showed that in a feline model of ischemic-reperfusion injury, iNO application possesses extra-pulmonary bioactivity in the mesenteric vasculature, preventing neutrophil adhesion.[204] NO inhalation inhibited myocardial injury in animals and patients, had anti-inflammatory effects in patients undergoing knee surgery, protected hepatocytes before liver transplantation, and inhibited the inflammatory response in the sepsis model.[205-208]

Taken together, the aforementioned studies depicted the importance of restoring NO levels to physiological levels in various diseases by using NO-based therapeutic approaches. However, using a molecule with a vast range of action brings unwanted systemic effects such as reduced blood pressure. Therefore, changes in the application route of NO, i.e., by inhalation, may offer new ways to recover NO levels only where it is necessary to regain homeostatic conditions.

3. Aim of the thesis

The current study aimed to investigate the anti-inflammatory effects of inhaled NO after experimental stroke. Special attention was given to how iNO is transported from the lung to the brain, whether iNO affects leukocyte-endothelial interactions after ischemic stroke, and to possible downstream signaling mechanisms of iNO.

II. Material and Methods

A detailed list of the used equipment, consumables, kits, chemicals/reagents, and software used in this study can be found in the appendix section.

1. Animals

Male C57BL/6 mice (6–8 weeks, weight 24–26 g; Charles River Laboratories, Wilmington, MA, USA) were used for the current study. Animals had free access to tap water and food. Animal experiments were conducted under institutional guidelines approved by the government of Upper Bavaria (license number 17-152).

2. Randomization

Animals were randomly assigned to the different experimental groups (sham, MCAo, and MCAo + inhaled nitric oxide (iNO)). To blind the researcher, data was renamed by an assistant before analysis with respect to the treatment groups.

3. Time course of acute cerebral ischemia experiments

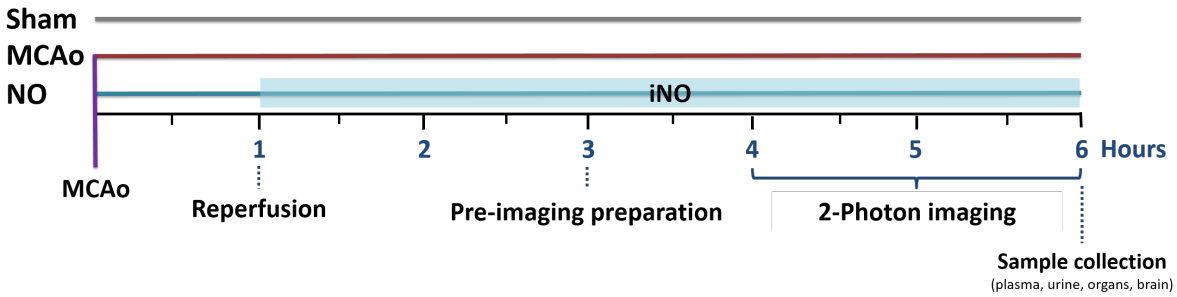

Figure 6: Experimental design of acute stroke

4. Transient focal cerebral ischemia

For postoperative analgesia, buprenorphine (0.1 mg/kg; Schering-Plough, Kenilworth, NJ, USA) was administered subcutaneously (s.c.) at least 30 minutes before surgery. The surgical procedure was carried out under isoflurane (Cp-pharma, Burgdorf, Germany) inhalation. For induction of anesthesia, a 5% (v/v) isoflurane/air mixture was introduced in a dark Plexiglas chamber for approx. 60 seconds until all motor reactions have ceased. During the surgical procedure (< 25 minutes), anesthesia was maintained with an isoflurane/air/oxygen mixture (ratio 2/60/50% (v/v)) using a nasal mask. Body temperature was maintained at 37.0 ± 0.1°C with a feed-back controlled heating pad (FHC, Bowdoinham, ME, USA).

For constant regional cerebral blood flow (rCBF) monitoring, the animal was placed on the abdomen, and a lateral, longitudinal 0.5 cm skin incision between the eye and ear was made to expose the temporal muscle. After loosening the base of the temporal muscle, a flexible laser Doppler probe (0.5 mm diameter; MT B500-0L240 Straight Microtip, Perimed, Järfälla, Sweden) was glued onto the exposed left parietal skull over the territory of the middle cerebral artery (MCA) for continuous monitoring of the regional cerebral blood flow with a Laser-Doppler fluxmeter (PeriFlux system 5000, Perimed, Järfälla, Sweden).

Focal cerebral ischemia was induced by occlusion of the MCA with a silicone-coated filament (0.19 mm diameter; Doccol Corporation, Sharon, MA, USA). To do so, the mouse was placed in a supine position, and a midline skin incision was made on the neck. Mandibular salivary glands were bluntly pushed laterally, and the proximal part of the common carotid artery (CCA) and the external carotid artery (ECA) were ligated distal to the carotid bifurcation. The distal internal carotid artery (ICA) was temporarily blocked with a microvascular clip (Fine Science Tools, Heidelberg, Germany), and the CCA was loosely wrapped with a silk thread (Fine Science Tools, Heidelberg, Germany). The filament was inserted into the vessel via an incision in the CCA and, after loosening the clip, advanced into the ICA until the rCBF measurement indicated the occlusion of the MCA. The filament was fixed in this position with the pre-knotted silk thread. In sham-operated animals, the filament was advanced as described above without vessel occlusion. After occlusion, the wound was temporarily sutured (Covidien, Dublin, Ireland). The animal was placed in a preheated recovery box (30°C; Peco Services Ltd, Brough, UK) and checked regularly for spontaneous breathing and motor activity.

To induce reperfusion, the animal was re-anesthetized after a neurological test (modified Bederson score [209]), and the wound was reopened. The filament was removed after 60 minutes, and the CCA was ligated distal to the incision, and the wound was closed subsequently. Finally, Carprofen (4mg/kg; Zoetis, Parsippany, NJ, USA) was injected s.c. for analgesia, and the animal was placed in the recovery box (30°C). During the wake-up phase (approx. two hours), the mouse was checked regularly for spontaneous breathing and motor activity.

For the rest of the observation period, the animals were returned to their cage, which was placed in a cabinet (Scanbur, Karlslunde, Denmark) with a temperature of 25-27°C for three days. For pain management, during the postoperative period, Carprofen (4 mg/kg) was injected s.c. with physiological saline (Berlin-Chemie AG, Berlin, Germany) as a liquid reservoir (1 mL) once daily. In addition, to ease food and water intake, mice received powdered food (Ssniff, Soest, Germany) and hydrogel (Clearh2o, Westbrook, ME, USA) placed on the cage floor for up to one week after surgery.

Weight development, general condition, and the degree of neurological impairment were assessed daily according to a score sheet and used as outcome parameters. Further, animals were tested for their neurological behavior, cranial nerve functions, motor and sensory deficits, and body coordination using the modified Bederson test (0-5 points).

5. Nitric Oxide (NO) inhalation

iNO treatment was given directly after reperfusion. The animals were placed in a custom-designed NO induction box (30x 17x 17 cm) depicted in Figure 4, which was placed in a heat-controlled incubator. The air inside the box was supplemented with 50 ppm NO (Linde, Dublin, Ireland) for two hours. NO, and nitrogen dioxide (NO_2) levels were constantly monitored with a multi-gas monitor device (Industrial Scientific, Pittsburgh, PA, USA). After two hours, animals were prepared for *in vivo* imaging. iNO supplementation was continued with an endotracheal tube during the preparation and imaging. In total, animals were treated with iNO for five hours.

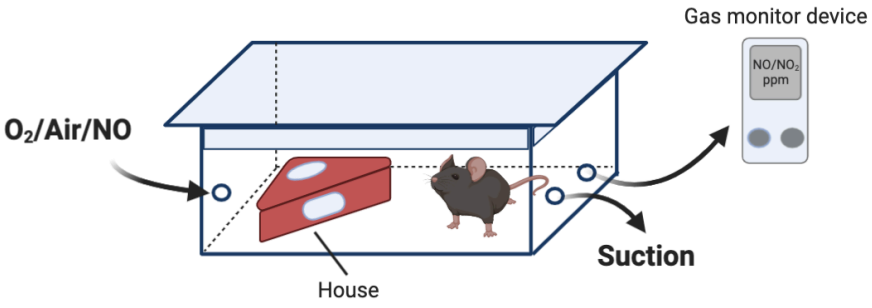

Figure 7: NO induction box (created with BioRender.com)

6. Intravital microscopy

Cranial window implantation

For induction of anesthesia, a 5% (v/v) isoflurane/air mixture was introduced to a dark Plexiglas chamber where the animal was placed for approx. 60 seconds until all motor reactions have ceased. Deep anesthesia for cranial window implantation and imaging was introduced by intraperitoneal (i.p.) injection of a combination of medetomidine (0.5 mg/kg), midazolam (5 mg/kg), and fentanyl (0.05 mg/kg) combination. Eye ointment (Bayer AG, Leverkusen, Germany) was applied to the cornea to prevent dehydration. Mice were intubated endotracheally (Vasofix® Safety (20G), B. Braun, Melsungen, Germany) and mechanically ventilated (MiniVent Type 845, Hugo Sachs Elektronik, March, Germany) with oxygen-enriched air (30/70% O_2/Air mixture). End-tidal carbon dioxide ($_{ET}CO_2$) was measured using a capnograph (Type 340, Hugo Sachs Elektronik, March, Germany) and kept constant between 20 and 30

mmHg. A feedback heating plate was used to maintain the body temperature of 37°C during anesthesia. Heart rate and peripheral oxygen saturation (pO_2) were monitored using a pulse oximeter (PhysioSuite PS-03, Kent Scientific, Torrington, CT, USA) attached to the hind paw. All physiological parameters were recorded with a Power lab system (AD Instruments, Sydney, Australia) and analyzed with LabChart software (Version 8; AD Instruments, Sydney, Australia). To maintain anesthesia, one-third of the initial dose was injected every hour.

The animal's head was fixed with a nose clip (David Kopf Instruments, Tujunga, CA, USA) on a custom-made imaging platform, and a midline incision was made on the scalp. After applying a local anesthetic (2% lidocaine, B. Braun, Melsungen, Germany), the periosteum was carefully removed. Next, a craniotomy (4x4 mm^2) was performed using a high-speed dental drill (Rewatronik, Wald-Michelbach, Germany), leaving the dura mater intact. Next, bleedings from bridging veins were stopped using a fibrin sealant patch (TachoSil, Takeda Pharmaceutical, Tokyo, Japan). Next, a cover glass (Warner Instruments, Holliston, MA, USA) with the exact size of the craniotomy was placed on top of the exposed dura mater and fixed with bone cement. Finally, a titanium ring was glued around the cover glass. The ring was used to fix the mouse head under the intravital microscope and to keep a pool of water between the cover glass and the water immersion objective (Plan Apochromat, NA 1.0; Zeiss, Oberkochen, Germany) used for *in vivo* imaging.

Catheterization

To allow the continuous measurement of arterial blood pressure and for the application of fluorescent dyes (fluorescein isothiocyanate (FITC) –dextran or Rhodamin6G; 0.5% (v/v) in PBS, Sigma-Aldrich, St. Louis, MO, USA), a catheter was inserted into the left femoral artery. The anesthetized mouse was placed in a supine position for the procedure, and one leg was stretched out to the side. An incision from the knee to the lateral abdomen exposed the femoral artery. The vessel was ligated distally and temporarily closed proximally with a vessel clip. A previously heparinized-saline (1%) polythene tube (Smiths Medical, Minneapolis, MN, USA) was inserted into the opened vessel and fixed with two silk threads. The wound and the catheter were fixed with cyanoacrylate adhesive (Drechseln und mehr, Weiden, Germany). The brain vasculature and circulating immune cells were stained by injection of 50 µL of the previously mentioned dyes before the imaging procedure. Shortly before finishing the experiment, a blood sample was taken from the femoral catheter to measure the blood gases (Blood gas analyzer Rapidlab 348, Siemens, Munich, Germany).

In vivo two-photon microscopy

Following cranial window implantation, the animal was transferred to a two-photon microscope (LSM 7 MP, Zeiss, Oberkochen, Germany) equipped with a Li:Ti laser Chameleon (Coherent, Santa Clara, CA, USA). A 20x water immersion objective (Zeiss, Oberkochen, Germany) was selected and dipped into the water pool depicted in Figure 5. The excitation wavelength was set to 840 nm, and a 500-550 nm band pass filter (green fluorescence) and a 565-610 nm band pass filter (red fluorescence) were used to detect fluorescence emission by GaAsP-NDD detectors.

Figure 8: Animal position under the two-photon microscope (created with BioRender.com)

Three regions of interest (ROI) were selected and imaged. ROIs were chosen to include the ischemic core, the penumbra, and the distal part of the ischemic core regions. Two main features of leukocyte behavior after inflammation, rolling, and adhesion were investigated three hours after reperfusion. To explore the rolling, time series over one minute with a size of 327 x 76.64 µm were recorded. To analyze the adhesion, Z-stacks with a size of 607.28 x 607.28 µm and a step distance of one micrometer were performed to a depth of 400 µm (Figure 9).

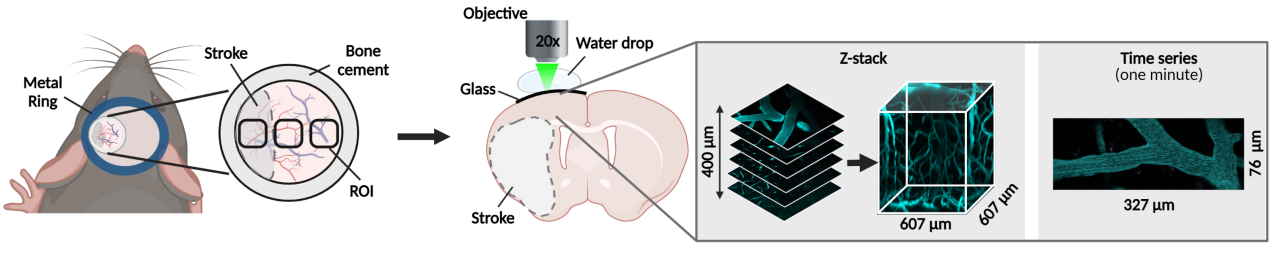

Figure 9: Region locations selected for Z-stack and time series via two-photon microscopy (created with BioRender.com)

The blood flow velocity was measured by line scanning, that is, by measuring the velocity of individual erythrocyte shadows traveling within the imaged vessel. For this purpose, randomly selected pial arterioles were rapidly scanned over a length of 20-50 µm along their longitudinal axis. The slope of each dark streak is inversely proportional to the speed of the erythrocyte. (Figure 10)

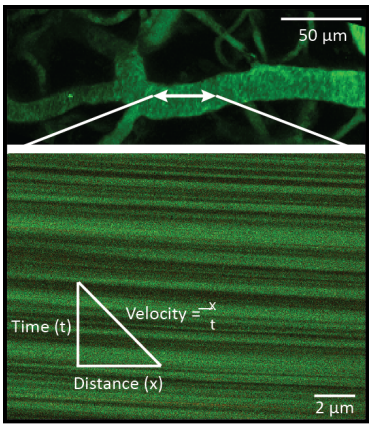

Figure 10: Line scan and velocity calculation image

Two-photon data quantification

To analyze rolling, time-series recordings (x: 390.35 µm, y: 91.49 µm) over one minute were acquired. Rhod6G$^+$ cells in venules were considered to roll if their speed was slower than the blood flow. For analyzing leukocyte adhesion, two Z-stack images with a depth of 400 µm from the same ROI were recorded five minutes apart and processed using Imaris software (Version 9.4, Bitplane AG, Zürich, Switzerland). The first stack was taken as a baseline, and adhered Rhod6G$^+$ cells were quantified in venules and capillaries.

Time series and Z-sacks were also used to assess the mean diameter of venules and capillaries. Three vessels were selected in each ROI, and the diameter was measured at five positions along the vessel with ImageJ (Version 1.53i, National Institute of Health, Bethesda, MD, USA).

Blood flow velocity was calculated by dividing the traveled distance of erythrocytes (µm) by the respective traveled time (msec.).

7. Sample collection

Animals were anesthetized with a mixture of medetomidine (1.5 mg/kg), midazolam (15 mg/kg), and fentanyl (0.15 mg/kg) as previously described. Urine was collected by aspiration directly from the bladder using a syringe with an injection needle (25G; B. Braun, Melsungen, Germany) after laparotomy. A thoracotomy was performed to collect blood samples using a syringe with an injection needle (25G) from the left ventricle before transcardial perfusion. The blood samples were collected in EDTA coated tubes (Sarstedt, Nümbrecht, Germany). Plasma was obtained by centrifugation of the collected blood samples at 13,000 x g for five minutes at 4°C. Immediately after

centrifugation, plasma was transferred into a new tube and snap-frozen until further use. For transcardial perfusion, a pressure perfusion system (Leica Biosystems, Wetzlar, Germany) was used. With a pressure of 125 mmHg, 4% paraformaldehyde (PFA) or saline was pumped through in two and a half minutes to wash out all blood cells and fix the tissue with consistency. Depending on the subsequent experiments, the tissues of interest were removed and stored at different temperatures (Table 1).

Table 1: Tissue storage conditions depending on the analysis

Tissue	Perfusion solution	Storage temperature	Analysis
Plasma	-	fresh	FACS
		-20°C	NO analysis, ELISA
Urine	-	-20°C	NO analysis
Lung	saline	-20°C	NO analysis, ELISA
Brain	PFA	4°C	Immunofluorescence (IF)
	saline	-20°C	NO analysis, ELISA, Gene expression analysis, Cresyl Violet staining
Isolated vessels	saline	4°C	Immunofluorescence
		-20°C	Protein expression analysis

8. Enzyme-linked immunosorbent assay (ELISA)

According to the respective manufacturers ' protocol, tissue cyclic GMP, IL-6, TNF-α, and MMP-9 concentrations were measured using commercially available ELISA kits (Table 2).

Table 2: ELISA kits

Product name	Catalog number	Company
Cyclic GMP Complete ELISA Kit	ab133052	Abcam (Cambridge, UK)
Mouse IL-6 ELISA Kit	ab222503	Abcam (Cambridge, UK)
Mouse TNF-α ELISA Kit	ab208348	Abcam (Cambridge, UK)
Mouse Total MMP-9	MMPT90	R & D Systems (Minneapolis, MN, USA)

Briefly, frozen brain and lung samples were weighed and homogenized in 10 volumes of 0.1 M hydrochloric acid (HCl) using a Precellys tissue homogenizer (Bertin Instruments, Montigny-le-Bretonneux, France). The homogenate was centrifuged at >600 x g for 10 minutes to pelletize the debris. Before the assay, the supernatant was diluted 5 to 10-fold with 0.1 M HCl.

The protein concentration of the tissue lysates was determined by the colorimetric bicinchoninic acid (BCA) assay (Thermo Fisher Scientific, Waltham, MA, USA). Bovine serum albumin (BSA) protein (Sigma-Aldrich, St. Louis, MO, USA) standards ranging from 20-2000 µg/mL in 0.1 M HCl were prepared. 25 µL protein sample and standard triplets were pipetted into a 96-flat bottom well plate (Thermo Fisher Scientific, Waltham, MA, USA). 200 µL of the working reagent (mixed according to the manufactures manual) was added to each well and incubated at 37°C for 30 minutes. The absorbance was measured with a plate reader (iMark Microplate Absorbance Reader, Bio-Rad Laboratories, Hercules, CA, USA) at a wavelength of 595 nm and used to calculate the protein concentration.

Standards and samples were added to the well plate and incubated at room temperature with gentle shaking as indicated in the respective manual. Once the standards and samples were discarded and the plate washed with the provided wash solution, the respective detection antibody was added to each well and incubated. After another washing step, the plate was incubated with HRP-streptavidin solution. Finally, a one-step substrate reagent was added, and after an incubation period, the stop solution was added before the measurement with a plate reader.

To quantify the concentration of the target molecule, the mean absorbance of each duplicate/triplet of the standards and samples were calculated, and the average blank absorbance value was subtracted. The sample concentration was determined from the standard curve and multiplied by the dilution factor.

9. Flow cytometry analysis

Myeloid cells population distribution

Blood samples were collected in EDTA tubes and diluted 1:1 with PBS. 1 µL of a CD16/CD32 monoclonal antibody mix (Thermo Fisher Scientific, Waltham, MA, USA) was added to block non-specific Fc domains to minimize false-positive results. 10 µL of the antibody master mix (

Table 3) was added to the sample and incubated for 30 minutes at 4°C. Samples were washed with 2 mL PBS and centrifuged at 500 x g for five minutes. Data were acquired using a BD FACSverse flow cytometer (Becton Dickinson, Franklin Lakes, NJ, USA) and analyzed using FlowJo software (v10.7, Becton Dickinson, Franklin Lakes, NJ, USA).

Table 3: Myeloid antibody panel

Antibody	Conjugate	Clone	Concentration	REF	Company
CD3	FITC	17A2	0.5 mg/ml	11-0032-82	Invitrogen (Waltham, MA, USA)
CD11b	PerCP-Cy5.5	M1/70	0.2 mg/ml	45-0112-82	Invitrogen (Waltham, MA, USA)
CD11c	BV510	HL3	0.2 mg/ml	562949	BD Horizon (Franklin Lakes, NJ, USA)
CD19	APC-Cy7	eBio1D3(1D3)	0.2 mg/ml	47-0193-82	Invitrogen (Waltham, MA, USA)
CD45	eFlour 450	30-F11	0.2 mg/ml	48-0451-82	Invitrogen (Waltham, MA, USA)
Ly6C	APC	HK1.4	0.2 mg/ml	17-5932-82	eBioscience (San Diego, CA, USA)
Ly6G(Gr-1)	PE-Cy7	RB6-8C5	0.2 mg/ml	25-5931-82	eBioscience (San Diego, CA, USA)
MHCII (I-A)	PE	NIMR-4	0.2 mg/ml	12-5322-81	eBioscience (San Diego, CA, USA)

-> Master Mix prepared in staining buffer

Adhesion molecule expression on myeloid cells

To exclude non-specific antibody binding, blood samples were stained with an isotype control master mix (Table 4).

Table 4: Isotype control antibody panel

Antibody	Conjugate	Clone	Concentration	REF	Company
Rat IgG2b	PE-CY7	RTK4530	0.2 mg/ml	400617	BioLegend (San Diego, CA, USA)
Rat IgG2c	PE-CY7	RTK4174	0.2 mg/ml	400721	BioLegend (San Diego, CA, USA)
rat IgG2a	PE-CY7	RTK2758	0.2 mg/ml	400521	BioLegend (San Diego, CA, USA)
Rat IgG1	PE	eBRG1	0.2 mg/mL	12-4301-81	Invitrogen (Waltham, MA, USA)
Rat IgG2b	FITC	RTK4530	0.5 mg/ml	400633	BioLegend (San Diego, CA, USA)
Rat IgG2a	PE/Cyanine5	RTK2758	0.2 mg/ml	400531	BioLegend (San Diego, CA, USA)
Rat IgG1	APC	eBRG1	0.2 mg/ml	17-4301-81	Invitrogen (Waltham, MA, USA)

-> Master Mix prepared in staining buffer

The blood samples were diluted 1:1 with PBS. 1 µL of a CD16/CD32 monoclonal antibody was added to block non-specific Fc domains to minimize false-positive results. Equal volumes of blood were distributed into four round-bottom tubes, and 10 µL of the target protein antibody master mix (

Table 5) was added for differentiating between immune cell populations. Sample tubes were incubated for 30 minutes at 4°C before data were acquired on a BD FACSverse flow cytometer. The samples were washed multiple times by adding 2 mL PBS and a centrifuging step at 500 x g for five minutes. Data were analyzed with FlowJo software (v10.7).

Table 5: Adhesion molecule antibody panel

	Antibody	Conjugate	Clone	Concentration	REF	Company
Every tube	CD45	eF450	30-F11	0.2 mg/ml	48-0451-82	Invitrogen (Waltham, MA, USA)
	CD11b	APC CY7	M1/70	0.2 mg/ml	101216	BioLegend (San Diego, CA, USA)
	PSGL-1	PE	4RA10	0.2 mg/mL	12-1621-82	Invitrogen (Waltham, MA, USA)
	CD49d	FITC	R1-2	0.5 mg/ml	103606	BioLegend (San Diego, CA, USA)
	L-selectin	Cy 5.5	MEL-14	0.2 mg/ml	104432	BioLegend (San Diego, CA, USA)
	CD18	APC	H155-78	0.2 mg/ml	141009	BioLegend (San Diego, CA, USA)
Individual tube	CD3	PE-CY7	17A2	0.2 mg/ml	100220	BioLegend (San Diego, CA, USA)
	CD19	PE-CY7	6D5	0.2 mg/ml	115520	BioLegend (San Diego, CA, USA)
	Ly6C	PE-CY7	HK1.4	0.2 mg/ml	128018	BioLegend (San Diego, CA, USA)
	Ly6G	PE-CY7	1A8-Ly6g	0.2 mg/ml	560601	BD Pharmingen (San Diego, CA, USA)

-> Master Mix prepared in staining buffer

10. Nitrite/Nitrate analysis

Sample preparation

Tissue samples (brain, lung) were weighed, and five volumes of PBS protease inhibitor solution was added (Table 6). Homogenization was carried out in soft tissue tubes (Bertin Instruments, Montigny-le-Bretonneux, France) with a tissue homogenizer followed by a centrifugation step at 10,000 x g for five minutes at 4°C.

To purify and concentrate the nitrite/nitrate amount, samples were cleaned with centrifugal concentrators (Sartorius, Göttingen, Germany). The concentrators were thoroughly cleaned before use, following the subsequent description. 200 µL of ultra-pure water was dispensed into each filter and centrifuged at 14,000 x g at room temperature for 10 minutes. This step was repeated once. Water was removed from the filters and tubes using a vacuum pump and kept in the fridge until further use.

400 µL tissue supernatant were transferred in previously cleaned concentrators and centrifuged for 90 minutes at 14,000 x g at 4°C. Plasma samples were also centrifuged through the filters with the same speed but only for 60 minutes. The eluate was stored at -80°C until further use. Urine samples were used without prior processing steps.

Table 6: Protease inhibitor composition

Inhibitor	Final conc.	Catalog number	Company
Benzamidine	1 mg/L (5.7 µM)	#B6506	Sigma-Aldrich, St. Louis, MO, USA
Antipain	1 mg/L (1.5 µM)	#A6191	
Aprotinin	1 mg/L	#A1153	
Leupeptin	2 mg/L (4.2 µM)	#L0649	
Pepstatin A	1 µM	#P-5318	
AEBSF	400 µM	#76307	

Chemiluminescence assay

To measure the nitrite/nitrate amount in liquid samples, the nitric oxide analyzer (NOA 280i, Analytix, Boldon, UK) was used. The device uses a gas-phase chemiluminescent reaction between nitric oxide and ozone (O_3). The apparatus was set up according to the manufacture's manual (Figure 11).

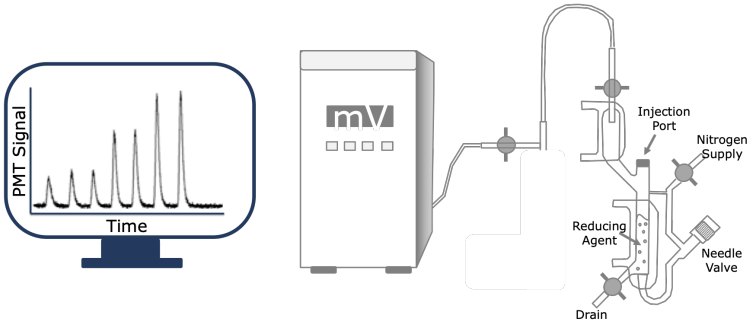

Figure 11: Nitrite measurement setup

Nitrite (NO_2) measurements were performed in a nitrite reduction solution (Table 7), necessary to convert nitrite to nitric oxide. A standard solution of 1 mM sodium nitrite was prepared for the measurements, and three dilutions of the standard (10 µM, 1 µM, 100 nM) were used for calibration.

Table 7: Nitrite reduction solution

	Volume
Potassium iodide (KI)	0.15 g
Ultra-pure water	1.5 mL
Acidic acid (100%)	13.5 mL

For measuring Nitrate (NO_3^-) in liquid samples, vanadium (III) chloride in hydrochloric acid was needed as a reducing solution to convert nitrate to nitric oxide (Table 8). To attain an efficient conversion, the reduction was carried out at 90°C. Therefore, the setup had to be changed slightly.

A gas bubbler with sodium hydroxide (1 M) was added between the purge vessel and the nitric oxide detector to prevent damage of the analyzer from the hydrochloric acid vapor (Figure 12).

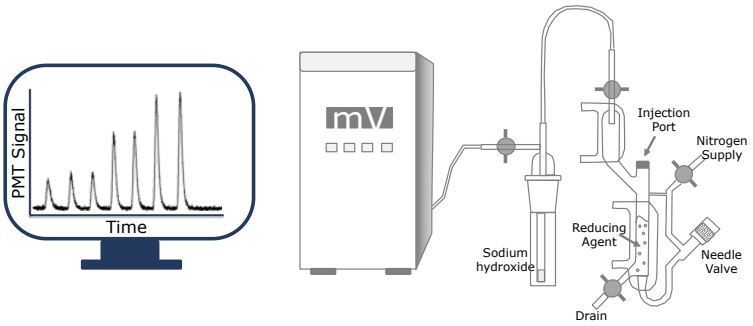

Figure 12: Nitrate measurement setup.

Before measuring the sample, a standard solution of 1 mM sodium nitrate was prepared, and three dilutions (100 µM, 10 µM, 1 µM) were used for a calibration curve**.**

Table 8: Nitrate reduction solution

	Volume
Vanadium chloride (VCl_3)	1 g
1M Hydrochloric acid (HCl)	100 mL
-> filter (0.2 µm); store at 4°C	

Data Quantification

Nitrite quantification values can be directly taken from the generated table by the NO analyzer software. To obtain nitrate values, the nitrite value has to be subtracted from nitrate values as measuring nitrate in this way gives nitrogen oxide values.

11. Gene expression analysis

Isolation of total RNA

Mouse brain hemispheres were separated, and RNA was extracted with 1 mL QIAzol Lysis Reagent (Qiagen, Hilden, Germany) added. For homogenization, one stainless steel bead (5 mm diameter, Qiagen, Hilden, Germany) was added to the tissue. The tube was placed into the TissueLyser (Qiagen, Hilden, Germany) for three minutes at 50 Hz and two minutes at 20 Hz. The homogenate was incubated for five minutes at room temperature. MaXtract high-density tubes (Qiagen, Hilden, Germany) were used to separate the aqueous RNA-containing phase, followed by a column purification with the RNeasy Mini kit (Qiagen, Hilden, Germany) according to the manufacturer´s protocol. Genomic DNA was removed by incubation with RNase-Free DNase (Qiagen, Hilden, Germany) directly on a column for 15

minutes. RNA quality and quantity were checked using the NanoDrop ND-1000 spectrophotometer (PEQLAB, Erlangen, Germany).

Reverse transcription-polymerase chain reaction (RT-PCR)

The Omniscript Reverse Transcription Kit Quick-Start (Qiagen, Hilden, Germany) was used for RNA transcription. For this purpose, 1 µg RNA was added to the master mix (Table 9). The synthesis was carried out at 37°C for one hour. The cDNA obtained was stored at -20°C.

Table 9: Master Mix components for cDNA synthesis

	Volume [µL]
10x Buffer RT	2
dNTP Mix (5 mM each dNTP)	2
Oligo dT primer (10 µM)	2
Omniscript Reverse Transcriptase	1

Quantitative real-time PCR (qRT-PCR)

The QuantiFast SYBR Green RT-PCR kit (Quanta, Hilden, Germany) was used for qRT-PCR. 2 µL cDNA (1:5 diluted in RNase-free H_2O) was supplemented with specific murine targeting primers (Table 11) and the gene expression master mix (Table 10). 12 µL sample of the mixture was transferred to a 96-well qRT plate and covered with an adhesive film. RNase-free water was used as a negative control. All samples were analyzed in triplets. The measurements were performed using a LightCycler 480 (Roche Life Science, Penzberg, Germany) and a standard program (Table 12). The mRNA levels were normalized by *Gapdh* as housekeeping gene and expressed as % contralateral hemisphere values calculated using the ΔΔCt-method.

Table 10: Master Mix components for quantitative real-time PCR

	Volume [µL]
2x QuantiFast SYBR Green RT-PCR Master Mix	6
Primer forward	0.24
Primer reverse	0.24
H_2O	3.52
cDNA	2

Table 11: List of primers for qRT-PCR

Target	Sequence 5' to 3'	Sequence 3' to 5'	Company
ICAM-1	CAA TTT CTC ATG CCG CAC AG	AGC TGG AAG ATC GAA AGT CCG	
VCAM-1	TCT TAC CTG TGC GCT GTG AC	ACT GGA TCT TCA GGG AAT GAG T	
E-selectin (CD62E)	CCG TCC CTT GGT AGT TGC A	CAA GTA GAG CAA TGA GGA CGA TGT	
Gapdh	ATT GTC AGC AAT GCA TCC TG	ATG GAC TGT GGT CAT GAG CC	
IL-1β	AGT GAC GGA CCC CAA AAG	AGC TGG ATG CTC TCA TCA GG	
TNF-α	TCT TCT CAT TCC TGC TTG TGG	GGT CTG GGC CAT AGA ACT GA	
IL-6	GCT ACC AAA CTG GAT ATA ATC AGG A	CCA GG AGC TAT GGT ACT CCA GAA	
P-Selectin (CD62P)	GCC ATT CAG TGT GCT GAC TC	CGG AAA CTC TGG ACA TTG C	Metabion,
MMP-9	AGA CGA CAT AGA CGG CAT CC	TCG GCT GTG GTT CAG TTG T	Planegg,
sGCα	TCT CCC TGG TAT CAT TAA AGC GG	CAC AAA CTC GGT ACA GTC ACT TC	Germany
sGCβ	TGC TGG TGA TCC GCA ATT ATG	GGT TGA GGA CTT TGC TTG CAG	
PKGα	GAC AGC GAC CGT CAA GAC TC	GAG GAT TTC ATC AGG AAG GCT C	
PKGβ	ACC CTG CGG GAT TTA CAG TAT	CGT CCT TCT GAT CCA ACT CCA	
A20	AGT GTC CAG GCT TCC CTG G	GGC AGT TTC CAT CAC CAT TGG	
IκBα	ACG AGC AAA TGG TGA AGG AG	ATG ATT GCC AAG TGC AGG A	
eNOS	CGA AGC GTG TGA AGG CAA C	TTG TAC GGG CCT GAC ATT TCC	
nNOS	CTG GTG AAG GAA CGG GTC AG	CCG ATC ATT GAC GGC GAG AAT	

Table 12: Thermal cycling program conditions for qRT-PCR

	Temperature [°C]	Time	Repetitions
Stage 1	95	5 min.	1x
Stage 2	95	15 sec.	40x
	60	1 min.	

12. Cerebral vessel isolation

The murine cerebral vessel isolation was based on the previous protocol by Zellner et al. [210] Briefly, frozen brain hemispheres were used to isolate cerebral vessels of sham, MCAo, and iNO treated animals. First, tissue was cut into small pieces with a scalpel and transferred into a glass tissue grinder (DWK Life Sciences, Wertheim, Germany). After adding 15 mL cold minimum essential medium (MEM, Thermo Fisher Scientific, Waltham, MA, USA), homogenization was performed by 20-40 up and down strokes. Next, the homogenate was mixed with 30% (w/v) Ficoll/MEM solution to a final concentration of 15%, followed by a centrifugation step at 6,000 x g for 20 minutes at 4 °C. The supernatant was discarded, and the formed pellet was vigorously dissolved in 1% (w/v) bovine serum albumin (BSA) diluted in PBS to enable a transfer onto a 40 µm cell strainer (Becton Dickinson,

Franklin Lakes, NJ, USA) for thorough washing with cold PBS. The purified vessels were collected by washing the inverted cell strainer with PBS and centrifuged at 3,000 x g for 5 minutes. The collected pellet consisted of purified vessels. As isolated vessels have high adherence to plastic, all materials used were coated with 1% (w/v) BSA. The purity was determined with a light microscope (Eclipse TS 100, Nikon, Tokyo, Japan). (Figure 13)

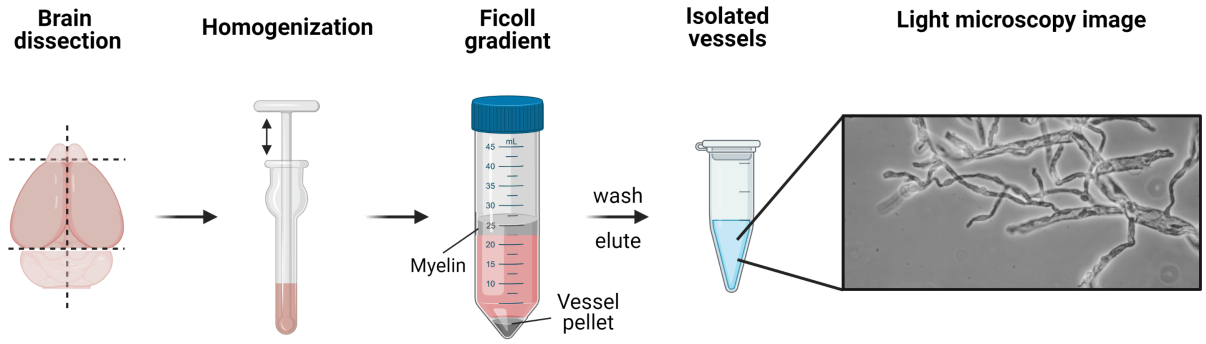

Figure 13: Cerebral vessel isolation steps (created with BioRender.com)

13. Protein expression analysis

Total protein isolation

To extract protein from isolated cerebral vessel a SDT lysis buffer (4% (w/v) SDS, 100 mM Tris-HCl pH 7.6, 100 mM DTT) was used. Samples were incubated for 30 minutes at room temperature and afterwards homogenized by Precellys tissue homogenizer (5x 30 sec., 10,000 rpm, 30 sec. pause). Homogenates were heated for five minutes at 95°C and subsequently sonicated with a VialTweeter sonicator (5 times, 30 sec., amplitude 100%, duty cycle 50%) (Hielscher, Teltow, Germany). A centrifugation step at 18,000 x g for 30 minutes at 15°C followed. The supernatant was collected in a fresh tube and stored at -20°C for further use.

Protein concentration measurement

Protein concentration was measured using the colorimetric 660-nm assay supplemented with ionic detergent compatibility reagent (Thermo Fisher Scientific, Waltham, MA, USA) according to the manufacturer's manual. Briefly, a protein standard was prepared to contain one-third of SDT buffer. Samples were diluted three-fold, and 5 µL of sample and standard transferred into a flat bottom 96-well plate. 75 µL of the 660 nm assay reagent was added, and the colorimetric change was immediately measured at 655 nm using a plate reader. The concentration was calculated using the four-parameter logistic regression model.

SDS polyacrylamide gel electrophoresis (PAGE)

Protein lysates were separated according to their size by sodium dodecyl sulfate-polyacrylamide gel electrophoresis (SDS-PAGE) using the XCell SureLock Mini-Cell Electrophoresis System (Thermo Fisher Scientific, Waltham, MA, USA) according to the manufacturer´s manual. Empty cassettes (Thermo Fisher Scientific, Waltham, MA, USA) were used to cast 10% separating gel and 4% stacking gel (Table 13). Samples were mixed with 4x Laemmli sample buffer (Bio-Rad Laboratories, Hercules, CA, USA) and dithiothreitol (DTT; final concentration 100 mM) and boiled at 95°C for five minutes. The electrophoresis was carried out in running buffer (25 mM Tris, 192 mM glycine, 1% (w/v) SDS) at 150 V for 90 minutes.

Table 13: Stacking and separation gel composition

Solution	Separating gel (10%)	Stacking gel (4%)
AcrylamideBis Solution (30%)	4 mL	555 µL
Tris-HCl 1.5 M pH 8.8	3 mL	
Tris-HCl 0.5 M pH 6.8		1.02 mL
Water	4.88 mL	2.94 mL
Ammonium persulfate (APS; 10%)	100 µL	45 µL
Tetramethylethylendiamine (TEMED)	10 µL	4.5 µL

Volumes are sufficient for two gels.

To transfer the separated protein onto a 0.2 µm polyvinylidene fluoride (PVDF) membrane (Bio-Rad Laboratories, Hercules, CA, USA), a Mini Trans-Blot system (Bio-Rad Laboratories, Hercules, CA, USA) was used. The transfer was conducted at 100 V for 90 minutes at 4°C. A 0.1% (w/v) Ponceau S solution (Sigma-Aldrich, St. Louis, MO, USA) was used to investigate the successful transfer of proteins onto the membrane.

After thoroughly washing with Tris-buffered saline with Tween 20 (TBS-T) buffer (10 mM Tris-HCl pH 8.0, 150 mM NaCl, 0.05% (v/v) Tween 20), the membrane was incubated with blocking buffer (5% (w/v) skim milk/TBS-T) for 1 hour at room temperature while gently shaking.

Subsequently, primary antibodies (Table 14) were diluted either in 5% (w/v) skim milk/TBS-T or 5% (w/v) BSA/TBS-T according to manufacturer's recommendations and incubated overnight at 4°C constantly shaking.

On the second day, membranes were washed thoroughly with TBS-T before adding the HRP-conjugated secondary antibody (Table 14) diluted in blocking buffer for one hour at room temperature under constant shaking. After a final washing step with TBS-T, HRP substrate was added as recommended by the manufacturer to detect the chemiluminescence signal with the

imaging system Fusion FX7 (Vilber, Eberhardzell, Germany). The signal intensity was quantified using ImageJ software.

Table 14: List of antibodies for WB

	Antibody	Species	Dilution	Manufacturer
primary	anti-ICAM-1 (ab222736)	rabbit	1:1000	Abcam, Cambridge, UK
	anti-PKG-1 (#3248)	rabbit	1:1000	Cell Signaling, Danvers, MA, USA
	anti- Guanylate Cyclase β1 subunit (# 160897)	rabbit	1:200	Caymanchem, Ann Arbor, MI, USA
	anti-β-Actin HRP conjugated (# A3854)	mouse	1:50.000	Sigma-Aldrich, St. Louis, MO, USA
	anti-rabbit IgG (#31464)	goat	1:7500	Thermo, Waltham, MA, USA

14. Histology

Cresyl Violet staining

Cresyl violet staining was performed to highlight the structural features and viability of neurons. First, the brains were cut with a cryostat (NX70, Thermo Fisher Scientific, Waltham, MA, USA). Frozen brain tissue was covered with embedding medium (Sakura Finetek, Alphen aan den Rijn, Netherlands) for cutting 10 µm thick coronal sections from rostral to caudal. Sections were transferred and mounted on super frost plus slides. The staining was sequentially performed in jars, as shown in Table 15. The section was embedded in Eukitt mounting medium (Sigma-Aldrich, St. Louis, MO, USA) and stored at room temperature.

Table 15: Cresyl violet staining procedure

Solution	Time (minutes)
70% Ethanol	2
Cresyl violet solution (1:5)	15
H_2O distilled I	rinse shortly
H_2O distilled II	rinse shortly
70% Ethanol	immerse briefly
96% Ethanol	immerse briefly
100% Ethanol	immerse briefly
100% Isopropanol	2
Rotihistol I	5
Rotihistol II	5

To quantify the infarct volume, slides were scanned with an Axio M2 inverted microscope (Carl Zeiss, Oberkochen, Germany). Brain hemispheres and infarct area were measured with ImageJ. Infarct volume was calculated by taking the sum of the infarcted area from rostral to caudal and multiplying the distance between sections (0.75).

Immunofluorescence (IF)

Isolated vessels (procedure explained in section 12) were mixed with 0.2% (w/v) BSA solution and stored at 4°C for immunofluorescence staining. For the staining procedure, a liquid-repellent slide marker pen (Science Services, Munich, Germany) was used to create a hydrophobic barrier around a drop of isolated vessel sample placed on a glass slide (SuperFrost Plus, Thermo Fisher Scientific, Waltham, MA, USA). The sample was dried at room temperature, and pure chilled acetone (100%) was used for 10 minutes at -20°C to fix and permeabilize the cell membranes. Thereafter, the slides were washed three times with PBS for five minutes. A 5% (w/v) BSA/PBS solution was added for one hour at room temperature to prevent unspecific binding. Next, primary antibodies (Table 16) were diluted in 0.2% (w/v) BSA/PBS and incubated overnight at 4°C. The next day, slides were washed with PBS and incubated with fluorophore-coupled secondary antibodies (Table 16) diluted in 0.2% (w/v) BSA/PBS for two hours at room temperature. Finally, slides were washed, incubated with DAPI solution (1:10,000 in PBS), and mounted with aqueous mounting media (Sigma-Aldrich, St. Louis, MO, USA). Images were taken with a confocal microscope (LSM 800, Carl Zeiss, Oberkochen, Germany).

Table 16: List of antibodies for IF

	Antibody	Species	Conjugate	Dilution	Manufacturer
primary	anti-ICAM-1 (ab222736)	rabbit		1:100	Abcam
	anti-Col-IV (ab235296)	goat		1:100	Abcam
	anti-αSMA (ab7817)	mouse		1:100	Abcam
secondary	anti-rabbit	donkey	Alexa 594	1:500	Jackson
	anti-goat	donkey	Alexa 697	1:500	Jackson
	anti-mouse	donkey	Alexa 594	1:500	Jackson

To quantify the ICAM-1 intensity of isolated vessels, ten ROIs per hemisphere from each animal were analyzed with ImageJ. The intensity of ICAM-1 was measured and normalized to Col-IV intensity in the same area. Smooth muscle actin (α-SMA) was used to identify arterioles.

15. Statistical analysis

GraphPad Prism 9 software (GraphPad Software Inc., San Diego, CA, USA) was used to perform statistical analysis for all data sets. If not stated otherwise, experiments were illustrated as means ± standard deviation (SD) of at least eight independent experiments. Initially, data were tested for normality. One-way ANOVA was used for normally distributed data, and the Kruskal-Wallis test was used if the data did not follow a Gaussian distribution. A statistically significant difference between groups was assumed at a p-value below 0.05.

III. Results

1. Standardization of the MCA occlusion model

To validate the MCA occlusion (MCAo) model, a standardization procedure was carried out. To do so, animals were subjected to one hour of MCAo followed by 24 hours of reperfusion. Thereafter, animals were sacrificed, and the infarct volume was analyzed.

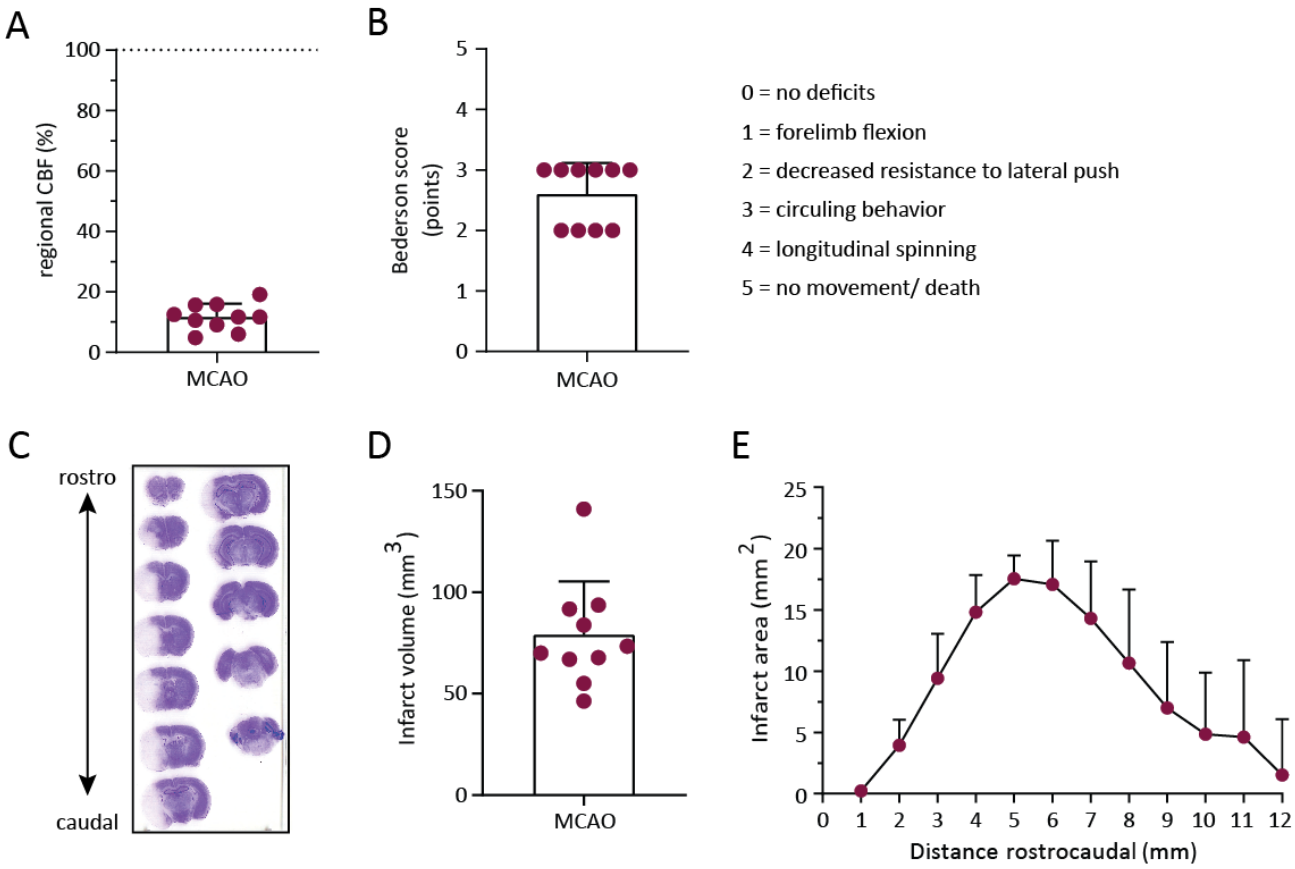

Figure 14: Distribution and size of cerebral infarct by MCA occlusion. C57BL/6 mice were subjected to one hour of MCA occlusion with a reperfusion time of 24 hours. **A)** Regional cerebral blood flow after MCA occlusion. **B)** Neurological deficits before reperfusion assessed by the Bederson test. **C)** Consecutive cresyl violet stained brain sections from one mouse sacrificed 24 hours after MCAo. The infarct remains unstained (white area). **D)** Infarct volume 24 hours after one-hour MCA occlusion. **E)** Rostrocaudal distribution of the infarct area. Data are given as means ± SD of 10 independent experiments.

The regional cerebral blood flow was monitored during surgery. A flow reduction by 80-90% indicated the correct placement of the filament and was therefore used to verify successful MCA occlusion (Figure 14A). Shortly before reperfusion, neurological deficits are determined via the Bederson score test as another indication for the induction of ischemia (Figure 14B). Histological analysis of the stained sections showed that infarcts were evenly distributed along the rostrocaudal axis in C57BL/6 animals (Figure 14E). The infarct volume was approximately around 80 mm^3 (Figure

14D). These data indicate that the MCAo model could be carried out reliably in a standardized manner.

2. Adhesion of leukocytes to cerebral vessels following ischemic stroke

The inhaled nitric oxide experiments were performed after the standardization of the MCA occlusion model. Therefore *in vivo* two-photon microscopy was used for visualizing and tracking immediate temporal and spatial leukocyte-endothelial interactions (LEI) after stroke.

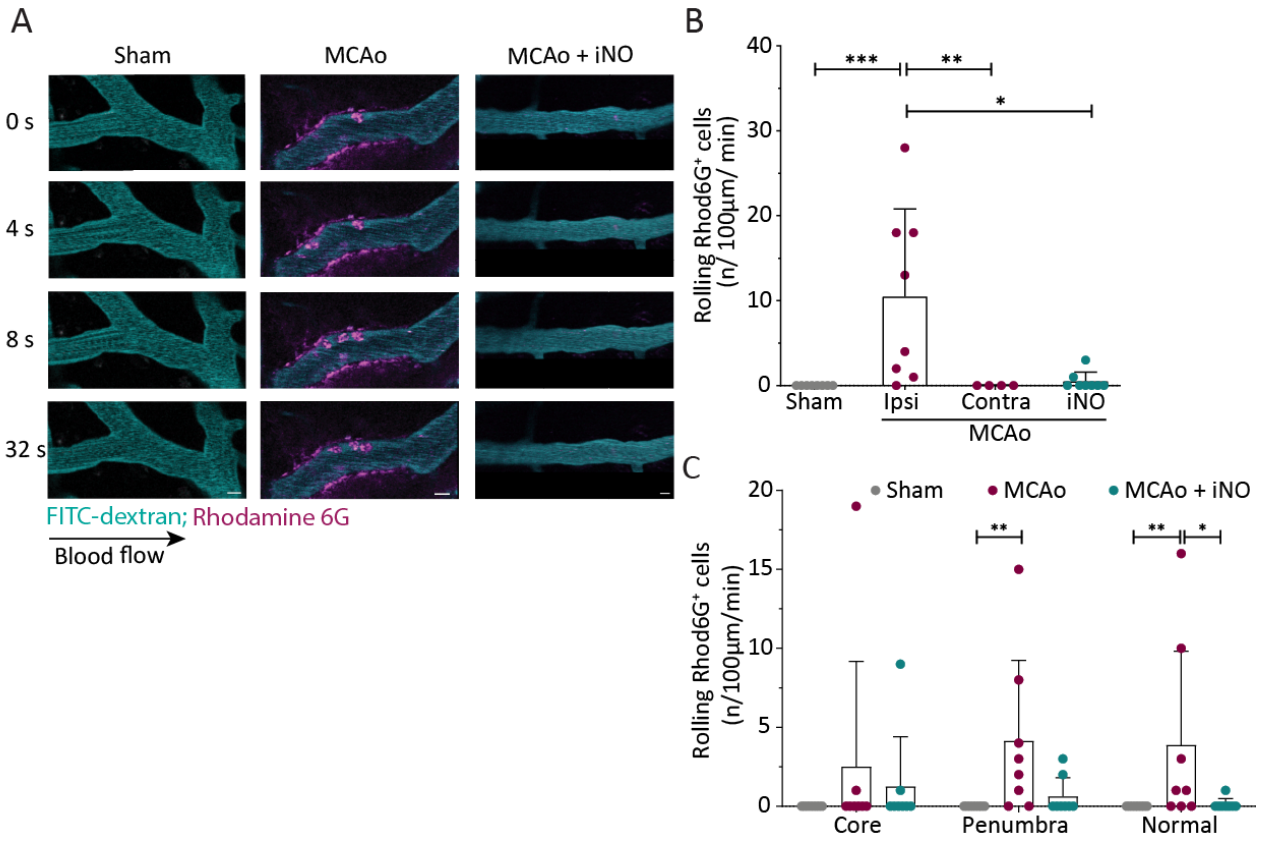

Figure 15: Rolling behavior of Rhod6G⁺ cells (leukocytes) after MCAo in cerebral venules.

A) Rolling leukocytes along the wall of cerebral venules five hours after sham surgery (left), reperfusion (center) or reperfusion and iNO (right) (scale bar = 10 µm); leukocytes and plasma stained with Rhodamine 6G (magenta) and FITC-dextran (cyan), respectively. **B)** Quantification of rolling of leukocytes onto the vascular endothelium. **C)** Quantification of leukocyte rolling in different areas of the ischemic territory. MCAo vs. sham or iNO: *p < 0.05, **p < 0.01, ***p < 0.001, Kruskal-Wallis test. Data are given as means ± SD of n=4-8.

No rolling leukocytes were observed in the sham group. However, a ten-fold increase of rolling Rhod6G⁺ cells was observed in venules of the ischemic hemisphere compared to the same hemisphere of sham-operated mice or the non-ischemic contralateral hemisphere (Figure 15B). Administration of iNO reduced the number of rolling leukocytes to control levels (Figure 15B). A closer look into the different areas of the ischemic territory revealed a rise of rolling cells in all

investigated regions, including normally appearing tissue outside the ischemic penumbra (Figure 15C).

The next step in the process of LEI after rolling along the vessel wall is the firm adhesion of immune cells to the endothelium. Rhod6G$^+$ cells were defined as “adherent” when stationary for at least five minutes.

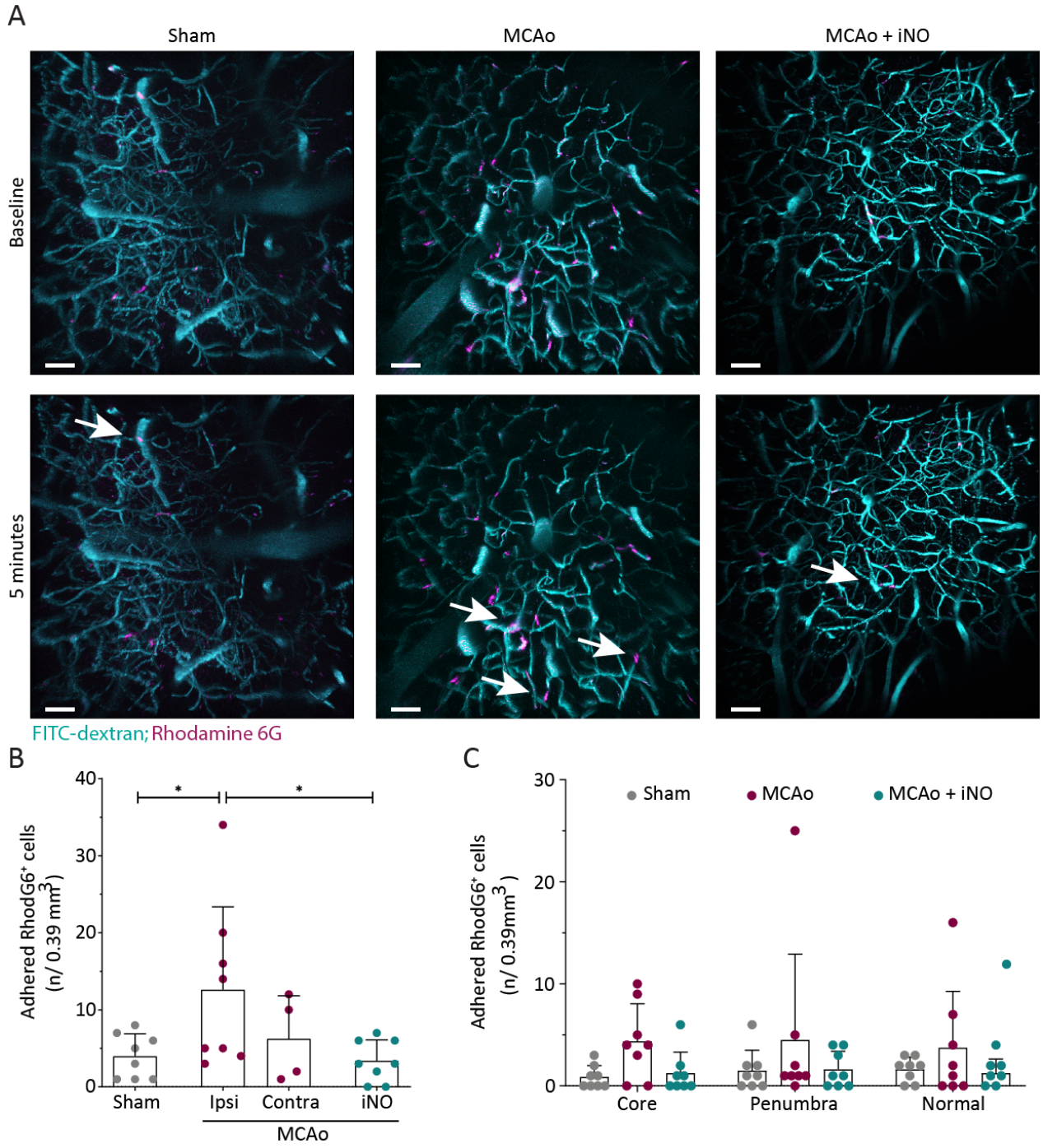

Figure 16: Adhered Rhod6G$^+$ cells in venules and capillaries five hours after reperfusion. A) Representative images of adhered leukocytes (magenta) and cerebral vasculature (cyan) (scale bar = 50 µm) **B)** Quantification of the total number of adhered leukocytes to the endothelium, and **C)** quantification of adhered leukocytes in different areas of the ischemic territory. MCAo vs. sham or MCAo vs iNO: *p < 0.05, one-way ANOVA. Data were given as means ± SD of n=4-8.

Investigation of sham-operated animals revealed a physiological adhesion of on average four leukocytes per 0.39 mm^3. The number of adhered leukocytes increased significantly five hours after reperfusion in the stroked hemisphere with up to 12 leukocytes per 0.39 mm^3 compared to sham animals. MCAo resulted in a three-fold increase of leukocytes (12 cells/ 0.39 mm^3). iNO resulted in a three-fold decrease in adhered leukocytes following reperfusion (4 cells/ 0.39 mm^3). Another group of mice was used to investigate LEI in the contralateral hemisphere after stroke. The amount of adhered leukocytes in the contralateral side of the stroked animals reached an average of 6 cells per 0.39 mm^3, which shows that stroke induction did not affect the basal adhesion at the contralateral hemisphere (Figure 16B).

Adhesion stayed high in other ROIs such as stroke core, penumbra, or normal tissue after MCAo and diminished with iNO application (Figure 16C).

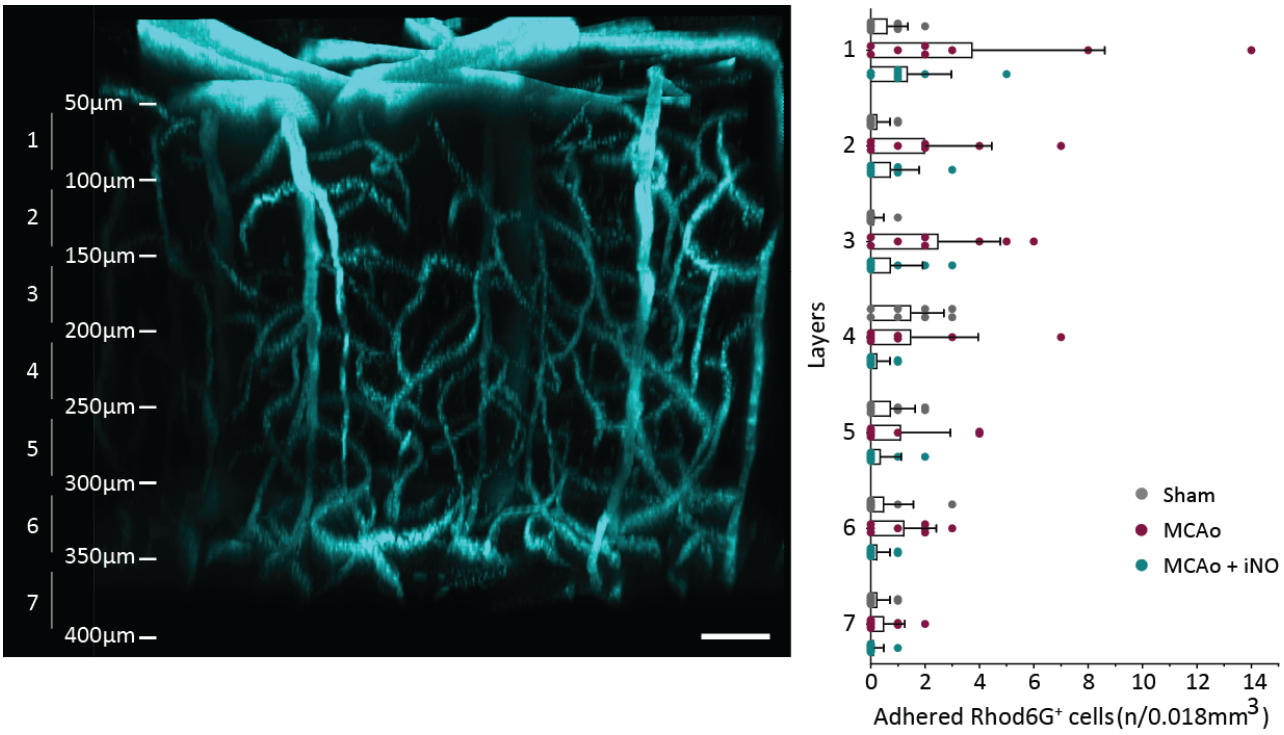

Figure 17: Adhered Rhod6G⁺ cells distribution five hours after reperfusion. Representative image of adhered cerebral vasculature (cyan) and quantification of leukocyte adhesion from the cortical surface to a depth of 400 µm (scale bar = 50 µm). Data were given as means ± SD of n=8.

Depth distribution analysis of adhered leukocytes revealed that the adhesion was more pronounced close to the cortical surface and decreased through the parenchyma (Figure 17).

To exclude implications of iNO on physiological parameters, the hemodynamics and vascular diameter were quantified in the three-dimensional (3D) two-photon images. The vital parameters were continuously monitored through the femoral catheter and recorded.

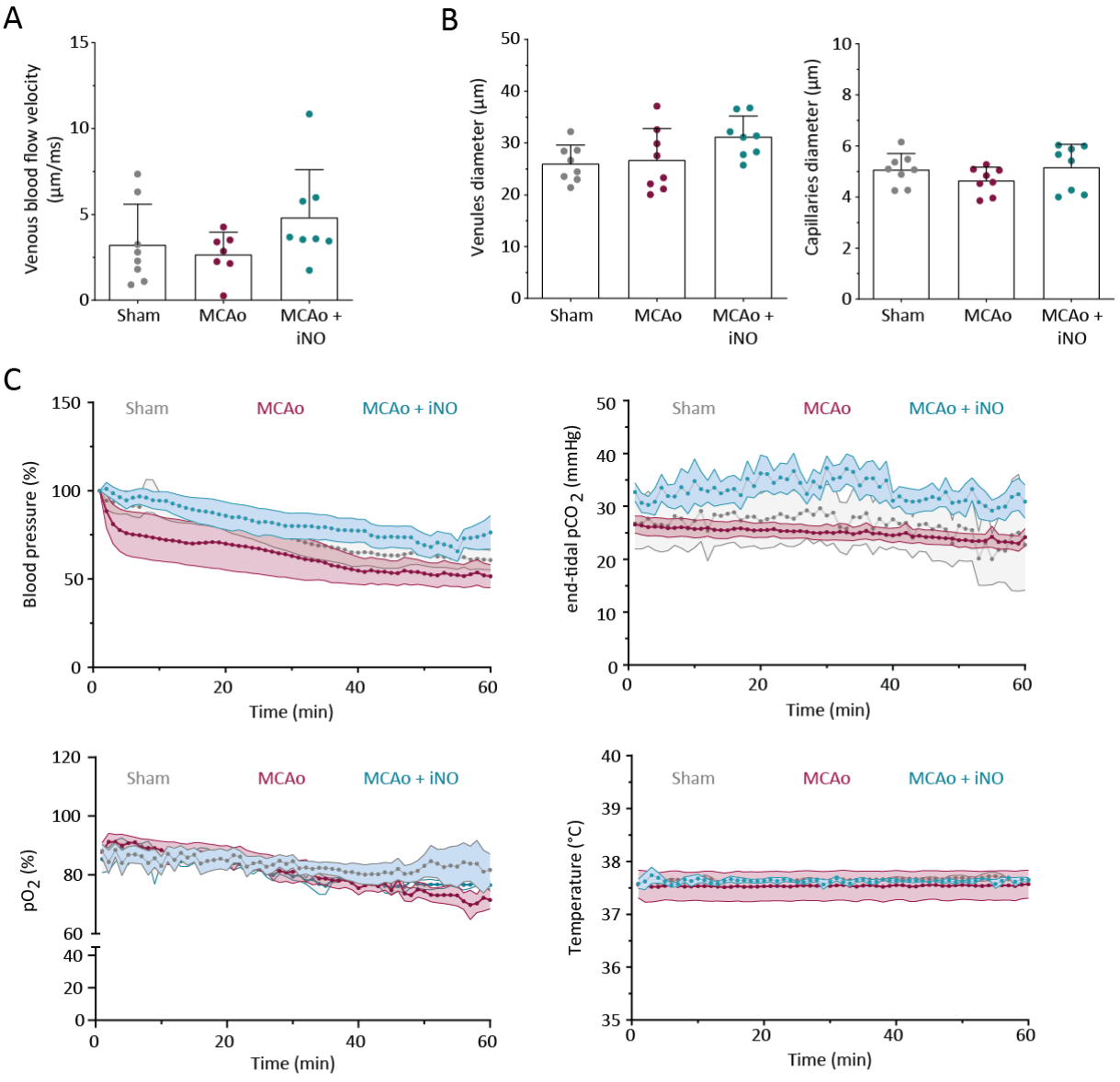

D

Parameter	Sham	MCAo	MCAo + iNO
pH	7,19 ± 0,10	7,15 ± 0,10	7,21 ± 0,17
pCO_2 (mmHg)	59,14 ± 14,91	56,43 ± 9,89	53,63 ± 17,36
pO_2 (mmHg)	110,68 ± 22,49	104,01 ± 34,65	95,23 ± 63,87
Na^+ (mmol/L)	158,80 ± 9,78	155,57 ± 7,83	152 ± 3,00
K^+ (mmol/L)	5,29 ± 0,29	5,63 ± 0,52	5,94 ± 2,08
Ca^{2+} (mmol/L)	1,39 ± 0,23	1,20 ± 0,19	1,39 ± 0,04

Figure 18: Physiological parameters during *in vivo* imaging. A) Venous blood flow velocity was measured in vivo by performing a line scan and dividing the traveled distance of erythrocytes (µm) by the respective traveled time (msec.). **B)** Diameter of venules and capillaries was measured in a randomly chosen vessel from the 3D two-photon images with ImageJ. **C)** Vital parameters were measured and monitored throughout the entire surgery via LabChart software. **D)** Blood sample was measured with a blood gas analyzer. Data were given as means ± SD **(A and B)** or SEM **(C)**, n=8.

No significant variations were detected regarding the blood flow velocity in cerebral venules five hours after reperfusion in animals with or without iNO administration (Figure 18A). MCAo did not cause vasoconstriction in cerebral venules or capillaries compared to sham-operated animals.

Additionally, iNO had no aberrant vasodilation effect upon application (Figure 18B). No alterations in blood pressure, exhaled carbon dioxide (end-tidal pCO_2), oxygen saturation (O_2), and temperature were observed in any of the experimental groups (Figure 18C).

To investigate circulating immune cells after stroke, peripheral blood was collected by cardiac puncture, and leukocyte subsets were quantified by FACS analysis.

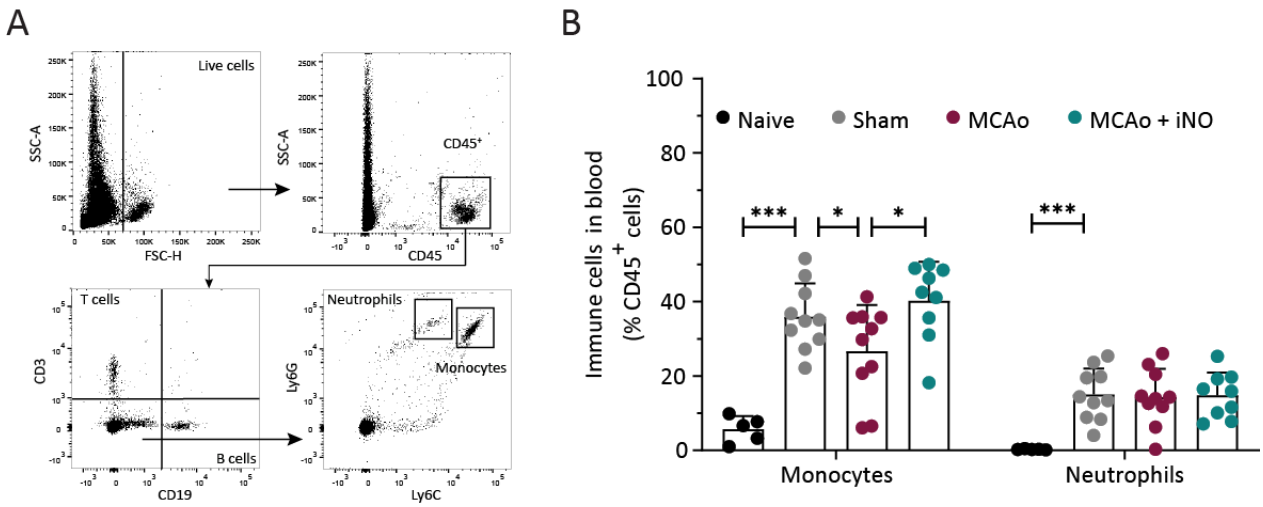

Figure 19: Immune cell population counts in blood in naive mice after sham surgery or MCAo. Myeloid cells were isolated five hours after reperfusion and analyzed by flow cytometry. **A)** Flow cytometry gating strategy to analyze immune cells in the blood. **B)** Quantification of Ly6G high (neutrophils) and Ly6C high (monocytes) cells. Naive vs. sham and MCAo vs. sham or MCAo + iNO: *p < 0.05, **p < 0.01, ***p < 0.001, one-way ANOVA test. Data are given as means ± SD of n=5-10.

Sham-operated animals showed a significant increase in circulating monocytes and neutrophils compared to naive animals (Figure 19B). Monocytes decreased after MCAo, and this effect could be reversed by iNO (Figure 19B).

3. Cytokine levels after MCA occlusion and inhaled NO treatment

Pro-inflammatory cytokines are small, secreted proteins that play a key role in the up-regulation of inflammatory processes in the peripheral and central nervous system. IL-1β, TNF-α, and IL-6 are among the first cytokines to be elevated, thus initiating the inflammatory cascade. In the current study, cytokine levels were analyzed in naive mice or five hours after stroke or sham surgery both in the brain and peripheral blood.

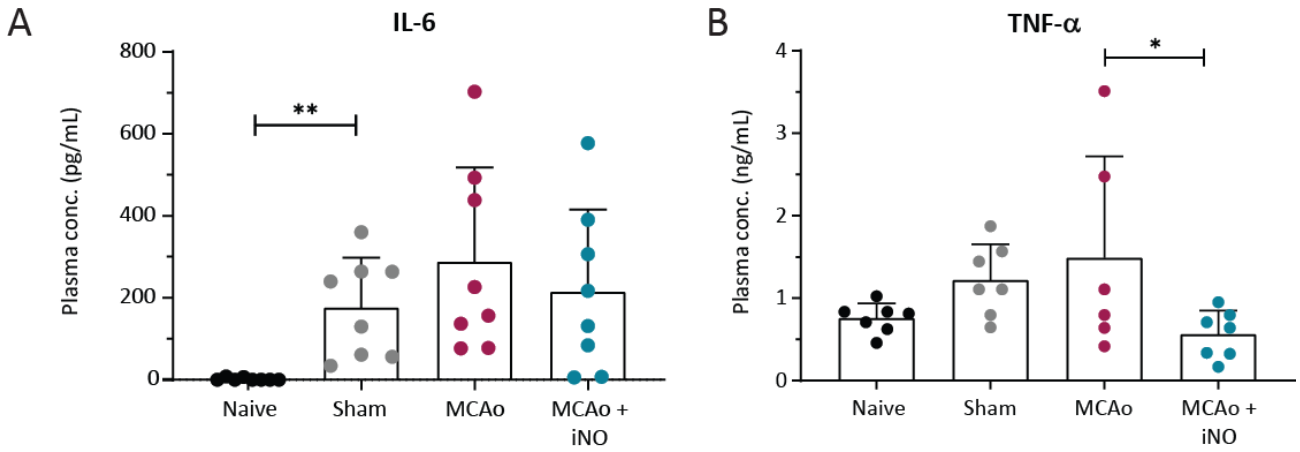

Figure 20: Pro-inflammatory cytokine levels in peripheral blood. Quantification of plasma **A)** IL-6 and **B)** TNF-α levels assessed by ELISA five hours after reperfusion. Naive vs. sham and MCAo vs. sham or MCAo + iNO: *p < 0.05, **p < 0.01, Kruskal-Wallis test (IL-6) or one-way ANOVA test (TNF-α). Data are given as means ± SD of n=6-8.

IL-6 plasma levels were almost undetectable in naive mice and were significantly elevated by up to 300-fold following sham surgery. MCAo did not cause any further significant increase (Figure 20A). Plasma TNF-α levels were detectable in naive mice and showed a tendency towards higher levels following sham operation and MCAo. iNO application significantly reduced plasma TNF-α levels to naive values (Figure 20B).

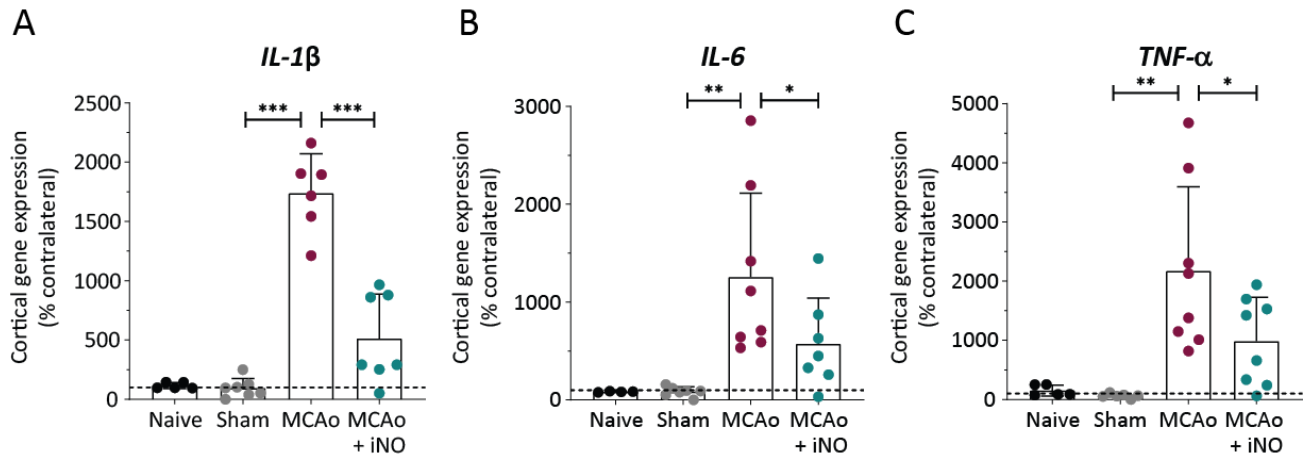

Figure 21: Pro-inflammatory cytokine levels in the cerebral cortex five hours after reperfusion. Quantification of **A)** *IL-1β*, **B)** *IL-6*, and **C)** *TNF-α* mRNA expression levels in brain hemispheres of sham, MCAo, and iNO mice measured by quantitative real-time PCR with *Gapdh* as a housekeeping gene. MCAo vs. sham or MCAo + iNO: *p < 0.05, **p < 0.01, ***p < 0.001, one-way ANOVA test. Data are given as means ± SD of n=6-8.

Low levels of pro-inflammatory cytokines were detected in sham-operated animals and the contralateral hemisphere of animals subjected to MCAo five hours after reperfusion. In contrast, pro-inflammatory cytokines were massively upregulated up to several thousand times after stroke

(Figure 21; red dots). Application of inhaled NO significantly decreased *IL-1β*, *Tnf-α*, and *IL-6* mRNA expression levels after MCAo by 50-70% (Figure 21; cyan dots).

Due to its importance in disrupting the BBB after ischemia, MMP-9 expression was investigated in the ischemic hemisphere and plasma five hours after reperfusion by qPCR and ELISA, respectively.

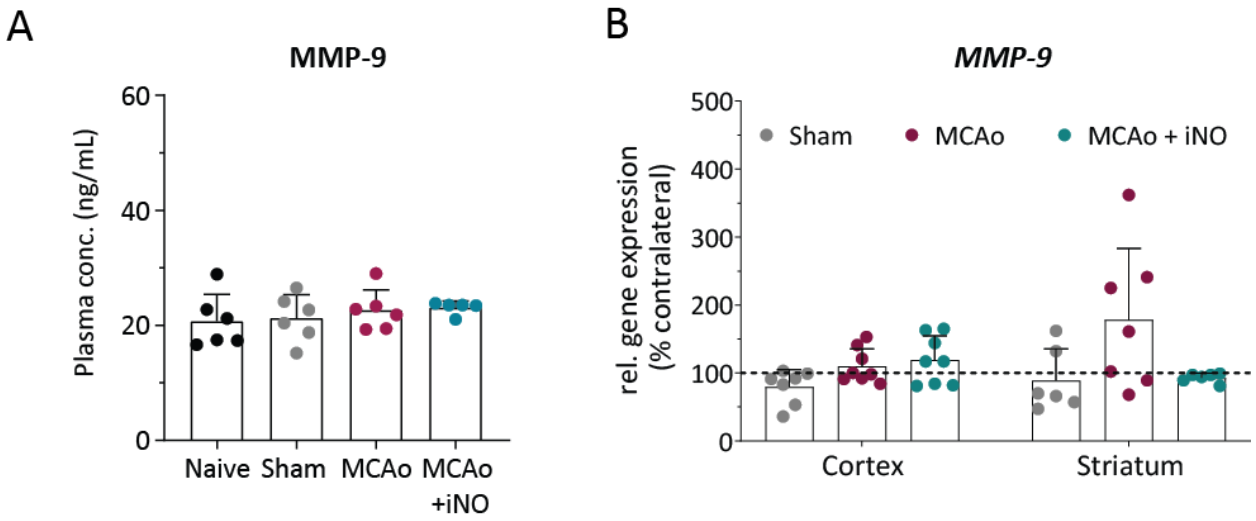

Figure 22: MMP-9 levels and expression in blood and brain. A) Plasma MMP-9 levels of naive, sham, MCAo, and MCAo + iNO mice were assessed by ELISA. **B)** Quantification of *MMP-9* mRNA expression levels determined in brain hemispheres of sham, MCAo, and MCAo + iNO mice by quantitative real-time PCR with *Gapdh* as a housekeeping gene. Data are given as means ± SD of n=4-7.

Plasma MMP-9 levels showed no changes in any group after stroke (Figure 22A). The only tendency towards elevated MMP-9 expression was observed in the ischemic core, i.e., in the striatum, of the infarct. iNO application reduced *MMP-9* mRNA expression in the striatum to sham levels (Figure 22B).

4. Adhesion molecule expression upon stroke induction

Endothelial cells

The next step was to investigate whether the stroke-induced increase in pro-inflammatory cytokines affects the expression of adhesion molecules such as selectins (P- and E- selectin) and integrin ligands (ICAM-1 and VCAM-1) in the ischemic brain since these molecules mediate rolling and firm adhesion of immune cells to the vascular wall of post-capillary venules.

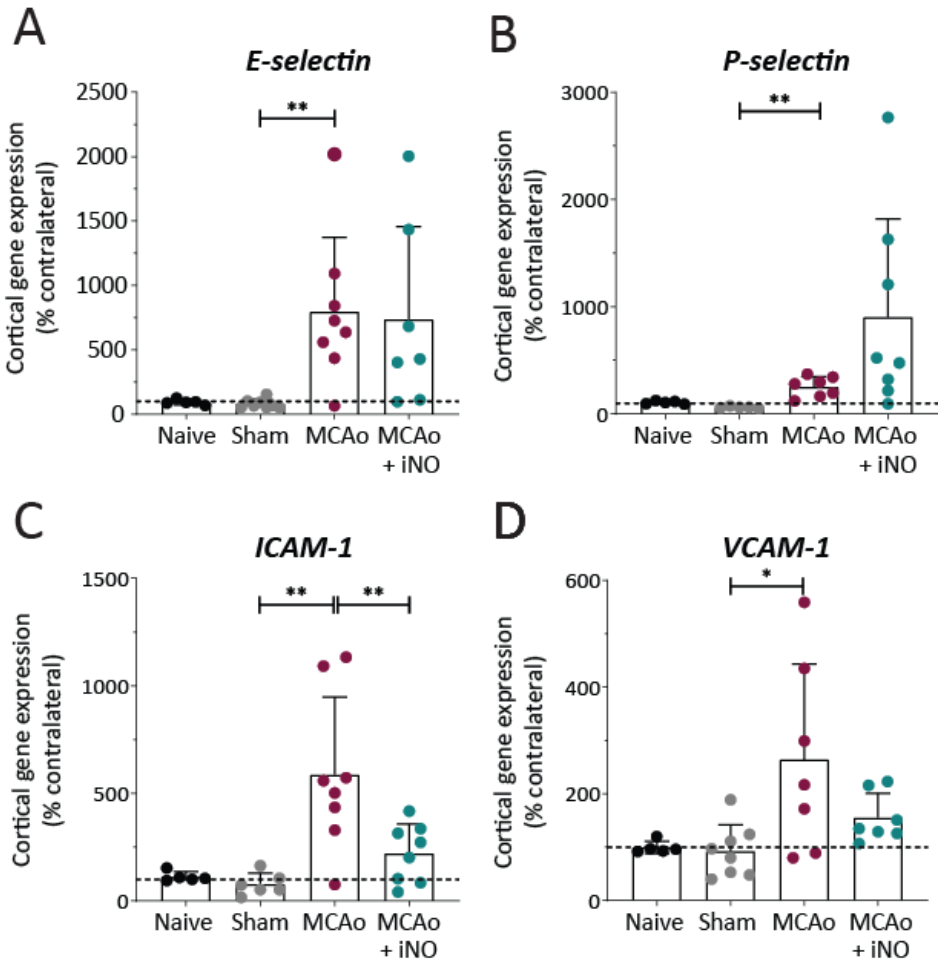

Figure 23: Adhesion molecule expression in the brain. Expression levels of **A-B)** *selectins* and **C-D)** *integrin ligands* were determined in cerebral cortex hemispheres of sham, MCAo, and MCAo + iNO mice five hours after reperfusion by quantitative real-time PCR with *Gapdh* as a housekeeping gene. MCAo vs. sham or MCAo + iNO: *p < 0.05, **p < 0.01, Kruskal-Wallis (selectins) or one-way ANOVA (integrin ligands). Data are given as means ± SD of n=6-8.

The mRNA expression of all adhesion molecules significantly increased by up to seven-fold five hours after stroke induction. Treatment with iNO after stroke did not change the expression levels of E- and P-selectins (Figure 23A-B) however, *ICAM-1* mRNA expression was significantly reduced in comparison to the MCAo group (Figure 23C). *VCAM-1* mRNA expression levels were also reduced by about 50% upon iNO application however, this reduction did not reach statistical significance (Figure 23D).

To instigate whether the changes of *ICAM-1* expression observed on the mRNA level translate to protein expression, we isolated brain vessels and performed immunohistochemistry and western blot analysis.

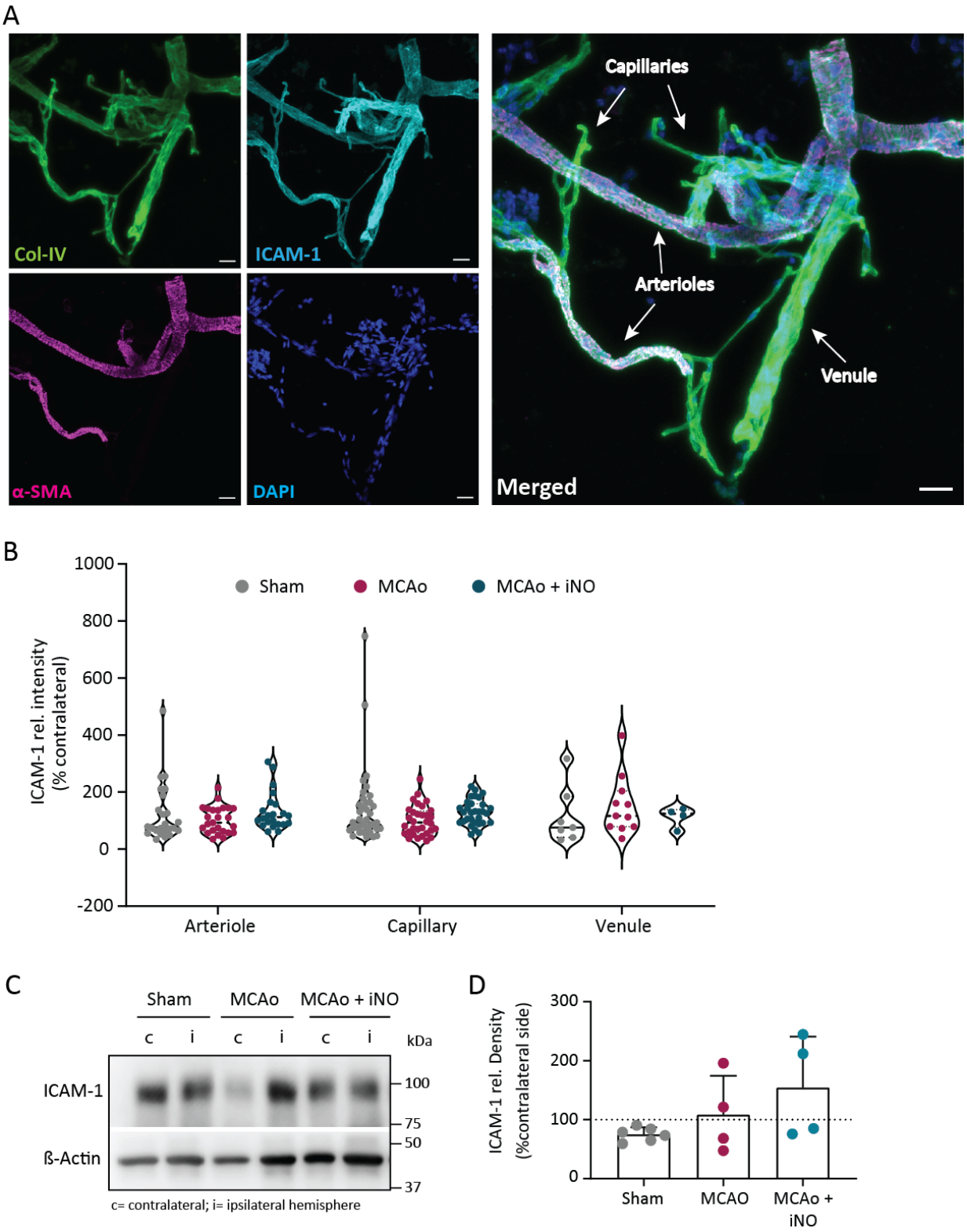

Figure 24: ICAM-1 expression in isolated brain vessels. A) Representative immunofluorescence confocal images of isolated brain vessels. Arterioles, capillaries, and venules were differentiated due to their thickness and expression of alpha-smooth muscle actin (α-SMA). (Scale bar = 20 µm) **B)** Quantification of ICAM-1 pixel intensity in isolated cerebral vessels, normalized to Col-IV expression, depicted as percentage of the contralateral hemisphere. (Dots represent selected ROIs) **C-D)** Western blots and quantification of ICAM-1 from isolated vessel specimens, where β-actin was used as a housekeeping protein. Data are given as means ± SD of n=4-6.

Using α-SMA as a marker, we could nicely differentiate arterioles (strong staining) from venules (no staining; Figure 24A). Collagen-IV and ICAM-1 were expressed at a higher level in venules however, when correcting for Col-IV expression and comparing results to vessels isolated from the contralateral non-ischemic hemisphere, we did not observe a difference in ICAM-1 intensity between experimental groups (Figure 24B). These results were corroborated by Western blot analysis (Figure 24D). These results were quite surprising since not even an increase of ICAM-1 expression after ischemia, which is evident by PCR analysis, could be demonstrated on the protein level.

Leukocytes

Circulating immune cells also contain the counterpart of adhesion molecules on endothelial cells. To analyze this, circulating myeloid cells were isolated from the blood and analyzed for expression changes by flow cytometry following stroke and iNO application.

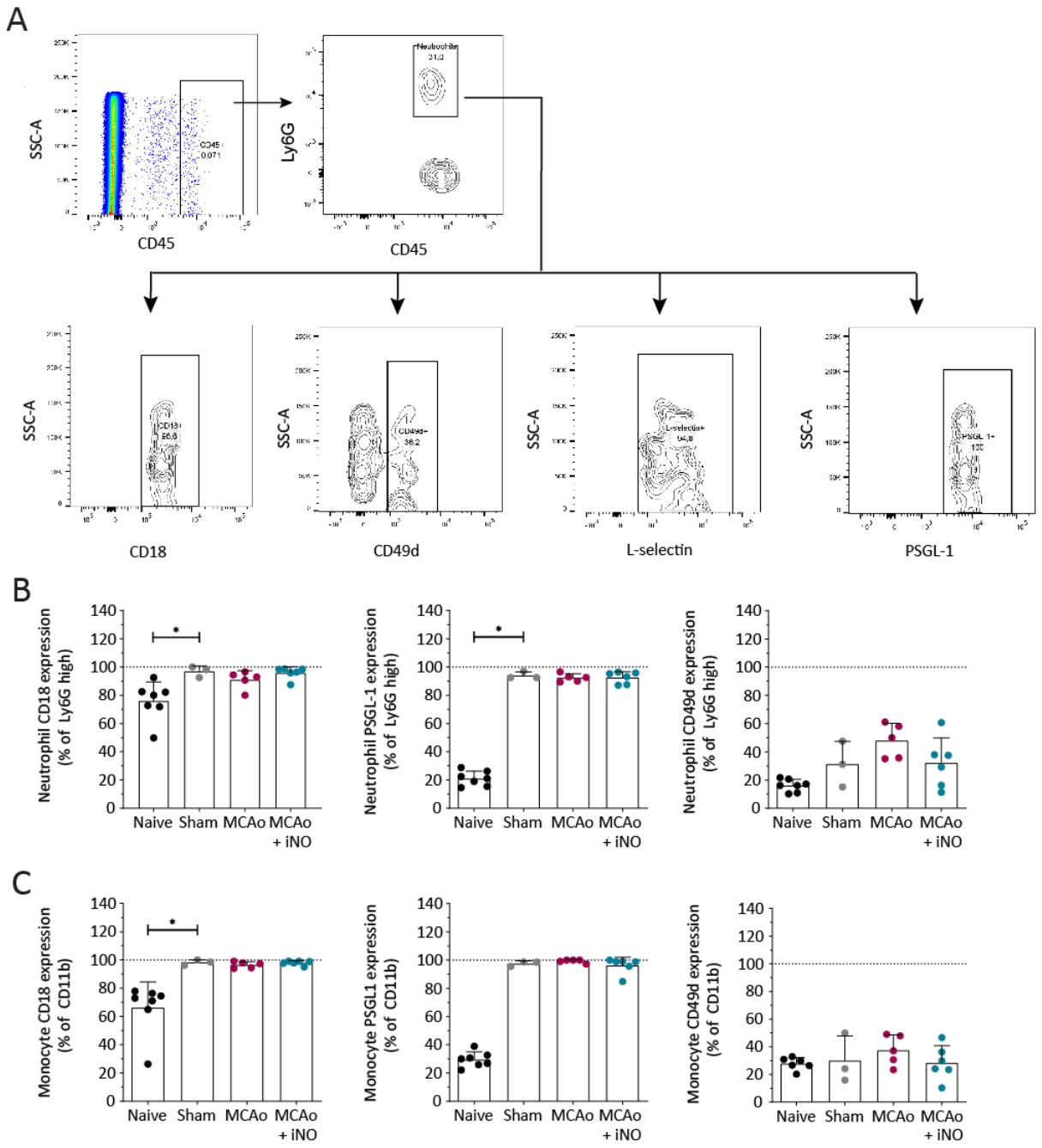

Figure 25: Adhesion molecule markers on circulating leukocytes five hours after reperfusion. A) Representative gating strategy for flow cytometry analysis. Quantification of **B)** Ly6G high (neutrophils) and **C)** CD11b high (monocytes) cells and their surface adhesion molecule presentation. Naive vs. sham: *p < 0.05, Kruskal-Wallis test. Data are given as means ± SD of n=3-7.

CD18 and PSGL-1 were already upregulated by sham surgery, and neither MCAo nor MCAo + iNO affected this increase. The same was observed for CD49d, however, on a much lower level (Figure 25).

5. NO signaling after cerebral ischemia

To analyze the endogenous NO production machinery (see Figure 5), NOSs, the NO receptor sGC, the sGC product cGMP, and PKG protein expression were analyzed in brain hemispheres and isolated brain vessel specimens.

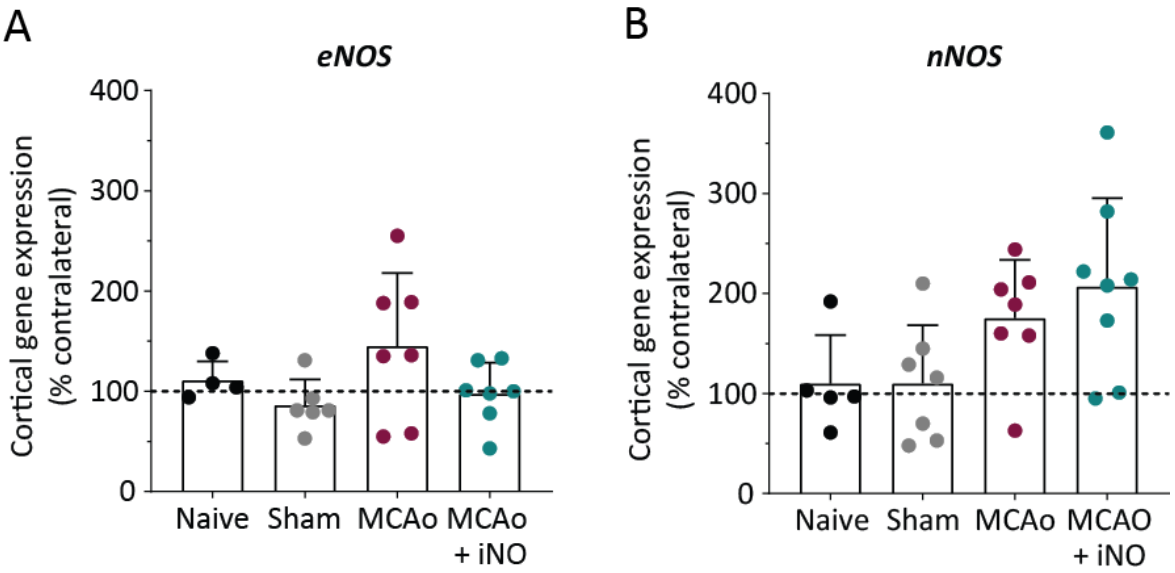

Figure 26: NOS mRNA levels in brain tissue. Quantification of **A)** *eNOS* and **B)** *nNOS* mRNA levels in cerebral cortex hemispheres of sham, MCAo, and MCAo + iNO mice five hours after reperfusion by quantitative real-time PCR with *Gapdh* as a housekeeping gene. Data are given as means ± SD of n=6-7.

Both *eNOS* and *nNOS* mRNA expression levels showed a tendency towards an increase after stroke induction by about 50% (Figure 26A and B; n.s.). Inhaled NO lowered *eNOS* mRNA expression to almost sham levels (Figure 26A) but did not affect *nNOS* mRNA expression (Figure 26B). Inducible NOS could not be detected in any of the groups in this early phase after stroke (data not shown).

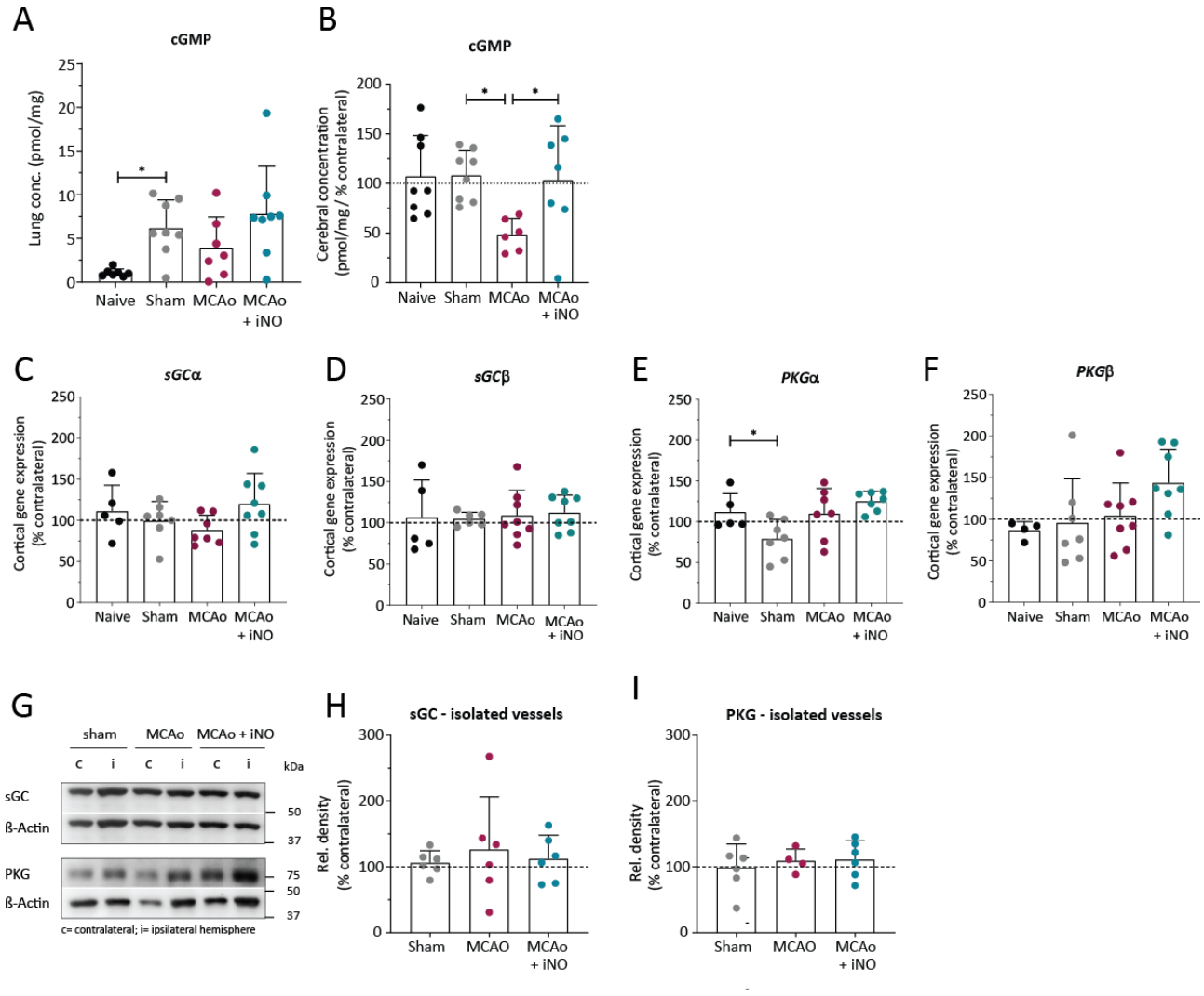

Figure 27: NO downstream molecule expression. A-B) cGMP levels in lung and brain hemisphere samples, measured by ELISA five hours after reperfusion. mRNA expression of **C-D)** *sGC* and **E-F)** *PKG* in cerebral cortex hemispheres of sham, MCAo, and MCAo + iNO mice five hours after reperfusion by quantitative real-time PCR with *Gapdh* as a housekeeping gene. **G)** Representative western blot images and quantification for **H)** sGC and **I)** PKG protein expression in isolated vessel samples with β-actin as housekeeping protein. MCAo vs. sham or iNO: *p < 0.05, one-way ANOVA. Data are given as means ± SD of n=4-8.

Next, downstream molecules of NO were analyzed. Sham-operated animals showed a significant increase of cGMP in the lung, whereas neither stroked nor iNO treated animals exhibited changes in the lung (Figure 27A). Cerebral cGMP levels displayed no changes in sham compared to naive animals. A significant decline was present in brain tissue after MCA occlusion that could be increased to sham values by inhaled NO (Figure 27B).

Quantitative gene expression analysis displayed a tendency of decreased *sGCα* subunit in stroked animals compared to sham-operated animals (Figure 27C). Inhaled NO restored *sGCα* subunit to sham levels and even slightly higher (Figure 27C). On the contrary, the β-*subunit of sGC* presented no significant changes between the different experimental groups (Figure 27D). *PKGα* subunit was

significantly increased in stroked compared to sham-operated animals (Figure 27E). Furthermore, no changes could be revealed by applying iNO (Figure 27E). Apart from that, the β-*subunit of PKG* was not different between experimental groups (Figure 27F).

Isolated cerebral vessels of stroked animals reveal no alterations in the sGC (Figure 27H) nor PKG (Figure 27I) protein amount compared to sham animals. Likewise, the application of inhaled NO had no impact on the protein expression of sGC and PKG quantity in endothelial cells (Figure 27G-I).

The NF-κB is a ubiquitously expressed transcription factor, activated by diverse immune-stimulatory ligands activating gene expression of cytokines, cell adhesion molecules, immunoreceptors, and others. Therefore, the transcriptional activity of NF-κB is tightly regulated to maintain homeostasis. IκBα is itself an NF-κB target gene and contributes to the inhibition of NF-κB signaling in a negative feedback loop. Another inhibitor of NF-κB is the A20 deubiquitinase.

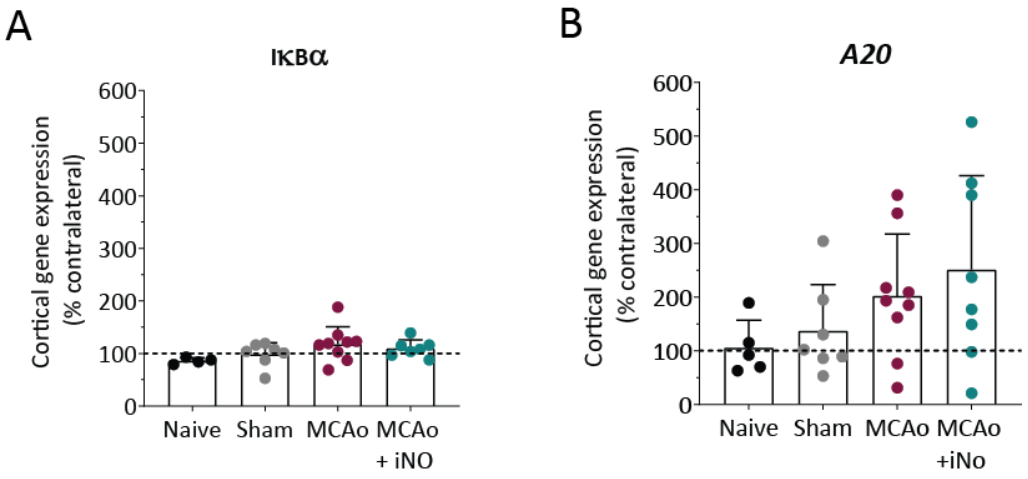

Figure 28: Inhibitory molecules of the NF-κB signaling pathway. Quantification of **A)** *IκBα* and **B)** *A20* mRNA levels in cortical hemispheres of sham, MCAo, and MCAo + iNO mice five hours after reperfusion by quantitative real-time PCR with *Gapdh* as a housekeeping gene. Data are given as means ± SD of n=7-9.

Cortical homogenates of stroked animals indicated a tendency towards an increased IκBα expression (Figure 28A). A similar trend was observed for the expression of *A20* (Figure 28B). Giving inhaled NO to stroked animals did not significantly change *IκBα* or *A20* expression.

6. NO metabolites after inhalation

NO can be oxidized to nitrite (NO_2^-) and nitrate (NO_3^-). These metabolites serve as storage forms of NO in mammals.

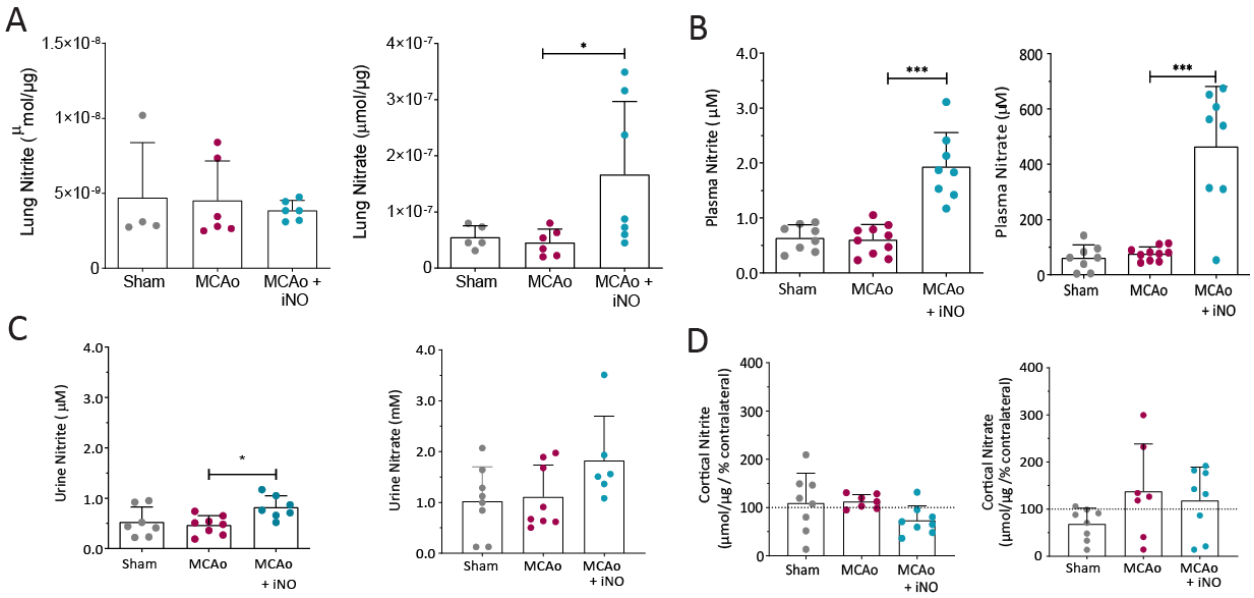

Figure 29: Nitrite and nitrate levels after stroke induction. Nitrite and nitrate measurement in **A+D)** lung and brain, **B+C)** in plasma and urine collected four hours after reperfusion and analyzed by a chemiluminescent assay. MCAo vs. sham or MCAo + iNO: *p < 0.05, ***p < 0.001 one-way ANOVA. Data are given as means ± SD of n=4-10.

No alterations in nitrite/nitrate levels in lung and plasma were observed after stroke. iNO supplementation did not affect the nitrite levels, whereas the nitrate levels significantly increased in the lung (Figure 29A). However, iNO substantially boosted the nitrite and nitrate amount in plasma by almost two times and four times, respectively (Figure 29B). Brain levels of NO metabolites revealed no changes in stroked or iNO treated mice (Figure 29D). If not transformed, NO metabolites are eliminated via renal excretion, which is shown by the high concentration of nitrite and nitrate in the urine of NO-treated rodents (Figure 29C).

IV. Discussion

Stroke initiates a complex molecular and cellular cascade that eventually contributes to ischemic tissue injury. The primary event after the arterial occlusion is hypoperfusion, which reduces glucose and oxygen availability in the brain. Lack of ATP results in tissue acidosis, loss of neuronal membrane potential, and high extracellular potassium and glutamate concentrations leading to excessive stimulation of neurons and subsequent damage or death of previously unaffected neuronal tissue.[86] Secondarily, cell lysis triggers post-ischemic inflammation, which starts with the activation of local inflammatory cells, release of pro-inflammatory cytokines and chemokines, and is followed by the recruitment of blood leukocytes through cerebral vessels, a process believed to contribute to ischemic brain injury.[23] Since strategies of neutralizing key pro-inflammatory cytokines (TNF-α, IL-1β, and IL-6) are successfully used in patients suffering from non-neurological inflammatory diseases,[106,211,212] pharmacological interventions targeting inflammation may also have a therapeutic potential after stroke.[213]

Among others, one potential strategy to treat cerebral ischemia is to address the NO-sGC-cGMP pathway. NO dilates cerebral vessels, and lack of NO after cerebral ischemia may lead to vasoconstriction and additional brain damage. To avoid systemic side effects, NO was previously applied by inhalation (iNO) and was proven to restore vascular function following small and large animal models of ischemic stroke, traumatic brain injury, and brain trauma.[196-198,200,202]

In addition to its vasoactive properties, NO is also known to have anti-adhesive properties.[204] Therefore, we hypothesized that inhalation of NO might reduce the interaction of leukocytes with the cerebrovascular endothelium, thereby providing neuroprotection after focal cerebral ischemia.

In this project, we demonstrated that iNO has anti-adhesive effects following ischemic stroke and reduces leukocyte adhesion in the cerebral vasculature after cerebral ischemia (Figure 15). Our study indicates that iNO causes a strong inhibition of leukocyte-endothelial interaction five hours after reperfusion *in vivo* (Figure 16). Deep brain two-photon microscopy made it possible to investigate that iNO reduced leukocyte rolling and adhesion to pre-ischemic levels in the living animal.

Former studies in non-neuronal tissues have shown that inhibition of NO production by pharmacological or genetic inhibition of NOS induces leukocyte adhesion.[204,214-216] Conversely, restoration of NO availability reduced leukocyte adhesion in the setting of ischemia/reperfusion injury in various organs.[204,207] Extension of these experimental results into the clinical scenario confirmed the anti-inflammatory potential of iNO. Patients who underwent knee surgery requiring

a tourniquet showed attenuated inflammatory effects by administering iNO for the duration of the surgery.[217] Additionally, iNO given during or after either liver or heart transplantation reduces inflammation and improved clinical outcome.[184,197] The anti-adhesive effect is further supported by an increase in the amount of circulating immune cells, predominantly monocytes, upon iNO treatment, which indicates that fever cells adhered to the vasculature of the inflamed organ, an observation also made in the current study (Figure 19).

NO's anti-adhesive effects were predominantly seen in capillaries and venules, as hypoperfusion has a much more substantial impact in those vessels due to an artery-to-vein oxygen gradient. A shift of hemoglobin deoxygenation towards arterioles under hypoxic conditions supports the notion that NO also inhibits leukocyte-endothelial interaction in arterioles.[218,219]

Many therapeutic strategies that increase NO's availability rely on the systemic application of NO precursors and have systemic side effects, such as systemic hypotension.[182] In contrast, NO inhalation has been shown to result in NO bioavailability exclusively in hypoxic-ischemic tissue without any effects on systemic hemodynamic effects.[200,205,207] These findings were corroborated in the current study (Figure 18): the recorded physiological data after iNO suggest that no adverse systemic effects are present. Thus iNO may represent a preferable route of administration, especially in diseases where systemic hypotension is unfavorable.

After observing reduced leukocyte adhesion following application of iNO to mice subjected to ischemic stroke *in vivo*, we aimed to investigate the underlying mechanisms. NO's anti-adhesive properties are related to transcriptional regulation of adhesion proteins on endothelial cells. Investigating transcriptional regulation of adhesion proteins, we found diminished *de novo* synthesis of messenger RNA (mRNA) for *ICAM-1* and *VCAM-1* in the cerebral cortex of ischemic mice treated with iNO (Figure 23), findings also observed by others in other disease models and non-neuronal organs.[220-226] This reduction of adhesion molecules is a good explanation of how iNO prevents leukocyte interaction with the endothelium and blocks leukocytes' transmigration into ischemic brain tissue.

In contrast to ICAM-1 and VCAM-1, molecules that promote firm adhesion, *E- or P-selectin* mRNA levels were not affected by iNO application (Figure 23). These results are controversial as other studies have observed a decline of selectins by NO.[225-227] These discrepancies may be due to differences in timing and duration of the application of agonist/antagonist, as well as the physiological condition of the investigated animals. [225-227] It seems like iNO effects rolling *in vivo* without altering the expression level of selectins. As leukocyte transmigration represents a dynamic

process, ICAM-1 also has a role in the rolling step, therefore iNO could reduce *in vivo* rolling via ICAM-1 down-regulation.[222,225]

The NF-κB pathway controls the transcriptional regulation of adhesion proteins and pro-inflammatory genes. Under physiological conditions, the protein is kept inactive in the cytosol via the inhibitory protein IκBα. The activation of cytokine receptors initiates the degradation of IκBα, thereby enabling NF-κB to translocate into the nucleus and to activate gene transcription.[228,229] S-nitrosylation via NO contributes to the inactivation of the NF-κB signaling pathway. The term S-nitrosylation is used to attach a NO group to the thiol group of the amino acid cysteine to form an S-nitrosothiol (SNO). Studies indicated that under basal conditions Iκκβ and p65, two important molecules of the canonical NF-κB activation cascade, can be S-nitrosylated, thereby keeping NF-κB in its inactive state.[230,231] Investigations revealed that inhibition of NO activity by ODQ (soluble guanylate cyclase inhibitor, primary NO receptor in the cytoplasm) activates NF-κB signaling, whereby stimulation of NO production had the opposite effect.[230,232,233] In line with these findings, we demonstrate in the current study that transcriptional levels of IκBα were reduced to near pre-ischemic conditions via inhalation of NO (Figure 28A). Additionally, we observed an increase of A20, another intrinsic NF-κB inhibitor protein, upon iNO administration (Figure 28B). The importance of A20 for maintaining nervous tissue homeostasis, preventing apoptosis, and downregulating inflammation has been shown previously.[234-238]

Another fast-inflammatory response that induces leukocyte adhesion is mediated through membrane clustering rather than transcriptional mechanisms. Under physiological conditions, the endothelial plasma membrane expresses only low levels of adhesion proteins. Upon inflammatory stimulation, adhesion proteins cluster within the cell membrane to increase their affinity for leukocytes integrins without the necessity to increase expression.[239,240] Small transmembrane proteins called tetraspanins connect to ICAM-1 and VCAM-1 to enable them to form clusters. Protein kinase C zeta (PKCz) additionally regulates ICAM-1 pooling. Stimulation via TNF-α showed to activate and translocate PKCz to the plasma membrane and to phosphorylate ICAM-1.[239-241] A study also suggests that VCAM-1 is transported from an intracellular pool to the endothelial surface after treatment with TNF-α.[242] In the current study, the protein expression for ICAM-1 was not changed upon iNO application (Figure 24). Many reports demonstrate that, next to its effects on NF-κB signaling, NO plays an important role in adhesion molecule transport and clustering.[243] Furthermore, eNOS prevents ICAM-1 clustering mediated by Src phosphorylation in endothelial cells.[244,245] In the current study, we did not detect any alterations of ICAM-1 expression on the protein level in isolated cerebral vessels isolated from iNO treated mice. Thus, the observed

reduction in leukocyte adhesion upon iNO might indeed is mediated by reduced clustering rather than reduced protein expression.

We investigated NOS expression in our experimental paradigm since iNO may have also affected endogenous NO production by NO synthases. Exogenous application of NO via inhalation following MCAo lowered eNOS expression to pre-ischemic conditions, whereas nNOS mRNA expression was increased (Figure 26). Possible mechanisms are the S-nitrosylation-induced inhibition of NF-κB activation by iNO. Under physiological conditions, NO derived from eNOS localized in the Golgi apparatus and neighboring caveolae inhibits NF-κB activation.[243,246,247] Activation of NF-κB signaling through a brief period of ischemia may thus activate eNOS expression, which is then restored by iNO though increased S-nitrosylation.[248,249]

Genetic deletion of iNOS indicated that NO from this source is responsible for the inhibition of NF-κB via nitrosylation in models of lung inflammation and colitis.[250,251] This could not be confirmed for the ischemic brain since no iNOS expression could be detected in the current study. The most likely reason is the relatively early time point of the investigation, which did not allow iNOS to be upregulated, as also suggested by others.[170]

This compares to contradictory investigations. One study reported that the NF-κB inactivation depends on NO concentrations beyond those reached by iNOS expression.[252] Another study in human vascular aortic smooth muscle cells demonstrated that NO is required for enhancing ICAM-1 expression if NOSs are unspecifically inhibited before LPS administration.[253] Overall, these results suggest that NF-κB activation or inhibition depends on the duration of inflammatory stimulation, the amount of NO, and where it originated. In summary, short-term inflammatory stimuli and optimal endogenous NO concentrations via eNOS inhibits adhesion molecule expression. The higher nNOS levels in the iNO treated group (Figure 26B) suggests a possible neuromodulatory role of nNOS after stroke. But so far, no data has indicated a connection between NF-κB and nNOS activation. Suggesting that exogenous restoration of NO levels creates homeostatic conditions in cerebral endothelial cells by inactivating the NF-κB signaling pathway and further NO production in the endothelium via eNOS was not needed. This is also substantiated by the decrease in cytokine (*IL-1*β, *IL-6, and TNF-α*) mRNA levels following iNO application which are also under the control of NF-κB signaling (Figure 21).

A further target regulated by NO is the protein expression on leukocytes, which are the counterparts of the adhesion molecules on endothelial cells. In this project, there was a tendency for CD49d (counterpart of VCAM-1) to be set to pre-ischemic levels upon iNO application following stroke (Figure 25). CD18 (counterpart of ICAM-1) expression, on the contrary, was not altered by iNO (Figure 25). Some studies point to the ability of NO to inhibit CD18.[217,254-256] The mechanism of action, however, is still unknown. One study suggests that CD18 inhibition on neutrophils through NO is linked to the activity of membrane-bound guanylate cyclase on the leukocytes.[254] That binding inhibits the conformational change of CD18 and hinders the binding to its counterpart ICAM-1 on the endothelium. Another study suggests a multifaceted series of events are responsible for the inhibition via the cytoskeleton of neutrophils.[256,257] Thus, despite some evidence from the literature, adhesion molecules on leukocytes do not seem to be the primary targets responsible for the observed anti-adhesive effect of iNO. Further research will need to address this point in more detail.

The route of NO application through the pulmonary circulation raises the question of whether NO reaches the desired location, in this case, the brain. Inhaled NO´s vascular action has been shown to extend beyond the former suggested pulmonary circulation by forming NO carriers involving nitrite, nitrate, or S-nitrosothiols (hemoglobin, cysteine, glutathione, albumin).[204,258,259] The increase of nitrite and nitrate in the circulating blood (Figure 29B) is consistent with this concept and has been supported by other studies using iNO and suggests that these intermediates, alone or together, may contribute to the observed neuroprotective effects of NO. In the presence of oxygenated hemoglobin, nitrite is known to be quickly oxidized to nitrate, explaining the much higher nitrate levels in the blood, also seen in the current study (Figure 29B).[152] Under conditions of reduced tissue oxygenation and acidosis seen in cerebral ischemia, NO is locally generated and released directly from the heme group along with oxygen, S-nitroso-albumin, or nitrite reduction.[259,260] Thus, iNO can execute its endogenous vasodilator effect beyond the pulmonary compartment, where it is already successfully established as therapeutic for pulmonary hypertension, to reach the cerebral vasculature and rescue the ischemic penumbra by increasing collateral blood flow.[200]

After being sufficiently confident that inhaled NO exerts NO activity in the brain, it would be interesting to know whether iNO activates the NO-sGC-CGMP signaling pathway in brain tissue. On the transcriptional level, iNO restored sGCα to pre-ischemic conditions, whereas sGCß was not altered (Figure 27C/D). Hence, iNO prevented the degradation of the central cGMP-forming enzyme that loses its function post-stroke due to reducing the sGCα subunit.[181,261,262] By preserving sGC

function, iNO was also able to restore cGMP levels after stroke (Figure 27B/I). Of note, iNO also maintained PGK function, a molecule with strong neuroprotective properties following ischemic stroke.[263] Hence, iNO did not only suppress pro-inflammatory upregulation of adhesion molecules but also restored neuroprotective signaling via the sGC-cGMP signaling pathway.

Despite the suggested positive characteristics of iNO, potential side effects should also be considered. In the presence of high oxygen concentrations, NO is oxidized to nitrogen dioxide that further reacts with superoxide to generate peroxynitrite. This can cause damage to a wide range of molecules such as DNA and proteins.[264] This can be overcome by applying only low NO concentration by inhalation of 50 ppm or below in combination with physiological oxygen concentrations. Therefore, under clinical conditions which require high concentrations of inspired oxygen rather than NO donors, then iNO should be applied.[265] Additionally, NO may also react with oxyhemoglobin, thereby forming methemoglobin, a form of hemoglobin that cannot bind and transport oxygen. Usually, this problem is of minor importance since reductases in red blood cells cleave met-hemoglobin efficiently. Nevertheless, patients receiving iNO should be monitored for methemoglobinemia. This is especially true for pediatric patients who express only low levels of met-Hb reductase.[266]

A promising approach to circumvent potential adverse effects of inhaled NO is the use of nanocarriers. In a rodent stroke model, nanoparticles loaded with L-arginine achieved a rapid targeting of the stroke lesion with the guidance of a magnetic field. This resulted in a local NO production that prompted vasodilation, recovery of blood flow, and reperfusion of the microvasculature.[267]

There is ample evidence that inflammatory processes contribute to injury formation following cerebral ischemia. The current study demonstrates that inhaled NO inhibits leukocyte adhesion and suppresses pro-inflammatory signaling within the brain parenchyma next to its vasoactive function. Thus, iNO influences multiple stroke-related pathophysiological pathways and may therefore represent a promising novel and safe therapeutic approach worth to be evaluated for therapeutic efficacy in stroke patients.

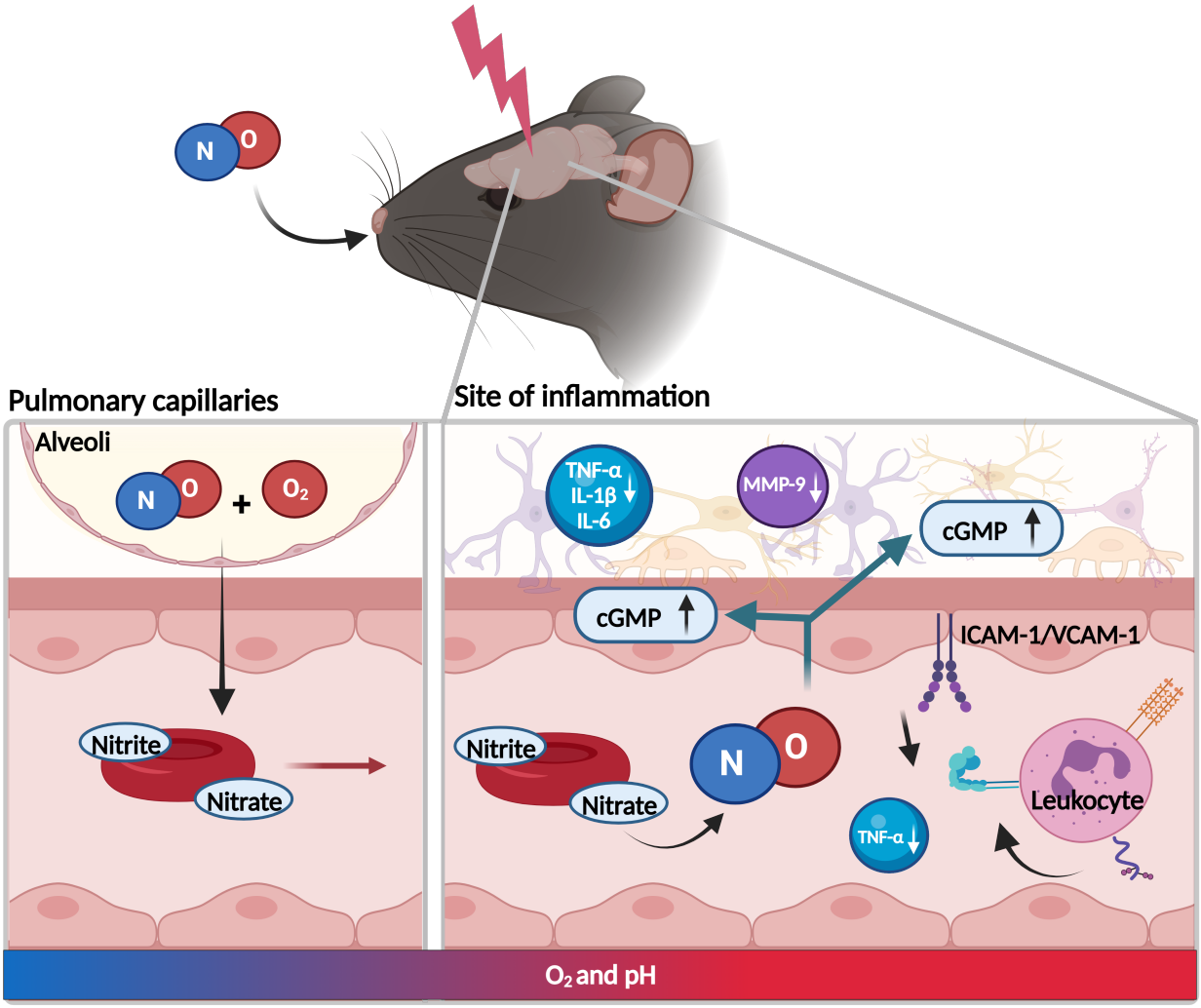

Figure 30: Graphical abstract of key findings regarding stroke and inhaled nitric oxide. These findings demonstrate that inhaled NO is transported through nitrite/nitrate to the site of inflammation, where it inhibits leukocyte-endothelial interaction, pro-inflammatory cytokines and restores cGMP levels in the brain tissue reducing vascular inflammation following ischemic stroke. (created with BioRender.com)

V. Appendix

1. Abbreviations

AMPA	α-amino-3-hydroxy-5-methyl-4-isoxazolepropionic acid
AMPK	AMP-activated protein kinase
Aß	ß-amyloid
ATP	adenosine triphosphate
BBB	blood-brain barrier
BCA	bicinchoninic acid
BSA	Bovine serum albumin
CaM	calmodulin
CaMKII	calmodulin-dependent protein kinase II
CCA	common carotid artery
cGMP	guanosine 3',5'-cyclic monophosphate
CNS	central nervous system
DAMP	danger-associated molecular patterns
DTT	Dithiothreitol
ECA	external carotid artery
EDFR	endothelium-derived relaxing factor
EDTA	Ethylenediaminetetraacetic acid
ELISA	Enzyme-linked immunosorbent assay
eNOS	endothelial nitric oxide synthase
ENOS	efficacy of nitric oxide in stroke trial
$_{ET}CO_2$	End-tidal carbon dioxide
FAD	flavin adenine dinucleotide
FITC	fluorescein isothiocyanate
FMN	Flavin mononucleotide
GMP	guanosine monophosphate
GTP	guanosine 5'-triphosphate
HCl	hydrochloric acid
HMGB1	high-mobility group protein1
Hsp90	heat shock protein 90

ICA	internal carotid artery
ICAM-1	intercellular adhesion molecule 1
IF	Immunofluorescence
Ig	immunoglobulin
IL-1ß	interleukin-1ß
IL-6	interleukin-6
INFγ	interferon-γ
iNO	inhaled nitric oxide
iNOS	inducible nitric oxide synthase
JAM	junctional adhesion molecule
LFA-1	lymphocyte function-associated antigen 1
LPS	lipopolysaccharide
Mac-1	macrophage-1 antigen
MCAo	middle cerebral artery occlusion
MEM	minimum essential medium
MMP	matrix metalloportease
mRNA	messenger RNA
mtDNA	mitochondrial DNA
NAPDH	nicotinamide adenine dinucleotide phosphate
NF-κB	nuclear factor kappa B
NMDA	N-methyl-D-aspartate receptor
nNOS	neuronal nitric oxide synthase
NO	Nitric oxide
NO_2	nitrite
NO3-	Nitrate
NOD	nitric oxide donors
NOS	nitric oxide synthase
PAGE	Polyacrylamide gel electrophoresis
PBS	Phosphate-buffered saline
PDE	phosphodiesterase
PFA	paraformaldehyde
PKA	protein kinase A
PKG	Protein kinase G

pO_2	peripheral oxygen
PSGL-1	P-selectin glycoprotein ligand-1
PVDF	Polyvinylidene fluoride
qrt-PCR	Quantitative real-time PCR
rCBF	regional cerebral blood flow
RIGHT	Rapid Intervention with GTN in Hypertensive stroke Trial
ROCK	Rho kinase
ROI	regions of interest
qRT-PCR	Reverse transcription-polymerase chain reaction
SAH	subarachnoid hemorrhage
SD	Standard deviation
SDS	sodium dodecyl sulphate
sGC	soluble guanylate cyclase
TBI	traumatic brain injury
TEMED	Tetramethylethylendiamine
TLR	toll like receptors
TNF-α	tumor necrosis factor-α
tPA	tissue-type plasminogen activator
Tris-HCL	tris(hydroxymethyl)aminomethane- hydrochloric acid
VCAM-1	vascular cell adhesion molecule 1
VEGF	vascular endothelial growth factor
VLA-4	very late antigen-4
WB	Western blotting

2. Equipment and consumables

Equipment (Catalogue #)	**Manufacturer**
Axio Imager M2 inverted microscope	Carl Zeiss, Oberkochen, Germany
Blood gas analyzer Rapidlab 348	Siemens, Munich, Germany
Capnograph Type 340	Hugo Sachs Elektronik, March, Germany
Centrifuge 5810 R	Eppendorf, Hamburg, Germany
Centrifuge Avanti J25	Beckmann-Coulter, Brea, CA, USA
Confocal laser scanning microscope LSM 800	Carl Zeiss, Oberkochen, Germany
Cryostat NX70	Thermo Fisher Scientific, Waltham, MA, USA
Dental drill	Rewatronik, Wald-Michelbach, Germany
Eclipse TS 100 microscope	Nikon, Tokio, Japan
FACSverse flow cytometer	Becton Dickinson, Franklin Lakes, NJ, USA
Forceps	Fine Science Tools, Heidelberg, Germany
Freezer -20°C mediLine	Liebherr, Kirchdorf an der Iller, Germany
Freezer -80°C Herafreeze	Thermo Fisher Scientific, Waltham, MA, USA
Fridge 4°C MediLine	Liebherr, Kirchdorf an der Iller, Germany
Fusion FX7	Vilber, Eberhardzell, Germany
Heater Control Module	FHC, Bowdoinham, ME, USA
Heating Cabinet	Scanbur, Karlslunde, Denmark
iMark Microplate Absorbance Reader	Bio-Rad Laboratories, Hercules, CA, USA
Immersion Objective Plan Apochromat, NA 1.0	Zeiss, Oberkochen, Germany
ITX Multi-gas monitor	Industrial Scientific, Pittsburgh, PA, USA
Li:Ti laser Chameleon	Coherent, Santa Clara, CA, USA
LightCycler 480	Roche Life Science, Penzberg, Germany
LSM 7 MP microscope	Zeiss, Oberkochen, Germany
MediHeat Fluid Heating Cabinet	Peco Services Ltd, Brough, UK
Microcentrifuge 5424 R	Eppendorf, Hamburg, Germany
Microvascular clip (# 18055-04)	Fine Science Tools, Heidelberg, Germany
Mini Trans-Blot® Cell	Bio-Rad Laboratories, Hercules, CA, USA
MiniVent Type 845	Hugo Sachs Elektronik, March, Germany
NanoDrop ND-1000 spectrophotometer	PEQLAB, Erlangen, Germany
Nitric oxide analyzer NOA 280i	Analytix, Boldon, UK
PeriFlux system 5000	Perimed, Järfälla, Sweden
Power lab system	AD Instruments, Sydney, Australia
Precellys tissue homogenizer	Bertin Instruments, Montigny-le-Bretonneux, France
Pressure perfusion system	Leica Biosystems, Wetzlar, Germany
Pulse oximeter PhysioSuite PS-03	Kent Scientific, Torrington, CT, USA
ROCKER 3D digital	Ika, Staufen, Germany

Stainless Steel Beads, 5 mm	Qiagen, Hilden, Germany
Stereomicroscope Leica M80	Leica Biosystems, Wetzlar, Germany
Stereotactic instrument	David Kopf Instruments, Tujunga, CA, USA
Thermomixer basic	CellMedia, Zeitz, Germany
TissueLyser LT	Qiagen, Hilden, Germany
VialTweeter sonicator	Hielscher, Teltow, Germany
Wheaton glass tissue grinder	DWK Life Sciences, Wertheim, Germany
XCell SureLock Mini-Cell Electrophoresis System	Thermo Fisher Scientific, Waltham, MA, USA

Consumables (Catalogue #)	**Manufacturer**
96-flat bottom well plate	Thermo Fisher Scientific, Waltham, MA, USA
96-well qRT plate	Applied Biosystems, Waltham, MA, USA
Bovine serum albumin (BSA)	Sigma-Aldrich, St. Louis, MO, USA
CA-Kleber Maxi-Cure	Drechseln und mehr, Weiden, Germany
CD16/CD32 Monoclonal Antibody (#14-0161-81)	Thermo Fisher Scientific, Waltham, MA, USA
Cell strainer (# 352340)	Becton Dickinson, Franklin Lakes, NJ, USA
Conical tubes	Becton Dickinson, Franklin Lakes, NJ, USA
Cover glass (4x4 mm)	Warner Instruments, Holliston, MA, USA
Cyano Veneer (# 152261)	Hager & Werken, Duisburg, Germany
Eye ointment Bepanthen	Bayer AG, Leverkusen, Germany
Ficoll p400	Sigma-Aldrich, St. Louis, MO, USA
Fine Polythene Tube (# 10793527)	Smiths Medical, Minneapolis, MN, USA
Hydrogel (# 70-01-1062)	Clearh2o, Westbrook, ME, USA
Immun-Blot® PVDF Membrane (# 1620177)	Bio-Rad Laboratories, Hercules, CA, USA
K3 EDTA tubes (#41.3395.005)	Sarstedt, Nümbrecht, Germany
MaXtract high-density tubes (# 129056)	Qiagen, Hilden, Germany
Minimum essential medium (MEM)	Thermo Fisher Scientific, Waltham, MA, USA
MT B500-0L240 Straight Microtip (# 91-00123)	Perimed, Järfälla, Sweden
Novex Empty Cassettes (# NC2015)	Thermo Fisher Scientific, Waltham, MA, USA
Petri dish (10 cm)	Greiner Bio-One, Kremsmünster, Austria
Precision Plus Protein Standards (#1610373)	Bio-Rad Laboratories, Hercules, CA, USA
Protein LoBind tubes (0.5 mL/ 1.5 mL)	Eppendorf, Hamburg, Germany
Round-Bottom Polystyrene Tubes	Corning, Corning, NY, USA
Scalpel No. 21	Feather, Osaka, Japan
Serological pipettes (10 mL/ 25 mL)	Greiner Bio-One, Kremsmünster, Austria
Silicone-coated filament (# 701912PK5Re)	Doccol Corporation, Sharon, MA, USA
Silk thread (# 18020-50)	Fine Science Tools, Heidelberg, Germany
Soft tissue homogenizing CK14(# 03961-1-203)	Bertin Instruments, Montigny-le-Bretonneux, France

Ssniff V1534	Ssniff, Soest, Germany
Super PAP Pen Liquid Blocker (# N71310-N)	Science Services, Munich, Germany
SuperFrost Plus slides	Thermo Fisher Scientific, Waltham, MA, USA
Suture (# SCD-3058G)	Covidien, Dublin, Ireland
Syringe (1 mL) with needle (25G) (# 9166033V)	B. Braun, Melsungen, Germany
TachoSil	Takeda Pharmaceutical, Tokio, Japan
Vasofix® Safety (20G) (# 4269110S-01)	B. Braun, Melsungen, Germany
Vivaspin 500 Centrifugal Concentrators (# VS0192)	Sartorius, Göttingen, Germany

3. Kits

Kits	**Manufacturer**
660 nm Protein-Assay (# 22660)	Thermo Fisher Scientific, Waltham, MA, USA
Ionic detergent compatibility reagent (#22663)	Thermo Fisher Scientific, Waltham, MA, USA
Omniscript Reverse Transcription Kit Quick-Start (# 205113)	Qiagen, Hilden, Germany
Pierce BCA Protein-Assay kit (# 23227)	Thermo Fisher Scientific, Waltham, MA, USA
QuantiFast SYBR Green RT-PCR Kit (# 204156)	Quanta, Hilden, Germany
RNase-Free DNase Set (# 79256)	Qiagen, Hilden, Germany
RNeasy Mini kit (# 74106)	Qiagen, Hilden, Germany

4. Chemicals and Reagents

Chemical/Reagent (Catalogue #)	**Manufacturer**
Acetone (99.5% for synthesis)	AppliChem, Darmstadt, Germany
Acrylamide/Bis solution, 37.5:1 (30%)	SERVA, Heidelberg, Germany
Ammonium persulfate	Sigma-Aldrich, St. Louis, MO, USA
Bovine serum albumin	Sigma-Aldrich, St. Louis, MO, USA
Buprenorphine	Schering-Plough, Kenilworth, NJ, USA
Carprofen	Zoetis, Parsippany, NJ, USA
DAPI 4’,6-Diamidine-2’-phenylindole dihydrochloride	Roche, Penzberg, Germany
Dithiothreitol (DTT)	Sigma-Aldrich, St. Louis, MO, USA
Ethanol	Merck, Darmstadt, Germany
Eukitt mounting medium (# 03989)	Sigma-Aldrich, St. Louis, MO, USA
Flow Cytometry staining buffer (#00-4222-26)	Thermo Fisher Scientific, Waltham, MA, USA
Fluorescein isothiocyanate (FITC) –dextran (# FD2000S)	Sigma-Aldrich, St. Louis, MO, USA
Fluoromount Aqueous Mounting Medium(#F4680-25ML)	Sigma-Aldrich, St. Louis, MO, USA
Glucose solution	B. Braun, Melsungen, Germany
Immobilon western HRP substrate	Merck, Darmstadt, Germany
Isoflurane (# 1214)	Cp-pharma, Burgdorf, Germany
Isopropanol	Merck, Darmstadt, Germany

Kresylechtviolett für NISSL (#11128.00500)	Morphisto, Offenbach am Main, Germany
Laemmli sample buffer (4x)	Bio-Rad Laboratories, Hercules, CA, USA
Lidocaine (2%)	B. Braun, Melsungen, Germany
Nitric oxide gas (268 mg/m^3)	Linde, Dublin, Ireland
Paraformaldehyd (PFA) 4 % (#11762)	Morphisto, Offenbach am Main, Germany
Phosphate buffered saline (PBS)	Klinikum der Universität München, Munich, Germany
Ponceau S solution	Sigma-Aldrich, St. Louis, MO, USA
QIAzol Lysis Reagent (#79306)	Qiagen, Hilden, Germany
Rhodamin6G (# 252433)	Sigma-Aldrich, St. Louis, MO, USA
Rotihistol (# 6640.1)	Carl Roth, Karlsruhe, Germany
Saline	Berlin-Chemie AG, Berlin, Germany
Skim milk powder	Sigma-Aldrich, St. Louis, MO, USA
Sodium dodecyl sulfate	Sigma-Aldrich, St. Louis, MO, USA
Tetramethylethylendiamin (TEMED)	Carl Roth, Karlsruhe, Germany
Tissue-Tek embedding medium	Sakura Finetek, Alphen aan den Rijn, Netherlands
Tris base (Trizma)	Sigma-Aldrich, St. Louis, MO, USA
Tween 20	Carl Roth, Karlsruhe, Germany

5. Software

Software	**Manufacturer**
LabChart 8 Reader	AD Instruments, Sydney, Australia
Nucline NanoScan software (Version 3.04.014.0000)	Mediso, Budapest, Hungary
ImageJ (Version 1.53i)	National Institute of Health, Bethesda, MD, USA
LabChart software (Version 8.0)	ADInstruments, Sydney, Australia
GraphPad Prism 9.0 software	GraphPad Software Inc., San Diego, CA, USA
Imaris (Version 9.4)	Bitplane AG, Zürich, Switzerland
FlowJo software (Version v10.7)	Becton Dickinson, Franklin Lakes, NJ, USA
ZEN software (Version 14.0.0.201)	Zeiss, Oberkochen, Germany

6. List of figures

7. List of tables

8. References

1. Collaborators, G.S. Global, regional, and national burden of stroke, 1990-2016: a systematic analysis for the Global Burden of Disease Study 2016. *Lancet Neurol* **18**, 439-458 (2019).
2. Johnson, W., Onuma, O., Owolabi, M. & Sachdev, S. Stroke: a global response is needed. *Bull World Health Organ* **94**, 634-634a (2016).
3. Hankey, G.J. Stroke. *Lancet* **389**, 641-654 (2017).
4. Boehme, A.K., Esenwa, C. & Elkind, M.S. Stroke Risk Factors, Genetics, and Prevention. *Circ Res* **120**, 472-495 (2017).
5. Astrup, J., Siesjö, B.K. & Symon, L. Thresholds in cerebral ischemia - the ischemic penumbra. *Stroke* **12**, 723-725 (1981).
6. Tissue plasminogen activator for acute ischemic stroke. *N Engl J Med* **333**, 1581-1587 (1995).
7. Powers, W.J.*, et al.* Guidelines for the Early Management of Patients With Acute Ischemic Stroke: 2019 Update to the 2018 Guidelines for the Early Management of Acute Ischemic Stroke: A Guideline for Healthcare Professionals From the American Heart Association/American Stroke Association. *Stroke* **50**, e344-e418 (2019).
8. Khalessi, A.A.*, et al.* Acute stroke intervention. *JACC Cardiovasc Interv* **4**, 261-269 (2011).
9. Mair, G. & Wardlaw, J.M. Imaging of acute stroke prior to treatment: current practice and evolving techniques. *Br J Radiol* **87**, 20140216 (2014).
10. Henderson, S.J., Weitz, J.I. & Kim, P.Y. Fibrinolysis: strategies to enhance the treatment of acute ischemic stroke. *J Thromb Haemost* **16**, 1932-1940 (2018).
11. Jovin, T.G.*, et al.* Thrombectomy within 8 hours after symptom onset in ischemic stroke. *N Engl J Med* **372**, 2296-2306 (2015).
12. Saver, J.L.*, et al.* Stent-retriever thrombectomy after intravenous t-PA vs. t-PA alone in stroke. *N Engl J Med* **372**, 2285-2295 (2015).
13. O'Connor, R.E., McGraw, P. & Edelsohn, L. Thrombolytic therapy for acute ischemic stroke: why the majority of patients remain ineligible for treatment. *Ann Emerg Med* **33**, 9-14 (1999).
14. de Los Ríos la Rosa, F.*, et al.* Eligibility for Intravenous Recombinant Tissue-Type Plasminogen Activator Within a Population: The Effect of the European Cooperative Acute Stroke Study (ECASS) III Trial. *Stroke* **43**, 1591-1595 (2012).
15. Kernan, W.N.*, et al.* Guidelines for the prevention of stroke in patients with stroke and transient ischemic attack: a guideline for healthcare professionals from the American Heart Association/American Stroke Association. *Stroke* **45**, 2160-2236 (2014).
16. Nardi, K.*, et al.* Admission leukocytosis in acute cerebral ischemia: influence on early outcome. *J Stroke Cerebrovasc Dis* **21**, 819-824 (2012).
17. Burrows, F.E., Bray, N., Denes, A., Allan, S.M. & Schiessl, I. Delayed reperfusion deficits after experimental stroke account for increased pathophysiology. *J Cereb Blood Flow Metab* **35**, 277-284 (2015).
18. Enzmann, G., Kargaran, S. & Engelhardt, B. Ischemia-reperfusion injury in stroke: impact of the brain barriers and brain immune privilege on neutrophil function. *Ther Adv Neurol Disord* **11**, 1756286418794184 (2018).
19. Jiang, X.*, et al.* Blood-brain barrier dysfunction and recovery after ischemic stroke. *Prog Neurobiol* **163-164**, 144-171 (2018).
20. Balch, M.H.H., Nimjee, S.M., Rink, C. & Hannawi, Y. Beyond the Brain: The Systemic Pathophysiological Response to Acute Ischemic Stroke. *J Stroke* **22**, 159-172 (2020).
21. Meisel, C., Schwab, J.M., Prass, K., Meisel, A. & Dirnagl, U. Central nervous system injury-induced immune deficiency syndrome. *Nat Rev Neurosci* **6**, 775-786 (2005).

22. Langhorne, P.*, et al.* Medical complications after stroke: a multicenter study. *Stroke* **31**, 1223-1229 (2000).
23. Anrather, J. & Iadecola, C. Inflammation and Stroke: An Overview. *Neurotherapeutics* **13**, 661-670 (2016).
24. Kawabori, M. & Yenari, M.A. Inflammatory responses in brain ischemia. *Curr Med Chem* **22**, 1258-1277 (2015).
25. Abbas, A.K., Lichtman, A.H. & Pillai, S. *Cellular and molecular immunology*, (Elsevier Saunders, Philadelphia, PA, 2015).
26. Ishikawa, M.*, et al.* Platelet-leukocyte-endothelial cell interactions after middle cerebral artery occlusion and reperfusion. *J Cereb Blood Flow Metab* **24**, 907-915 (2004).
27. Okada, Y.*, et al.* P-selectin and intercellular adhesion molecule-1 expression after focal brain ischemia and reperfusion. *Stroke* **25**, 202-211 (1994).
28. Wu, F., Liu, L. & Zhou, H. Endothelial cell activation in central nervous system inflammation. *J Leukoc Biol* **101**, 1119-1132 (2017).
29. Huang, J.*, et al.* Postischemic cerebrovascular E-selectin expression mediates tissue injury in murine stroke. *Stroke* **31**, 3047-3053 (2000).
30. Suzuki, H.*, et al.* Postischemic expression of P-selectin immunoreactivity in rat brain. *Neurosci Lett* **228**, 151-154 (1997).
31. Hentzen, E.R.*, et al.* Sequential binding of CD11a/CD18 and CD11b/CD18 defines neutrophil capture and stable adhesion to intercellular adhesion molecule-1. *Blood* **95**, 911-920 (2000).
32. Arumugam, T.V.*, et al.* Contributions of LFA-1 and Mac-1 to brain injury and microvascular dysfunction induced by transient middle cerebral artery occlusion. *Am J Physiol Heart Circ Physiol* **287**, H2555-2560 (2004).
33. Campanella, M., Sciorati, C., Tarozzo, G. & Beltramo, M. Flow cytometric analysis of inflammatory cells in ischemic rat brain. *Stroke* **33**, 586-592 (2002).
34. Gidday, J.M., Park, T.S., Gonzales, E.R. & Beetsch, J.W. CD18-dependent leukocyte adherence and vascular injury in pig cerebral circulation after ischemia. *Am J Physiol* **272**, H2622-2629 (1997).
35. Kim, J.S.*, et al.* Adhesive glycoproteins CD11a and CD18 are upregulated in the leukocytes from patients with ischemic stroke and transient ischemic attacks. *J Neurol Sci* **128**, 45-50 (1995).
36. Fan, Z.*, et al.* Neutrophil recruitment limited by high-affinity bent β2 integrin binding ligand in cis. *Nat Commun* **7**, 12658 (2016).
37. Blann, A.*, et al.* Soluble intercelluar adhesion molecule-1, E-selectin, vascular cell adhesion molecule-1 and von Willebrand factor in stroke. *Blood Coagul Fibrinolysis* **10**, 277-284 (1999).
38. Stanimirovic, D., Shapiro, A., Wong, J., Hutchison, J. & Durkin, J. The induction of ICAM-1 in human cerebromicrovascular endothelial cells (HCEC) by ischemia-like conditions promotes enhanced neutrophil/HCEC adhesion. *J Neuroimmunol* **76**, 193-205 (1997).
39. Woodfin, A.*, et al.* JAM-A mediates neutrophil transmigration in a stimulus-specific manner in vivo: evidence for sequential roles for JAM-A and PECAM-1 in neutrophil transmigration. *Blood* **110**, 1848-1856 (2007).
40. Shihata, W.A., Michell, D.L., Andrews, K.L. & Chin-Dusting, J.P. Caveolae: A Role in Endothelial Inflammation and Mechanotransduction? *Front Physiol* **7**, 628 (2016).
41. McMenamin, P.G. Distribution and phenotype of dendritic cells and resident tissue macrophages in the dura mater, leptomeninges, and choroid plexus of the rat brain as demonstrated in wholemount preparations. *J Comp Neurol* **405**, 553-562 (1999).

42. Kivisäkk, P.*, et al.* Human cerebrospinal fluid central memory CD4+ T cells: evidence for trafficking through choroid plexus and meninges via P-selectin. *Proc Natl Acad Sci U S A* **100**, 8389-8394 (2003).
43. Hutchings, M. & Weller, R.O. Anatomical relationships of the pia mater to cerebral blood vessels in man. *J Neurosurg* **65**, 316-325 (1986).
44. Yilmaz, G. & Granger, D.N. Leukocyte recruitment and ischemic brain injury. *Neuromolecular Med* **12**, 193-204 (2010).
45. Emerich, D.F., Dean, R.L., 3rd & Bartus, R.T. The role of leukocytes following cerebral ischemia: pathogenic variable or bystander reaction to emerging infarct? *Exp Neurol* **173**, 168-181 (2002).
46. Ao, L.Y.*, et al.* Immune Cells After Ischemic Stroke Onset: Roles, Migration, and Target Intervention. *J Mol Neurosci* **66**, 342-355 (2018).
47. Dirnagl, U., Iadecola, C. & Moskowitz, M.A. Pathobiology of ischaemic stroke: an integrated view. *Trends Neurosci* **22**, 391-397 (1999).
48. Weston, R.M., Jones, N.M., Jarrott, B. & Callaway, J.K. Inflammatory cell infiltration after endothelin-1-induced cerebral ischemia: histochemical and myeloperoxidase correlation with temporal changes in brain injury. *J Cereb Blood Flow Metab* **27**, 100-114 (2007).
49. El Amki, M.*, et al.* Neutrophils Obstructing Brain Capillaries Are a Major Cause of No-Reflow in Ischemic Stroke. *Cell Rep* **33**, 108260 (2020).
50. Perez-de-Puig, I.*, et al.* Neutrophil recruitment to the brain in mouse and human ischemic stroke. *Acta Neuropathol* **129**, 239-257 (2015).
51. Enzmann, G.*, et al.* The neurovascular unit as a selective barrier to polymorphonuclear granulocyte (PMN) infiltration into the brain after ischemic injury. *Acta Neuropathol* **125**, 395-412 (2013).
52. Vallés, J.*, et al.* Neutrophil extracellular traps are increased in patients with acute ischemic stroke: prognostic significance. *Thromb Haemost* **117**, 1919-1929 (2017).
53. Kollikowski, A.M.*, et al.* Local Leukocyte Invasion during Hyperacute Human Ischemic Stroke. *Ann Neurol* **87**, 466-479 (2020).
54. Weisenburger-Lile, D.*, et al.* Harmful neutrophil subsets in patients with ischemic stroke. *Association with disease severity* **6**, e571 (2019).
55. Gelderblom, M.*, et al.* Temporal and spatial dynamics of cerebral immune cell accumulation in stroke. *Stroke* **40**, 1849-1857 (2009).
56. Buck, B.H.*, et al.* Early neutrophilia is associated with volume of ischemic tissue in acute stroke. *Stroke* **39**, 355-360 (2008).
57. Xue, J.*, et al.* Neutrophil-to-Lymphocyte Ratio Is a Prognostic Marker in Acute Ischemic Stroke. *J Stroke Cerebrovasc Dis* **26**, 650-657 (2017).
58. Chu, H.X.*, et al.* Immune cell infiltration in malignant middle cerebral artery infarction: comparison with transient cerebral ischemia. *J Cereb Blood Flow Metab* **34**, 450-459 (2014).
59. Garcia, J.H.*, et al.* Influx of leukocytes and platelets in an evolving brain infarct (Wistar rat). *Am J Pathol* **144**, 188-199 (1994).
60. Garcia-Bonilla, L.*, et al.* Spatio-temporal profile, phenotypic diversity, and fate of recruited monocytes into the post-ischemic brain. *J Neuroinflammation* **13**, 285 (2016).
61. ElAli, A. & Jean LeBlanc, N. The Role of Monocytes in Ischemic Stroke Pathobiology: New Avenues to Explore. *Front Aging Neurosci* **8**, 29 (2016).
62. Zrzavy, T.*, et al.* Dominant role of microglial and macrophage innate immune responses in human ischemic infarcts. *Brain Pathol* **28**, 791-805 (2018).
63. Kostulas, N.*, et al.* Dendritic cells are present in ischemic brain after permanent middle cerebral artery occlusion in the rat. *Stroke* **33**, 1129-1134 (2002).

64. Felger, J.C.*, et al.* Brain dendritic cells in ischemic stroke: time course, activation state, and origin. *Brain Behav Immun* **24**, 724-737 (2010).
65. Yilmaz, A.*, et al.* Transient decrease in circulating dendritic cell precursors after acute stroke: potential recruitment into the brain. *Clin Sci (Lond)* **118**, 147-157 (2009).
66. Feng, Y.*, et al.* Infiltration and persistence of lymphocytes during late-stage cerebral ischemia in middle cerebral artery occlusion and photothrombotic stroke models. *J Neuroinflammation* **14**, 248 (2017).
67. Gill, D. & Veltkamp, R. Dynamics of T cell responses after stroke. *Curr Opin Pharmacol* **26**, 26-32 (2016).
68. Jander, S., Kraemer, M., Schroeter, M., Witte, O.W. & Stoll, G. Lymphocytic infiltration and expression of intercellular adhesion molecule-1 in photochemically induced ischemia of the rat cortex. *J Cereb Blood Flow Metab* **15**, 42-51 (1995).
69. Llovera, G.*, et al.* The choroid plexus is a key cerebral invasion route for T cells after stroke. *Acta Neuropathol* **134**, 851-868 (2017).
70. Tuttolomondo, A.*, et al.* Peripheral frequency of CD4+ CD28- cells in acute ischemic stroke: relationship with stroke subtype and severity markers. *Medicine (Baltimore)* **94**, e813 (2015).
71. Kitamura, D., Roes, J., Kühn, R. & Rajewsky, K. A B cell-deficient mouse by targeted disruption of the membrane exon of the immunoglobulin mu chain gene. *Nature* **350**, 423-426 (1991).
72. Ren, X.*, et al.* Regulatory B cells limit CNS inflammation and neurologic deficits in murine experimental stroke. *J Neurosci* **31**, 8556-8563 (2011).
73. Yilmaz, G., Arumugam, T.V., Stokes, K.Y. & Granger, D.N. Role of T lymphocytes and interferon-gamma in ischemic stroke. *Circulation* **113**, 2105-2112 (2006).
74. Kleinschnitz, C.*, et al.* Early detrimental T-cell effects in experimental cerebral ischemia are neither related to adaptive immunity nor thrombus formation. *Blood* **115**, 3835-3842 (2010).
75. Doyle, K.P.*, et al.* B-lymphocyte-mediated delayed cognitive impairment following stroke. *J Neurosci* **35**, 2133-2145 (2015).
76. Prüss, H.*, et al.* Evidence of intrathecal immunoglobulin synthesis in stroke: a cohort study. *Arch Neurol* **69**, 714-717 (2012).
77. Mracsko, E.*, et al.* Antigen dependently activated cluster of differentiation 8-positive T cells cause perforin-mediated neurotoxicity in experimental stroke. *J Neurosci* **34**, 16784-16795 (2014).
78. Gan, Y.*, et al.* Ischemic neurons recruit natural killer cells that accelerate brain infarction. *Proc Natl Acad Sci U S A* **111**, 2704-2709 (2014).
79. Liu, Q.*, et al.* Brain Ischemia Suppresses Immunity in the Periphery and Brain via Different Neurogenic Innervations. *Immunity* **46**, 474-487 (2017).
80. Neumann, J.*, et al.* Beware the intruder: Real time observation of infiltrated neutrophils and neutrophil-Microglia interaction during stroke in vivo. *PLoS One* **13**, e0193970 (2018).
81. Neumann, J.*, et al.* Very-late-antigen-4 (VLA-4)-mediated brain invasion by neutrophils leads to interactions with microglia, increased ischemic injury and impaired behavior in experimental stroke. *Acta Neuropathol* **129**, 259-277 (2015).
82. Sato, M., Paschen, W., Pawlik, G. & Heiss, W.D. Neurologic deficit and cerebral ATP depletion after temporary focal ischemia in cats. *J Cereb Blood Flow Metab* **4**, 173-177 (1984).
83. Mies, G., Ishimaru, S., Xie, Y., Seo, K. & Hossmann, K.A. Ischemic thresholds of cerebral protein synthesis and energy state following middle cerebral artery occlusion in rat. *J Cereb Blood Flow Metab* **11**, 753-761 (1991).

84. Veldhuis, W.B.*, et al.* In vivo excitotoxicity induced by ouabain, a Na+/K+-ATPase inhibitor. *J Cereb Blood Flow Metab* **23**, 62-74 (2003).
85. Sibarov, D.A., Bolshakov, A.E., Abushik, P.A., Krivoi, II & Antonov, S.M. Na+,K+-ATPase functionally interacts with the plasma membrane Na+,Ca2+ exchanger to prevent Ca2+ overload and neuronal apoptosis in excitotoxic stress. *J Pharmacol Exp Ther* **343**, 596-607 (2012).
86. Ankarcrona, M.*, et al.* Glutamate-induced neuronal death: a succession of necrosis or apoptosis depending on mitochondrial function. *Neuron* **15**, 961-973 (1995).
87. Rothman, S.M. & Olney, J.W. Glutamate and the pathophysiology of hypoxic--ischemic brain damage. *Ann Neurol* **19**, 105-111 (1986).
88. Mori, T.*, et al.* Attenuation of a delayed increase in the extracellular glutamate level in the peri-infarct area following focal cerebral ischemia by a novel agent ONO-2506. *Neurochem Int* **45**, 381-387 (2004).
89. Zhao, Y.*, et al.* Chrysophanol attenuates nitrosative/oxidative stress injury in a mouse model of focal cerebral ischemia/reperfusion. *J Pharmacol Sci* **138**, 16-22 (2018).
90. Liesz, A.*, et al.* DAMP signaling is a key pathway inducing immune modulation after brain injury. *J Neurosci* **35**, 583-598 (2015).
91. Yamaguchi, A.*, et al.* Temporal expression profiling of DAMPs-related genes revealed the biphasic post-ischemic inflammation in the experimental stroke model. *Mol Brain* **13**, 57 (2020).
92. Goldstein, R.S.*, et al.* Elevated high-mobility group box 1 levels in patients with cerebral and myocardial ischemia. *Shock* **25**, 571-574 (2006).
93. Kono, H., Chen, C.J., Ontiveros, F. & Rock, K.L. Uric acid promotes an acute inflammatory response to sterile cell death in mice. *J Clin Invest* **120**, 1939-1949 (2010).
94. Bours, M.J., Swennen, E.L., Di Virgilio, F., Cronstein, B.N. & Dagnelie, P.C. Adenosine 5'-triphosphate and adenosine as endogenous signaling molecules in immunity and inflammation. *Pharmacol Ther* **112**, 358-404 (2006).
95. Quintana, F.J. & Cohen, I.R. Heat shock proteins as endogenous adjuvants in sterile and septic inflammation. *J Immunol* **175**, 2777-2782 (2005).
96. Kuboyama, K.*, et al.* Astrocytic P2Y(1) receptor is involved in the regulation of cytokine/chemokine transcription and cerebral damage in a rat model of cerebral ischemia. *J Cereb Blood Flow Metab* **31**, 1930-1941 (2011).
97. Zhang, Z., Chopp, M. & Powers, C. Temporal profile of microglial response following transient (2 h) middle cerebral artery occlusion. *Brain Res* **744**, 189-198 (1997).
98. Denes, A.*, et al.* Proliferating resident microglia after focal cerebral ischaemia in mice. *J Cereb Blood Flow Metab* **27**, 1941-1953 (2007).
99. Nayak, A.R.*, et al.* Time course of inflammatory cytokines in acute ischemic stroke patients and their relation to inter-alfa trypsin inhibitor heavy chain 4 and outcome. *Ann Indian Acad Neurol* **15**, 181-185 (2012).
100. Gregersen, R., Lambertsen, K. & Finsen, B. Microglia and macrophages are the major source of tumor necrosis factor in permanent middle cerebral artery occlusion in mice. *J Cereb Blood Flow Metab* **20**, 53-65 (2000).
101. Caso, J.R., Moro, M.A., Lorenzo, P., Lizasoain, I. & Leza, J.C. Involvement of IL-1beta in acute stress-induced worsening of cerebral ischaemia in rats. *Eur Neuropsychopharmacol* **17**, 600-607 (2007).
102. Barone, F.C.*, et al.* Tumor necrosis factor-alpha. A mediator of focal ischemic brain injury. *Stroke* **28**, 1233-1244 (1997).
103. Ritzel, R.M.*, et al.* Functional differences between microglia and monocytes after ischemic stroke. *J Neuroinflammation* **12**, 106 (2015).

104. Drieu, A., Levard, D., Vivien, D. & Rubio, M. Anti-inflammatory treatments for stroke: from bench to bedside. *Ther Adv Neurol Disord* **11**, 1756286418789854 (2018).
105. Emsley, H.C*., et al.* A randomised phase II study of interleukin-1 receptor antagonist in acute stroke patients. *J Neurol Neurosurg Psychiatry* **76**, 1366-1372 (2005).
106. Smith, C.J*., et al.* SCIL-STROKE (Subcutaneous Interleukin-1 Receptor Antagonist in Ischemic Stroke): A Randomized Controlled Phase 2 Trial. *Stroke* **49**, 1210-1216 (2018).
107. Kohler, E*., et al.* Intravenous minocycline in acute stroke: a randomized, controlled pilot study and meta-analysis. *Stroke* **44**, 2493-2499 (2013).
108. Malhotra, K*., et al.* Minocycline for acute stroke treatment: a systematic review and meta-analysis of randomized clinical trials. *J Neurol* **265**, 1871-1879 (2018).
109. Elkind, M.S.V*., et al.* Natalizumab in acute ischemic stroke (ACTION II): A randomized, placebo-controlled trial. *Neurology* **95**, e1091-e1104 (2020).
110. Elkins, J*., et al.* Safety and efficacy of natalizumab in patients with acute ischaemic stroke (ACTION): a randomised, placebo-controlled, double-blind phase 2 trial. *The Lancet Neurology* **16**, 217-226 (2017).
111. Krams, M*., et al.* Acute Stroke Therapy by Inhibition of Neutrophils (ASTIN): an adaptive dose-response study of UK-279,276 in acute ischemic stroke. *Stroke* **34**, 2543-2548 (2003).
112. Lees, K.R., Diener, H.C., Asplund, K. & Krams, M. UK-279,276, a neutrophil inhibitory glycoprotein, in acute stroke: tolerability and pharmacokinetics. *Stroke* **34**, 1704-1709 (2003).
113. Use of anti-ICAM-1 therapy in ischemic stroke: results of the Enlimomab Acute Stroke Trial. *Neurology* **57**, 1428-1434 (2001).
114. Liu, J., Zhang, C., Tao, W. & Liu, M. Systematic review and meta-analysis of the efficacy of sphingosine-1-phosphate (S1P) receptor agonist FTY720 (fingolimod) in animal models of stroke. *Int J Neurosci* **123**, 163-169 (2013).
115. Zhang, S*., et al.* Rationale and design of combination of an immune modulator Fingolimod with Alteplase bridging with Mechanical Thrombectomy in Acute Ischemic Stroke (FAMTAIS) trial. *Int J Stroke* **12**, 906-909 (2017).
116. O'Collins, V.E*., et al.* 1,026 experimental treatments in acute stroke. *Ann Neurol* **59**, 467-477 (2006).
117. Malone, K., Amu, S., Moore, A.C. & Waeber, C. The immune system and stroke: from current targets to future therapy. *Immunol Cell Biol* **97**, 5-16 (2019).
118. Ghimire, K., Altmann, H.M., Straub, A.C. & Isenberg, J.S. Nitric oxide: what's new to NO? *Am J Physiol Cell Physiol* **312**, C254-c262 (2017).
119. Priestley, J. & Hey, W. Observations on Different Kinds of Air. By Joseph Priestley, L L. D. F. R. S. *Philosophical Transactions (1683-1775)* **62**, 147-264 (1772).
120. Furchgott, R.F. Endothelium-derived relaxing factor: discovery, early studies, and identification as nitric oxide. *Biosci Rep* **19**, 235-251 (1999).
121. Ignarro, L.J., Buga, G.M., Wood, K.S., Byrns, R.E. & Chaudhuri, G. Endothelium-derived relaxing factor produced and released from artery and vein is nitric oxide. *Proc Natl Acad Sci U S A* **84**, 9265-9269 (1987).
122. Cyr, A.R., Huckaby, L.V., Shiva, S.S. & Zuckerbraun, B.S. Nitric Oxide and Endothelial Dysfunction. *Crit Care Clin* **36**, 307-321 (2020).
123. Dawson, T.M. & Dawson, V.L. Nitric Oxide Signaling in Neurodegeneration and Cell Death. *Adv Pharmacol* **82**, 57-83 (2018).
124. Bogdan, C. Nitric oxide and the immune response. *Nat Immunol* **2**, 907-916 (2001).
125. Pollock, J.S*., et al.* Characterization and localization of endothelial nitric oxide synthase using specific monoclonal antibodies. *Am J Physiol* **265**, C1379-1387 (1993).

126. Bredt, D.S*., et al.* Nitric oxide synthase protein and mRNA are discretely localized in neuronal populations of the mammalian CNS together with NADPH diaphorase. *Neuron* **7**, 615-624 (1991).
127. Nagpal, L. & Panda, K. Characterization of calmodulin-free murine inducible nitric-oxide synthase. *PLoS One* **10**, e0121782 (2015).
128. Griffith, O.W. & Stuehr, D.J. Nitric oxide synthases: properties and catalytic mechanism. *Annu Rev Physiol* **57**, 707-736 (1995).
129. Li, H. & Poulos, T.L. Structure-function studies on nitric oxide synthases. *J Inorg Biochem* **99**, 293-305 (2005).
130. Nathan, C. & Xie, Q.W. Nitric oxide synthases: roles, tolls, and controls. *Cell* **78**, 915-918 (1994).
131. Marsden, P.A*., et al.* Structure and chromosomal localization of the human constitutive endothelial nitric oxide synthase gene. *J Biol Chem* **268**, 17478-17488 (1993).
132. Abe, K*., et al.* Upregulation of protein-tyrosine nitration in the anterior horn cells of amyotrophic lateral sclerosis. *Neurol Res* **19**, 124-128 (1997).
133. Colasanti, M*., et al.* Expression of a NOS-III-like protein in human astroglial cell culture. *Biochem Biophys Res Commun* **252**, 552-555 (1998).
134. Reiling, N*., et al.* Nitric oxide synthase: expression of the endothelial, Ca2+/calmodulin-dependent isoform in human B and T lymphocytes. *Eur J Immunol* **26**, 511-516 (1996).
135. Helfrich, M.H*., et al.* Expression of nitric oxide synthase isoforms in bone and bone cell cultures. *J Bone Miner Res* **12**, 1108-1115 (1997).
136. Wang, R., Ghahary, A., Shen, Y.J., Scott, P.G. & Tredget, E.E. Human dermal fibroblasts produce nitric oxide and express both constitutive and inducible nitric oxide synthase isoforms. *J Invest Dermatol* **106**, 419-427 (1996).
137. García-Cardeña, G*., et al.* Dynamic activation of endothelial nitric oxide synthase by Hsp90. *Nature* **392**, 821-824 (1998).
138. Pritchard, K.A., Jr*., et al.* Heat shock protein 90 mediates the balance of nitric oxide and superoxide anion from endothelial nitric-oxide synthase. *J Biol Chem* **276**, 17621-17624 (2001).
139. Song, Y., Cardounel, A.J., Zweier, J.L. & Xia, Y. Inhibition of superoxide generation from neuronal nitric oxide synthase by heat shock protein 90: implications in NOS regulation. *Biochemistry* **41**, 10616-10622 (2002).
140. Gratton, J.P*., et al.* Reconstitution of an endothelial nitric-oxide synthase (eNOS), hsp90, and caveolin-1 complex in vitro. Evidence that hsp90 facilitates calmodulin stimulated displacement of eNOS from caveolin-1. *J Biol Chem* **275**, 22268-22272 (2000).
141. Drab, M*., et al.* Loss of caveolae, vascular dysfunction, and pulmonary defects in caveolin-1 gene-disrupted mice. *Science* **293**, 2449-2452 (2001).
142. Fulton, D*., et al.* Regulation of endothelium-derived nitric oxide production by the protein kinase Akt. *Nature* **399**, 597-601 (1999).
143. Schleicher, M*., et al.* The Akt1-eNOS axis illustrates the specificity of kinase-substrate relationships in vivo. *Sci Signal* **2**, ra41 (2009).
144. McCabe, T.J., Fulton, D., Roman, L.J. & Sessa, W.C. Enhanced electron flux and reduced calmodulin dissociation may explain "calcium-independent" eNOS activation by phosphorylation. *J Biol Chem* **275**, 6123-6128 (2000).
145. Bredt, D.S. & Snyder, S.H. Transient nitric oxide synthase neurons in embryonic cerebral cortical plate, sensory ganglia, and olfactory epithelium. *Neuron* **13**, 301-313 (1994).
146. Culcasi, M., Lafon-Cazal, M., Pietri, S. & Bockaert, J. Glutamate receptors induce a burst of superoxide via activation of nitric oxide synthase in arginine-depleted neurons. *J Biol Chem* **269**, 12589-12593 (1994).

147. Nakane, M., Mitchell, J., Förstermann, U. & Murad, F. Phosphorylation by calcium calmodulin-dependent protein kinase II and protein kinase C modulates the activity of nitric oxide synthase. *Biochem Biophys Res Commun* **180**, 1396-1402 (1991).
148. Cho, H.J.*, et al.* Calmodulin is a subunit of nitric oxide synthase from macrophages. *J Exp Med* **176**, 599-604 (1992).
149. Kamijo, R.*, et al.* Requirement for transcription factor IRF-1 in NO synthase induction in macrophages. *Science* **263**, 1612-1615 (1994).
150. Kato, C., Mikami, M. & Saito, K. Nitric oxide production and iNOS mRNA expression in mice induced by repeated stimulation with live Fusobacterium nucleatum. *Microbiol Immunol* **45**, 69-78 (2001).
151. Ding, M. & Merrill, J.E. The kinetics and regulation of the induction of type II nitric oxide synthase and nitric oxide in human fetal glial cell cultures. *Mol Psychiatry* **2**, 117-119 (1997).
152. Moncada, S., Palmer, R.M. & Higgs, E.A. Nitric oxide: physiology, pathophysiology, and pharmacology. *Pharmacol Rev* **43**, 109-142 (1991).
153. Lundberg, J.O., Carlstrom, M. & Weitzberg, E. Metabolic Effects of Dietary Nitrate in Health and Disease. *Cell Metab* **28**, 9-22 (2018).
154. Björne, H.H.*, et al.* Nitrite in saliva increases gastric mucosal blood flow and mucus thickness. *J Clin Invest* **113**, 106-114 (2004).
155. Benjamin, N.*, et al.* Stomach NO synthesis. *Nature* **368**, 502-502 (1994).
156. Zweier, J.L., Wang, P., Samouilov, A. & Kuppusamy, P. Enzyme-independent formation of nitric oxide in biological tissues. *Nat Med* **1**, 804-809 (1995).
157. Li, H., Samouilov, A., Liu, X. & Zweier, J.L. Characterization of the magnitude and kinetics of xanthine oxidase-catalyzed nitrate reduction: evaluation of its role in nitrite and nitric oxide generation in anoxic tissues. *Biochemistry* **42**, 1150-1159 (2003).
158. Webb, A.*, et al.* Reduction of nitrite to nitric oxide during ischemia protects against myocardial ischemia-reperfusion damage. *Proc Natl Acad Sci U S A* **101**, 13683-13688 (2004).
159. Cosby, K.*, et al.* Nitrite reduction to nitric oxide by deoxyhemoglobin vasodilates the human circulation. *Nat Med* **9**, 1498-1505 (2003).
160. Murad, F., Rapoport, R.M. & Fiscus, R. Role of cyclic-GMP in relaxations of vascular smooth muscle. *J Cardiovasc Pharmacol* **7 Suppl 3**, S111-118 (1985).
161. Buechler, W.A.*, et al.* Soluble guanylyl cyclase and platelet function. *Ann N Y Acad Sci* **714**, 151-157 (1994).
162. Horst, B.G. & Marletta, M.A. Physiological activation and deactivation of soluble guanylate cyclase. *Nitric Oxide* **77**, 65-74 (2018).
163. Montfort, W.R., Wales, J.A. & Weichsel, A. Structure and Activation of Soluble Guanylyl Cyclase, the Nitric Oxide Sensor. *Antioxid Redox Signal* **26**, 107-121 (2017).
164. Lorenz, R., Bertinetti, D. & Herberg, F.W. cAMP-Dependent Protein Kinase and cGMP-Dependent Protein Kinase as Cyclic Nucleotide Effectors. *Handb Exp Pharmacol* **238**, 105-122 (2017).
165. Kaupp, U.B. & Seifert, R. Cyclic nucleotide-gated ion channels. *Physiol Rev* **82**, 769-824 (2002).
166. Niwa, M.*, et al.* Time course of expression of three nitric oxide synthase isoforms after transient middle cerebral artery occlusion in rats. *Neurol Med Chir (Tokyo)* **41**, 63-72; discussion 72-63 (2001).
167. Gürsoy-Ozdemir, Y., Bolay, H., Saribaş, O. & Dalkara, T. Role of endothelial nitric oxide generation and peroxynitrite formation in reperfusion injury after focal cerebral ischemia. *Stroke* **31**, 1974-1980; discussion 1981 (2000).

168. Ito, Y.*, et al.* Nitric oxide production during cerebral ischemia and reperfusion in eNOS- and nNOS-knockout mice. *Curr Neurovasc Res* **7**, 23-31 (2010).
169. Liu, K., Li, Q., Zhang, L. & Zheng, X. The dynamic detection of NO during stroke and reperfusion in vivo. *Brain Inj* **23**, 450-458 (2009).
170. Iadecola, C., Zhang, F., Xu, S., Casey, R. & Ross, M.E. Inducible nitric oxide synthase gene expression in brain following cerebral ischemia. *J Cereb Blood Flow Metab* **15**, 378-384 (1995).
171. Suzuki, M., Tabuchi, M., Ikeda, M. & Tomita, T. Concurrent formation of peroxynitrite with the expression of inducible nitric oxide synthase in the brain during middle cerebral artery occlusion and reperfusion in rats. *Brain Res* **951**, 113-120 (2002).
172. Katsuyama, K., Shichiri, M., Marumo, F. & Hirata, Y. NO inhibits cytokine-induced iNOS expression and NF-kappaB activation by interfering with phosphorylation and degradation of IkappaB-alpha. *Arterioscler Thromb Vasc Biol* **18**, 1796-1802 (1998).
173. Iadecola, C., Zhang, F., Casey, R., Nagayama, M. & Ross, M.E. Delayed reduction of ischemic brain injury and neurological deficits in mice lacking the inducible nitric oxide synthase gene. *J Neurosci* **17**, 9157-9164 (1997).
174. Eliasson, M.J.*, et al.* Neuronal nitric oxide synthase activation and peroxynitrite formation in ischemic stroke linked to neural damage. *J Neurosci* **19**, 5910-5918 (1999).
175. Huang, Z.*, et al.* Enlarged infarcts in endothelial nitric oxide synthase knockout mice are attenuated by nitro-L-arginine. *J Cereb Blood Flow Metab* **16**, 981-987 (1996).
176. Yu, H.M.*, et al.* Coupling between neuronal nitric oxide synthase and glutamate receptor 6-mediated c-Jun N-terminal kinase signaling pathway via S-nitrosylation contributes to ischemia neuronal death. *Neuroscience* **155**, 1120-1132 (2008).
177. Gürsoy-Ozdemir, Y., Can, A. & Dalkara, T. Reperfusion-induced oxidative/nitrative injury to neurovascular unit after focal cerebral ischemia. *Stroke* **35**, 1449-1453 (2004).
178. Sehara, Y.*, et al.* Distribution of inducible nitric oxide synthase and cell proliferation in rat brain after transient middle cerebral artery occlusion. *Brain Res* **1093**, 190-197 (2006).
179. Corsani, L.*, et al.* Inducible nitric oxide synthase appears and is co-expressed with the neuronal isoform in interneurons of the rat hippocampus after transient ischemia induced by middle cerebral artery occlusion. *Exp Neurol* **211**, 433-440 (2008).
180. Sun, Y.*, et al.* Neuronal nitric oxide synthase and ischemia-induced neurogenesis. *J Cereb Blood Flow Metab* **25**, 485-492 (2005).
181. Atochin, D.N.*, et al.* Soluble guanylate cyclase alpha1beta1 limits stroke size and attenuates neurological injury. *Stroke* **41**, 1815-1819 (2010).
182. Bath, P.M., Krishnan, K. & Appleton, J.P. Nitric oxide donors (nitrates), L-arginine, or nitric oxide synthase inhibitors for acute stroke. *Cochrane Database Syst Rev* **4**, Cd000398 (2017).
183. Chen, Z.Q., Mou, R.T., Feng, D.X., Wang, Z. & Chen, G. The role of nitric oxide in stroke. *Med Gas Res* **7**, 194-203 (2017).
184. Morikawa, E.*, et al.* L-arginine infusion promotes nitric oxide-dependent vasodilation, increases regional cerebral blood flow, and reduces infarction volume in the rat. *Stroke* **25**, 429-435 (1994).
185. Willmot, M., Gray, L., Gibson, C., Murphy, S. & Bath, P.M. A systematic review of nitric oxide donors and L-arginine in experimental stroke; effects on infarct size and cerebral blood flow. *Nitric Oxide* **12**, 141-149 (2005).
186. Willmot, M.*, et al.* Transdermal glyceryl trinitrate lowers blood pressure and maintains cerebral blood flow in recent stroke. *Hypertension* **47**, 1209-1215 (2006).

187. Margaill, I., Allix, M., Boulu, R.G. & Plotkine, M. Dose- and time-dependence of L-NAME neuroprotection in transient focal cerebral ischaemia in rats. *Br J Pharmacol* **120**, 160-163 (1997).
188. Zhang, Z.G.*, et al.* ARL 17477, a potent and selective neuronal NOS inhibitor decreases infarct volume after transient middle cerebral artery occlusion in rats. *J Cereb Blood Flow Metab* **16**, 599-604 (1996).
189. Pérez-Asensio, F.J.*, et al.* Inhibition of iNOS activity by 1400W decreases glutamate release and ameliorates stroke outcome after experimental ischemia. *Neurobiol Dis* **18**, 375-384 (2005).
190. Amin-Hanjani, S.*, et al.* Mevastatin, an HMG-CoA reductase inhibitor, reduces stroke damage and upregulates endothelial nitric oxide synthase in mice. *Stroke* **32**, 980-986 (2001).
191. Becker, K., Tanzi, P., Kalil, A., Shibata, D. & Cain, K. Early statin use is associated with increased risk of infection after stroke. *J Stroke Cerebrovasc Dis* **22**, 66-71 (2013).
192. Jin, H.G.*, et al.* Hypoxia-induced upregulation of endothelial small G protein RhoA and Rho-kinase/ROCK2 inhibits eNOS expression. *Neurosci Lett* **408**, 62-67 (2006).
193. Shin, H.K.*, et al.* Rho-kinase inhibition acutely augments blood flow in focal cerebral ischemia via endothelial mechanisms. *J Cereb Blood Flow Metab* **27**, 998-1009 (2007).
194. Nakamura, T., Tsuruta, S. & Uchiyama, S. Cilostazol combined with aspirin prevents early neurological deterioration in patients with acute ischemic stroke: a pilot study. *J Neurol Sci* **313**, 22-26 (2012).
195. Rossaint, R.*, et al.* Inhaled nitric oxide for the adult respiratory distress syndrome. *N Engl J Med* **328**, 399-405 (1993).
196. Khan, M.F., Azfar, M.F. & Khurshid, S.M. The role of inhaled nitric oxide beyond ARDS. *Indian J Crit Care Med* **18**, 392-395 (2014).
197. Papadimos, T.J., Medhkour, A. & Yermal, S. Successful use of inhaled nitric oxide to decrease intracranial pressure in a patient with severe traumatic brain injury complicated by acute respiratory distress syndrome: a role for an anti-inflammatory mechanism? *Scand J Trauma Resusc Emerg Med* **17**, 5 (2009).
198. Vavilala, M.S., Roberts, J.S., Moore, A.E., Newell, D.W. & Lam, A.M. The influence of inhaled nitric oxide on cerebral blood flow and metabolism in a child with traumatic brain injury. *Anesth Analg* **93**, 351-353 , 353rd contents page (2001).
199. Kuebler, W.M.*, et al.* Inhaled nitric oxide induces cerebrovascular effects in anesthetized pigs. *Neurosci Lett* **348**, 85-88 (2003).
200. Terpolilli, N.A.*, et al.* Inhalation of nitric oxide prevents ischemic brain damage in experimental stroke by selective dilatation of collateral arterioles. *Circ Res* **110**, 727-738 (2012).
201. Terpolilli, N.A., Kim, S.W., Thal, S.C., Kuebler, W.M. & Plesnila, N. Inhaled nitric oxide reduces secondary brain damage after traumatic brain injury in mice. *J Cereb Blood Flow Metab* **33**, 311-318 (2013).
202. Pastor, P., Curvello, V., Hekierski, H. & Armstead, W.M. Inhaled nitric oxide protects cerebral autoregulation through prevention of impairment of ATP and calcium sensitive K channel mediated cerebrovasodilation after traumatic brain injury. *Brain Res* **1711**, 1-6 (2019).
203. Terpolilli, N.A.*, et al.* Nitric oxide inhalation reduces brain damage, prevents mortality, and improves neurological outcome after subarachnoid hemorrhage by resolving early pial microvasospasms. *J Cereb Blood Flow Metab* **36**, 2096-2107 (2016).

204. Fox-Robichaud, A*., et al.* Inhaled NO as a viable antiadhesive therapy for ischemia/reperfusion injury of distal microvascular beds. *J Clin Invest* **101**, 2497-2505 (1998).
205. Gianetti, J*., et al.* Supplemental nitric oxide and its effect on myocardial injury and function in patients undergoing cardiac surgery with extracorporeal circulation. *J Thorac Cardiovasc Surg* **127**, 44-50 (2004).
206. Lang, J.D., Jr*., et al.* Inhaled NO accelerates restoration of liver function in adults following orthotopic liver transplantation. *J Clin Invest* **117**, 2583-2591 (2007).
207. Hataishi, R*., et al.* Inhaled nitric oxide decreases infarction size and improves left ventricular function in a murine model of myocardial ischemia-reperfusion injury. *Am J Physiol Heart Circ Physiol* **291**, H379-384 (2006).
208. Da, J., Chen, L. & Hedenstierna, G. Nitric oxide up-regulates the glucocorticoid receptor and blunts the inflammatory reaction in porcine endotoxin sepsis. *Crit Care Med* **35**, 26-32 (2007).
209. Lourbopoulos, A., Karacostas, D., Artemis, N., Milonas, I. & Grigoriadis, N. Effectiveness of a new modified intraluminal suture for temporary middle cerebral artery occlusion in rats of various weight. *J Neurosci Methods* **173**, 225-234 (2008).
210. Zellner, A*., et al.* CADASIL brain vessels show a HTRA1 loss-of-function profile. *Acta Neuropathol* **136**, 111-125 (2018).
211. Shaw, S*., et al.* Discovery and characterization of olokizumab: a humanized antibody targeting interleukin-6 and neutralizing gp130-signaling. *MAbs* **6**, 774-782 (2014).
212. Scheinfeld, N. A comprehensive review and evaluation of the side effects of the tumor necrosis factor alpha blockers etanercept, infliximab and adalimumab. *J Dermatolog Treat* **15**, 280-294 (2004).
213. Lambertsen, K.L., Finsen, B. & Clausen, B.H. Post-stroke inflammation-target or tool for therapy? *Acta Neuropathol* **137**, 693-714 (2019).
214. Tsao, P.S., McEvoy, L.M., Drexler, H., Butcher, E.C. & Cooke, J.P. Enhanced endothelial adhesiveness in hypercholesterolemia is attenuated by L-arginine. *Circulation* **89**, 2176-2182 (1994).
215. Ma, X.L., Weyrich, A.S., Lefer, D.J. & Lefer, A.M. Diminished basal nitric oxide release after myocardial ischemia and reperfusion promotes neutrophil adherence to coronary endothelium. *Circ Res* **72**, 403-412 (1993).
216. Kubes, P., Suzuki, M. & Granger, D.N. Nitric oxide: an endogenous modulator of leukocyte adhesion. *Proc Natl Acad Sci U S A* **88**, 4651-4655 (1991).
217. Mathru, M., Huda, R., Solanki, Daneshvari R., Hays, S. & Lang, John D. Inhaled Nitric Oxide Attenuates Reperfusion Inflammatory Responses in Humans. *Anesthesiology* **106**, 275-282 (2007).
218. Vovenko, E.P. & Chuikin, A.E. Tissue oxygen tension profiles close to brain arterioles and venules in the rat cerebral cortex during the development of acute anemia. *Neurosci Behav Physiol* **40**, 723-731 (2010).
219. McMahon, T.J. & Doctor, A. Extrapulmonary effects of inhaled nitric oxide: role of reversible S-nitrosylation of erythrocytic hemoglobin. *Proc Am Thorac Soc* **3**, 153-160 (2006).
220. Shelton, J.L., Wang, L., Cepinskas, G., Inculet, R. & Mehta, S. Human neutrophil-pulmonary microvascular endothelial cell interactions in vitro: differential effects of nitric oxide vs. peroxynitrite. *Microvasc Res* **76**, 80-88 (2008).
221. Jiang, M.Z*., et al.* Effects of antioxidants and NO on TNF-alpha-induced adhesion molecule expression in human pulmonary microvascular endothelial cells. *Respir Med* **99**, 580-591 (2005).

222. Lo, H.P., Ackland-Berglund, C.E., Pritchard, K.A., Jr., Guice, K.S. & Oldham, K.T. Attenuated expression of inducible nitric oxide synthase in lung microvascular endothelial cells is associated with an increase in ICAM-1 expression. *J Pediatr Surg* **36**, 1136-1142 (2001).
223. Lelamali, K., Wang, W., Gengaro, P., Edelstein, C. & Schrier, R.W. Effects of nitric oxide and peroxynitrite on endotoxin-induced leukocyte adhesion to endothelium. *J Cell Physiol* **188**, 337-342 (2001).
224. Baatz, H. & Pleyer, U. Modulation of leukocyte-endothelium interaction by nitric oxide synthase inhibitors: effects on leukocyte adhesion in endotoxin-induced uveitis. *Inflamm Res* **50**, 534-543 (2001).
225. Liu, P.*, et al.* NO modulates P-selectin and ICAM-1 mRNA expression and hemodynamic alterations in hepatic I/R. *Am J Physiol* **275**, H2191-2198 (1998).
226. De Caterina, R.*, et al.* Nitric oxide decreases cytokine-induced endothelial activation. Nitric oxide selectively reduces endothelial expression of adhesion molecules and proinflammatory cytokines. *J Clin Invest* **96**, 60-68 (1995).
227. Ahluwalia, A.*, et al.* Antiinflammatory activity of soluble guanylate cyclase: cGMP-dependent down-regulation of P-selectin expression and leukocyte recruitment. *Proc Natl Acad Sci U S A* **101**, 1386-1391 (2004).
228. Pierce, J.W.*, et al.* Novel inhibitors of cytokine-induced IkappaBalpha phosphorylation and endothelial cell adhesion molecule expression show anti-inflammatory effects in vivo. *J Biol Chem* **272**, 21096-21103 (1997).
229. Collins, T.*, et al.* Transcriptional regulation of endothelial cell adhesion molecules: NF-kappa B and cytokine-inducible enhancers. *Faseb j* **9**, 899-909 (1995).
230. Reynaert, N.L.*, et al.* Nitric oxide represses inhibitory kappaB kinase through S-nitrosylation. *Proc Natl Acad Sci U S A* **101**, 8945-8950 (2004).
231. Kelleher, Z.T., Matsumoto, A., Stamler, J.S. & Marshall, H.E. NOS2 regulation of NF-kappaB by S-nitrosylation of p65. *J Biol Chem* **282**, 30667-30672 (2007).
232. Khan, M.*, et al.* S-Nitrosoglutathione Mimics the Beneficial Activity of Endothelial Nitric Oxide Synthase-Derived Nitric Oxide in a Mouse Model of Stroke. *J Stroke Cerebrovasc Dis* **28**, 104470 (2019).
233. Waldow, T., Witt, W., Weber, E. & Matschke, K. Nitric oxide donor-induced persistent inhibition of cell adhesion protein expression and NFkappaB activation in endothelial cells. *Nitric Oxide* **15**, 103-113 (2006).
234. Guedes, R.P.*, et al.* A20 deficiency causes spontaneous neuroinflammation in mice. *J Neuroinflammation* **11**, 122 (2014).
235. Wang, X.*, et al.* Astrocytic A20 ameliorates experimental autoimmune encephalomyelitis by inhibiting NF-κB- and STAT1-dependent chemokine production in astrocytes. *Acta Neuropathol* **126**, 711-724 (2013).
236. Miao, H.S., Yu, L.Y., Hui, G.Z. & Guo, L.H. Antiapoptotic effect both in vivo and in vitro of A20 gene when transfected into rat hippocampal neurons. *Acta Pharmacol Sin* **26**, 33-38 (2005).
237. Han, D.*, et al.* Clematichinenoside protects blood brain barrier against ischemic stroke superimposed on systemic inflammatory challenges through up-regulating A20. *Brain Behav Immun* **51**, 56-69 (2016).
238. Mc Guire, C., Rahman, M., Schwaninger, M., Beyaert, R. & van Loo, G. The ubiquitin editing enzyme A20 (TNFAIP3) is upregulated during permanent middle cerebral artery occlusion but does not influence disease outcome. *Cell Death Dis* **4**, e531 (2013).
239. Liu, G.*, et al.* Src phosphorylation of endothelial cell surface intercellular adhesion molecule-1 mediates neutrophil adhesion and contributes to the mechanism of lung inflammation. *Arterioscler Thromb Vasc Biol* **31**, 1342-1350 (2011).

240. Javaid, K.*, et al.* Tumor necrosis factor-alpha induces early-onset endothelial adhesivity by protein kinase Czeta-dependent activation of intercellular adhesion molecule-1. *Circ Res* **92**, 1089-1097 (2003).
241. Barreiro, O.*, et al.* Endothelial adhesion receptors are recruited to adherent leukocytes by inclusion in preformed tetraspanin nanoplatforms. *J Cell Biol* **183**, 527-542 (2008).
242. Mackesy, D.Z. & Goalstone, M.L. Insulin augments tumor necrosis factor-alpha stimulated expression of vascular cell adhesion molecule-1 in vascular endothelial cells. *J Inflamm (Lond)* **8**, 34 (2011).
243. Matsushita, K.*, et al.* Nitric oxide regulates exocytosis by S-nitrosylation of N-ethylmaleimide-sensitive factor. *Cell* **115**, 139-150 (2003).
244. Xu, S., Zhou, X., Yuan, D., Xu, Y. & He, P. Caveolin-1 scaffolding domain promotes leukocyte adhesion by reduced basal endothelial nitric oxide-mediated ICAM-1 phosphorylation in rat mesenteric venules. *Am J Physiol Heart Circ Physiol* **305**, H1484-1493 (2013).
245. Gao, F.*, et al.* Reduction of Endothelial Nitric Oxide Increases the Adhesiveness of Constitutive Endothelial Membrane ICAM-1 through Src-Mediated Phosphorylation. *Front Physiol* **8**, 1124 (2017).
246. Feron, O. & Balligand, J.L. Caveolins and the regulation of endothelial nitric oxide synthase in the heart. *Cardiovasc Res* **69**, 788-797 (2006).
247. Zhang, Q.*, et al.* Functional relevance of Golgi- and plasma membrane-localized endothelial NO synthase in reconstituted endothelial cells. *Arterioscler Thromb Vasc Biol* **26**, 1015-1021 (2006).
248. Sánchez, F.A.*, et al.* Functional significance of differential eNOS translocation. *Am J Physiol Heart Circ Physiol* **291**, H1058-1064 (2006).
249. Marín, N.*, et al.* S-Nitrosation of β-catenin and p120 catenin: a novel regulatory mechanism in endothelial hyperpermeability. *Circ Res* **111**, 553-563 (2012).
250. Vallance, B.A.*, et al.* Relative contributions of NOS isoforms during experimental colitis: endothelial-derived NOS maintains mucosal integrity. *Am J Physiol Gastrointest Liver Physiol* **287**, G865-874 (2004).
251. Kelleher, Z.T.*, et al.* NOS2 regulation of LPS-induced airway inflammation via S-nitrosylation of NF-{kappa}B p65. *Am J Physiol Lung Cell Mol Physiol* **301**, L327-333 (2011).
252. Qian, J. & Fulton, D.J. Exogenous, but not Endogenous Nitric Oxide Inhibits Adhesion Molecule Expression in Human Endothelial Cells. *Front Physiol* **3**, 3 (2012).
253. Heo, S.K., Yun, H.J., Noh, E.K., Park, W.H. & Park, S.D. LPS induces inflammatory responses in human aortic vascular smooth muscle cells via Toll-like receptor 4 expression and nitric oxide production. *Immunol Lett* **120**, 57-64 (2008).
254. Banick, P.D., Chen, Q., Xu, Y.A. & Thom, S.R. Nitric oxide inhibits neutrophil beta 2 integrin function by inhibiting membrane-associated cyclic GMP synthesis. *J Cell Physiol* **172**, 12-24 (1997).
255. Mitchell, D.J., Yu, J. & Tyml, K. Local L-NAME decreases blood flow and increases leukocyte adhesion via CD18. *Am J Physiol* **274**, H1264-1268 (1998).
256. Bhopale, V.M., Yang, M., Yu, K. & Thom, S.R. Factors Associated with Nitric Oxide-mediated β2 Integrin Inhibition of Neutrophils. *J Biol Chem* **290**, 17474-17484 (2015).
257. Thom, S.R.*, et al.* Nitric-oxide synthase-2 linkage to focal adhesion kinase in neutrophils influences enzyme activity and β2 integrin function. *J Biol Chem* **288**, 4810-4818 (2013).
258. Lundberg, J.O. & Weitzberg, E. NO generation from nitrite and its role in vascular control. *Arterioscler Thromb Vasc Biol* **25**, 915-922 (2005).
259. Cannon, R.O., 3rd*, et al.* Effects of inhaled nitric oxide on regional blood flow are consistent with intravascular nitric oxide delivery. *J Clin Invest* **108**, 279-287 (2001).

260. Ng, E.S.*, et al.* Enhanced S-nitroso-albumin formation from inhaled NO during ischemia/reperfusion. *Circ Res* **94**, 559-565 (2004).
261. Langhauser, F.*, et al.* A diseasome cluster-based drug repurposing of soluble guanylate cyclase activators from smooth muscle relaxation to direct neuroprotection. *npj Systems Biology and Applications* **4**, 8 (2018).
262. Nedvetsky, P.I., Kleinschnitz, C. & Schmidt, H.H.H.W. Regional distribution of protein and activity of the nitric oxide receptor, soluble guanylyl cyclase, in rat brain suggests multiple mechanisms of regulation. *Brain Research* **950**, 148-154 (2002).
263. Shvedova, M.*, et al.* cGMP-dependent protein kinase I in vascular smooth muscle cells improves ischemic stroke outcome in mice. *J Cereb Blood Flow Metab* **39**, 2379-2391 (2019).
264. Rubbo, H., Darley-Usmar, V. & Freeman, B.A. Nitric oxide regulation of tissue free radical injury. *Chem Res Toxicol* **9**, 809-820 (1996).
265. Moya, M.P.*, et al.* S-nitrosothiol repletion by an inhaled gas regulates pulmonary function. *Proc Natl Acad Sci U S A* **98**, 5792-5797 (2001).
266. Simons, M.*, et al.* Comparison of the oxidative reactivity of recombinant fetal and adult human hemoglobin: implications for the design of hemoglobin-based oxygen carriers. *Biosci Rep* **38**(2018).
267. Li, M.*, et al.* Platelet Membrane Biomimetic Magnetic Nanocarriers for Targeted Delivery and in Situ Generation of Nitric Oxide in Early Ischemic Stroke. *ACS Nano* **14**, 2024-2035 (2020).

9. Acknowledgments

Today I reach the finish line of my exciting Ph.D. adventure. Looking back, I would like to sincerely express my gratitude to all the people who supported me completing my thesis.

For the opportunity and trust in my ability to carry out this project, I would like to thank *Prof. Nikolaus Plesnila*. Through his critical advice and support, I had the chance to broaden and deepen my skills and knowledge. In addition, I wish to give my special regards *to Dr. Christof Haffner* for his support and for always having an open door.

I wish to express my deepest gratitude to *Dr. Burcu Seker* for her guidance, discussions, and tremendous support throughout my research. It was very inspiring to work with you, Burcu your encouraging nature helped me to continue also in struggling times.

My special regards go to my dear colleague *Uta Mamrak*. Thank you so much, Uta, for having infinite patients teaching me surgical procedures and sharing your experiences. I am grateful for the motivating and supportive advice for life and your open ear at all times.

I wish to thank all my colleagues (*Antonia, Andi, Anna-Lena, Barbara, Berni, Carina, Damian, Farida, Gemma, Hedwig, Igor, Janina, Katharina, Susi, Stefan*) whose scientific and non-scientific discussions and advice in one or the other coffee break were essential in the completion of this project. I am grateful for your help and open door in every situation.

Furthermore, I would like to thank the team of the ISD animal facility, *Dr. Manuela Schneider, Peggy Kunath, Stefanie Wurster, and Daniel Friedrich*, for taking great care of the animals.

Moreover, I would like to thank our collaboration partner *Dr. Amritha Ahluwalia* and her team. Especially *Tipparat Parakaw* and *Sven Van Eijl*, who warmly welcomed me in the lab and taught me new methods.

I want to thank my friends (*Babsi, Laura, Schafi, Storchi, Birgit, Helga*) who were there for me to share joy, adventures, and moral support. In particular, I want to gratefully acknowledge my best friend, *Karin*, for her strong support and the many experiences throughout over a decade of studies. Sharing moments of happiness and frustration strengthened our friendship, and I am infinitely grateful that I can always count on you.

Finally, I would like to sincerely thank my parents, *Iris and Robert*, and my sister *Caroline*. Your support, motivating words, patience, help, trust, and love eased my way to finishing another milestone in my life.